# Structural analysis of the specific inactivation of Toll-like receptor 2

Von der Fakultät für Lebenswissenschaften

der Technischen Universität Carolo-Wilhelmina

zu Braunschweig

zur Erlangung des Grades eines

Doktors der Naturwissenschaften

(Dr. rer. nat.)

genehmigte

D i s s e r t a t i o n

von Nils Kuklik

aus Peine

1. Referent: Professor Dr. Dieter Jahn
2. Referent: Professor Dr. Wolf-Dieter Schubert
eingereicht am: 11.07.2012
mündliche Prüfung (Disputation) am: 11.10.2012

Druckjahr 2012

## Vorveröffentlichungen der Dissertation

Teilergebnisse aus dieser Arbeit wurden mit Genehmigung der Fakultät für Lebenswissenschaften, vertreten durch den Mentor der Arbeit, in folgenden Beiträgen vorab veröffentlicht:

### Patent

"Toll-like Receptor 2 Binding Epitope and Binding Members thereto" eingereicht am 30.03.2012 beim "Intellectual Property Office", Großbritannien durch Opsona Therapeutics, Dublin, Irland (Antragsnummer: 1205633.9). Patent öffentlich zugänglich ab 01.10.2012.

### Tagungsbeiträge

Kuklik N., Schubert W.-D.: The benefits of silencing immune receptors. (Vortrag) Biotechnology Research Day, Bellville, Südafrika (2011). Zweiter Preis in der Kategorie "Bester PhD-Vortrag".

Kuklik N., Polle L., Wilke S., van den Heuvel J., Schubert W.-D.: Innate immune receptors. (Poster) Biotechnology Research Day, Bellville, Südafrika, (2010).

Kuklik N., Wilke S., van den Heuvel J., Schubert W.-D.: Producing Toll-like Receptors using Baculoviral Expression System for Structural- and Functional Analysis. (Poster) Workshop der Deutschen Gesellschaft für Kristallographie "Diffraction Data Collection Using Synchrotron Radiation", Berlin (2009).

Kuklik N., van den Heuvel J., Schubert W.-D.: Insect Cell Production of Toll-like Receptors 2 and 6. (Poster) 25$^{th}$ European Crystallography Meeting, Istanbul, Türkei (2009).

# Table of contents

# Abbreviations

| | |
|---|---|
| aa | amino acid(s) |
| AC | Affinity chromatography |
| AEC | Anion exchange chromatography |
| AIM2 | Absent in melanoma 2 |
| AP | Alkaline phosphatase |
| bp | base pairs |
| BCIP | 5-Bromo-4-chloro-3-indolyl phosphate |
| CARD | Caspase activation and recruitment domain |
| CCD | Charge coupled device |
| CD14 | Cluster of differentiation 14 |
| CD36 | Cluster of differentiation 36 |
| CDR | Complementary determining region |
| CHO cells | Chinese hamster ovary cells |
| DAI | DNA-dependent activator of IFN-regulatory factors |
| DAMP | Damage-associated molecular pattern |
| DNA | Deoxyribonucleic acid |
| *E. coli* | *Escherichia coli* |
| ECD | extracellular domain |
| EDTA | Ethylenediaminetetraacetic acid |
| EM | Electron microscopy |
| ESI-MS | Electrospray ionization mass spectrometry |
| Fab | Fragment antigen-binding |
| FACS | Fluorescence-activated cell sorting |
| Fc region | Fragment crystallizable region |
| FSC | Fourier shell correlation |
| GlcNAc | N-Acetylglucosamine |
| h | hour(s) |
| $His_6$ | His-His-His-His-His-His |
| hTLR2 | human Toll-like receptor 2 |
| hTLR6 | human Toll-like receptor 6 |
| HZI | Helmholtz Centre for Infection Research |
| IFN | Interferon |
| IgG | Immunoglobulin G |
| IL | Interleukin |
| I/R injury | Ischemia/reperfusion injury |
| IRF | Interferon regulatory factor |
| kD | kiloDalton |
| LB | Lysogeny broth |
| LPS | Lipopolysaccharide |
| LRR | Leucin rich repeat |
| LTA | Lipoteichoic acid |
| MAL | MyD88-adaptor-like |
| MALDI | Matrix assisted laser desorption ionization |
| MALP-2 | Macrophage-activating lipopeptide-2 kDa |
| Man | Mannose |
| MBL | Mannan-binding lectin |
| MOI | Multiplicity of infection |

| | |
|---|---|
| MS | Mass spectrometry |
| mTLR2 | murine Toll-like receptor 2 |
| mTLR6 | murine Toll-like receptor 6 |
| MW | Molecular weight |
| MyD88 | Myeloid differentiation primary response gene (88) |
| NEMO | NF-κB-essential modulator |
| NF-κB | Nuclear factor kappa-light-chain-enhancer of activated B cells |
| NLR | NOD-like receptors |
| NOD | Nucleotide oligomerization domain |
| NTA | Nitrilotriacetic acid |
| PAGE | Polyacrylamide gel electrophoresis |
| $Pam_2CSK_4$ | $Palmitoyl_2$-Cys-Ser-Lys-Lys-Lys-Lys-Lys |
| $Pam_3CSK_4$ | $Palmitoyl_3$-Cys-Ser-Lys-Lys-Lys-Lys-Lys |
| PAMP | Pathogen-associated molecular pattern |
| PCR | Polymerase chain reaction |
| PDB | Protein Data Bank |
| PEG | Polyethylene glycol |
| pFB | Expression vector pFastBac1 from Invitrogen |
| PGN | Peptidoglycan |
| pI | Isoelectric point |
| pfu | Plaque forming units |
| PNGase | Peptide:N-glycosidase F |
| PRR | Pattern-recognition receptor |
| PVDF | Polyvinylidene difluoride |
| PYD | Pyrin domain |
| RA | Rheumatoid arthritis |
| RIG | Retinoic acid-inducible gene |
| RLR | RIG-like receptors |
| RNA | Ribonucleic acid |
| rpm | Revolutions per minute |
| RT | Room temperature |
| SDS | Sodium dodecyl sulfate |
| SDS-PAGE | SDS-polyacrylamide gel electrophoresis |
| SEC | Size-exclusion chromatography |
| Sf21 cells | *Spodoptera frugiperda* 21 cells |
| SLE | Systemic lupus erythematosus |
| SPR | Surface plasmon resonance |
| TBS | Tris buffered saline |
| TCR | T-cell receptor |
| TEV | Tobacco etch virus |
| TIR | Toll/interleukin-1 receptor |
| TLR | Toll-like receptor |
| TNF | Tumor necrosis factor |
| TRAF | TNF receptor-associated factor |
| TRAM | TRIF-related adaptor molecule |
| TRIF | TIR-domain-containing adapter-inducing interferon-β |
| Tris | 2-Amino-2-(hydroxymethyl)-propan-1,3-diol |
| UV | Ultraviolet |
| UWC | University of the Western Cape |
| VLR | Variable lymphocyte receptor |

# Summary


## Inhibition of Toll-like receptor 2 with a monoclonal antibody

Over the last 2 decades, Toll-like receptors (TLRs) have emerged as critical first-line pattern recognition receptors for pathogen detection following microbial infections. In addition, they participate in responding to a variety of tissue damage-derived endogenous molecules. In both processes, TLRs initiate cellular immune responses. Evolutionarily TLRs constitute a rapid and efficient mechanism to stimulate the immune system through secreted inflammatory cytokines, leading to the phagocytosis of invading microbes or the endocytosis of damaged tissue. TLRs are further essential in developing adaptive immunity. Occasionally, however, the activation of TLRs can also result in severe diseases. This happens in situations where control over the release of pro-inflammatory mediators is lost. Examples include the septic shock pathology due to hyperactivation of immune cells following acute infection with bacteria, and chronic inflammation sustained by a cycle of endogenous ligand release, inflammatory cytokine production and cell necrosis. These and related diseases can effectively be treated by antagonistic drugs that inhibit the TLR-based pro-inflammatory response.

The monoclonal antibody OPN-305, an efficient inhibitor of TLR2, has successfully been used to treat septic shock, rheumatoid arthritis and ischemia/reperfusion injury in mice. However, whereas the efficacy of the antibody was well established, its molecular mechanism remained unexplained.

In this thesis, the complex between the extracellular domain of murine TLR2 and the fragment antigen-binding (Fab) domain of OPN-305 was generated and purified. A first structural description of this complex was achieved by negative stain electron microscopy (EM) at a resolution of ~22 Å. The three-dimensional reconstruction reveals that the antibody binds laterally to the central region of TLR2. Computational mapping of crystal structures of both TLR2 and an antibody Fab fragment into the EM-derived molecular envelope further identified the TLR1/TLR6 dimerization interface of TLR2 as the antibody interaction area. The docking experiments indicate that the leucine rich repeats (LRRs) 11 to 14 are involved in the protein-protein interaction allowing ten amino acids on the surface of TLR2 to be identified as constituting the probable, highly discontinuous epitope.

These results immediately suggest the mechanism of TLR2 inhibition and the antagonistic property of OPN-305 to derive from its ability to block the hetero-dimerization of TLR2 resulting in silencing of downstream signaling cascades.

Despite the wealth of information provided by the TLR2/OPN-305 complex structure, the precise determination of molecular conformations, exact atomic coordinates and the details of interaction await further characterization by techniques such as X-ray crystallography. Although the crystal structure of TLR2/OPN-305 could not be solved as part of this thesis, the complex was successfully crystallized, with crystals diffracting to a maximal resolution of 8 Å. This constitutes a first important step for further efforts to solve the crystal structure of TLR2/OPN-305.

## Producing mouse/human Toll-like receptors 2 and 6 in insect cells using the baculovirus expression system

TLRs, like most mammalian proteins, require expression systems evolutionarily closely related to the organism they originate from rather than traditional prokaryotic expression systems such as *E. coli*. The baculovirus expression system in insect cells is a well established technique to produce eukaryotic proteins. However, the low overall yield of protein and its purification remain bottlenecks during the procedure. In this work recombinant constructs for the expression of murine and human TLR2 and TLR6 have been designed comprising new secretion peptides and more efficient purification tags, providing protein for use in structural studies. Although cloning of recombinant baculovirus was successful and protocols for the virus production and protein purification were established, only TLR2 was produced in suitable amounts, and an increase in the overall protein yield was not achieved. Moreover, the additional Fc purification tag proved recalcitrant to enzymatic cleavage. The results of this thesis can support further optimization of the protein constructs.

# I Introduction

Higher organisms are continuously in contact with their direct environment, depending on it for sustenance but also under the constant threat of attack. Invading microorganisms including bacteria, viruses and parasites disrupt cellular homeostasis and lead to disease. Recognizing and eliminating invading pathogens rapidly is thus crucial. A large array of defense strategies has evolved collectively constituting the mammalian innate and adaptive immune systems. A first line of host defense against invading pathogens is the evolutionary conserved innate immune system that mediates the contact to microbial species via phagocytes including macrophages and dendritic cells (Akira et al., 2006). This is achieved by a limited number of membrane-associated pattern-recognition receptors (PRRs) eliciting an immune response of the organism. These receptors are essential to initiate and maintain an antipathogenic response while the more specific adaptive immune response develops (McCartney and Colonna, 2009). This elaborated system, however, can occasionally lead to auto-immune and inflammatory diseases, *inter alia* when PRR driven signaling pathways are disregulated. Using antagonists such as therapeutic antibodies represents a possible strategy to inhibit hyperactivated PRRs and has become a major research focus (Hennessy et al., 2010). First antagonistic drugs are close to product maturity while many more are in clinical trials (Aikawa et al., 2012; Farrar et al., 2011; Hennessy et al., 2010). Understanding the molecular principles of pathogen recognition by PRRs and their inhibition by medical drugs provides an important contribution to the development of new and the improvement of available drugs.

## IA Inhibition of TLR2 with a monoclonal antibody

### IA.1 The adaptive and innate immune system

Adaptive immunity derives from the development of a diverse repertoire of antigen receptors by T- and B-cells through gene rearrangement processes. Referred to as somatic hypermutation (Diaz and Flajnik, 1998) and V(D)J recombination (Jung and Alt, 2004), these processes are critical for the development of immunological memory (Akira, 2009). B-cells are part of the humoral immune response and generate highly specific antibodies. The T-cell receptors (TCRs), by contrast, are critical in cell-

mediated immunity (Figure IA-1). Antibodies and TCRs recognize specific antigens that either block infection or flags infected cells for destruction (McCartney and Colonna, 2009).

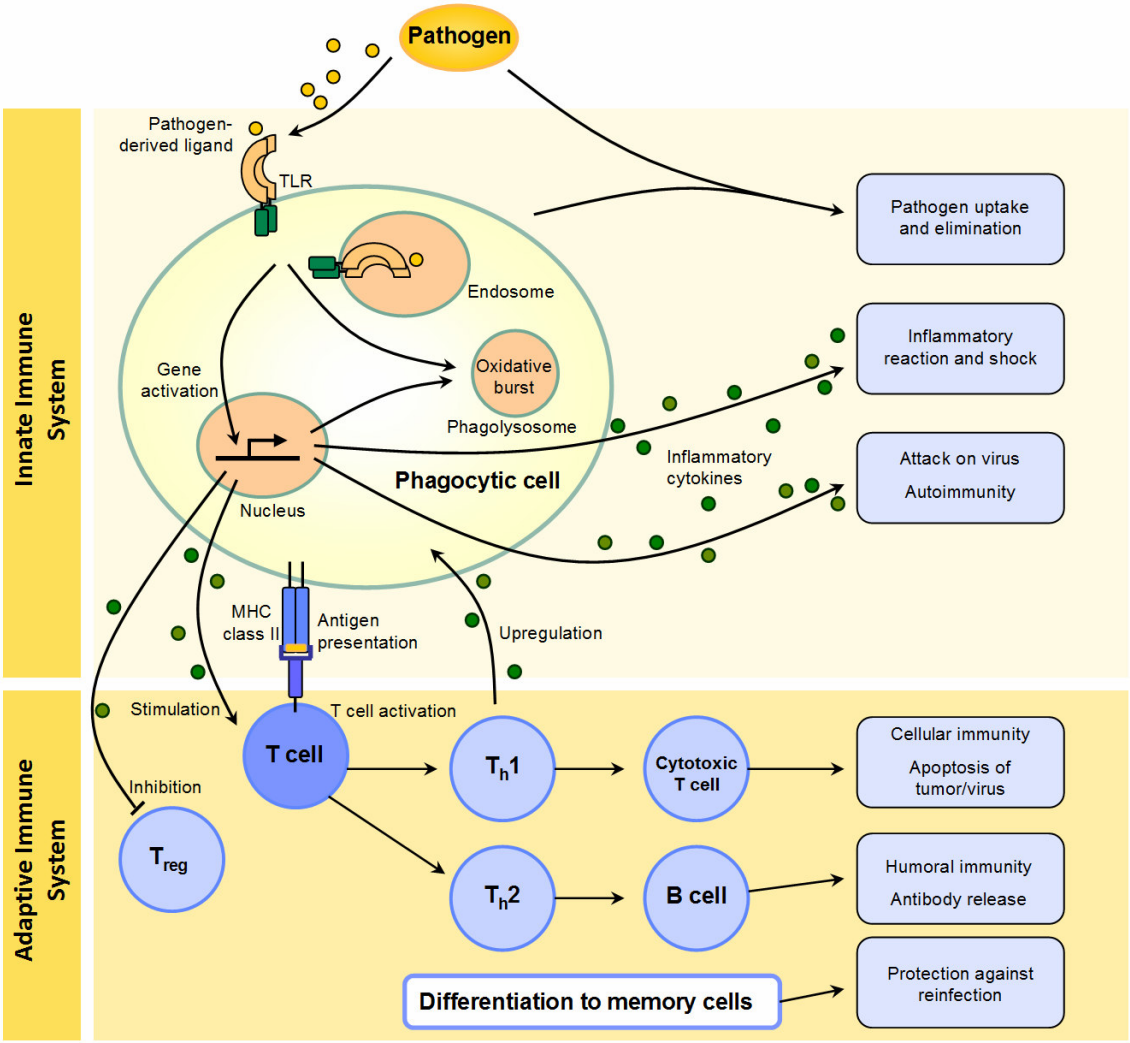


**Figure IA-1 The innate and adaptive immune system**
Dendritic cells, macrophages and other immune cells are involved in the activation of the innate and adaptive immune response. PRRs like Toll-like receptors link microbial signals to specific gene expression programs, which triggers the release of interferons and inflammatory cytokines. This induces the inflammatory response of the organism, and can in rare cases lead to autoimmunity reactions. Dendritic cells are antigen presenting cells and activate T cells through antigen expression on major histocompatibility complex (MHC) class II molecules on their surface. This in turn induces the proliferation of T helper cells ($T_h1$ and $T_h2$), the activation of cytotoxic T cells and B cells and the immunological memory. Innate and adaptive immune systems are further cross-regulated by cytokine release of phagocytes modulating the adaptive immunity by T cell stimulation and regulatory T cell ($T_{reg}$) inhibition, and upregulation of the innate immune system by release of immunological mediators by $T_h1$ cells.

As the adaptive immune response needs several days to develop, the innate immunity is the essential system during the first hours of infection. It is rapidly activated after

signaling molecules typical for attacking pathogens have been recognized (Kumar et al., 2009). However, adaptive and innate immune systems are intimately interwoven (Figure IA-1). Several regulatory pathways activated by the innate immune system also control many aspects of the adaptive immune response (Medzhitov, 2001). The combination of innate and adaptive immunity is thus central to the efficacy of the mammalian immune system. The innate immune system rapidly recognizes and eliminates invading microorganisms resulting in minimal self-damage, whereas the adaptive immune system mediates the protection against the re-infection with the same pathogen by generation of memory B and T cells (Palm and Medzhitov, 2009).

## IA.2 Pattern recognition receptors

Pattern recognition receptors (PRRs) are found in a wide array of eukaryotes including amoebae (Walk et al., 2011), insects (Anderson, 2000; Hashimoto et al., 1988), plants (Segonzac and Zipfel, 2011) and vertebrates (Janeway, Jr., 1992). The germ-line encoded receptors of the innate immune system recognize pathogens by characteristic molecules, generally referred to as “pathogen-associated molecular patterns” (PAMPs) (Janeway, Jr., 1989). PAMPs are signature molecules that are largely invariant, unique to large groups of evolutionarily related microorganisms, central to their metabolism or structure and hence essential for their survival. This principle allows microbial and host molecules to be distinguished permitting a limited number of receptors to recognize essentially all pathogens (Medzhitov, 2001).

PRRs may be categorized as follows (Figure IA-2): i) Membrane-bound PRRs. Examples include Dectin-1 for the detection of β-glucans in fungal cell walls (Goodridge et al., 2011), mannose receptor to bind mannose on the surface of microbes (Apostolopoulos and McKenzie, 2001), and the prominent class of Toll-like receptors (TLRs) that recognize a wide variety of microbial PAMPs and are located on cell or endosomal membranes (Mogensen, 2009). ii) Cytoplasmic receptors. Examples include the NOD-like receptors (NLRs) recognizing nucleotides and cell wall components (Fukata et al., 2009), RIG-like receptors (RLRs) for viral RNA (Ramos and Gale, Jr., 2011), and the “interferon stimulatory DNA” (ISD) sensors for viral DNA (Ishii et al., 2008). iii) Secreted PRRs recognize PAMPs, such as mannan-binding lectin (MBL) (Dommett et al., 2006). As part of the complement system of the innate immune

response, MBL is involved in the opsonization of the cell surface of microbes enhancing phagocytosis (Takahashi, 2011).

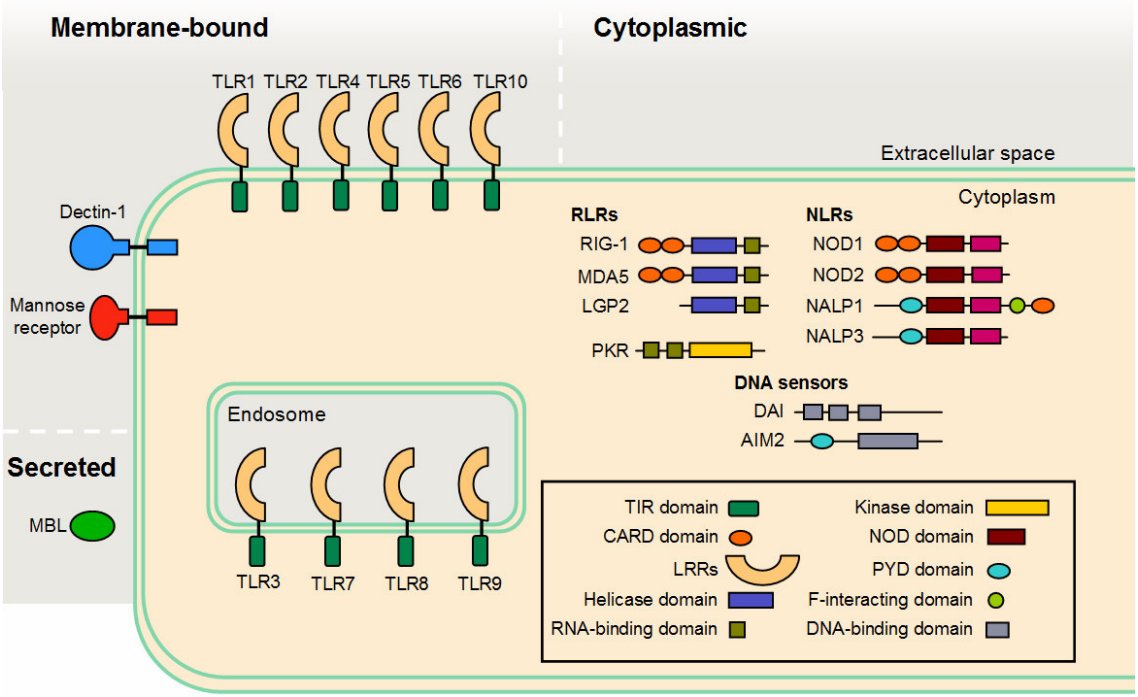


**Figure IA-2 The localization of pattern recognition receptors**
TLRs are membrane-spanning receptors on cellular or endosomal membranes. They bind PAMPs using leucine rich repeat (LRR) domains and initiate intracellular signaling through their C-terminal Toll/interleukin-1 receptor (TIR) domains. RLRs possess a helicase domain to bind viral RNA activating CARD-dependent signaling. NLRs have a central nucleotide-binding oligomerization domain (NOD), and a C-terminal LRR domain, which analogously to TLRs, recognizes the microbial molecules. DAI and AIM2 belong to the group of DNA sensor proteins, MBL opsonizes the cell surface of microbes enhancing phagocytosis. (Adapted from: Mogensen, 2009)

## IA.3 TLRs: Key players in the innate immune response

The most extensively studied class of PRRs is the family of Toll-like receptors (TLRs). TLRs derive their name from the homologous receptor Toll in *Drosophila melanogaster* (Medzhitov et al., 1997) discovered in 1988 as a protein central to establishing the embryonic dorsal-ventral pattern (Hashimoto et al., 1988). Toll was later linked to the activation of the immune response following fungal infection (Lemaitre et al., 1996). Structurally, TLRs are single-pass, type-1 transmembrane glycoproteins. The single, membrane-embedded α-helix connects an extracellular, ligand-binding domain primarily constituted by leucine-rich repeats (LRRs) with an intracellular Toll/interleukin-1 receptor (TIR) domain (Akira and Takeda, 2004; Slack et al., 2000). Extracellular recognition of suitable patterns leads to receptor dimerization which

initiates intracellular signaling culminating in the translocation of the transcription factors nuclear factor κB (NF-κB) and interferon regulatory factor 3 and 7 (IRF3 and IRF7) into the nucleus activating genes of the immune response (Gay and Gangloff, 2007).

### IA.3.1 The family of TLRs and their ligands

The human genome encodes eleven TLRs. However, the human gene for TLR11 is interrupted by a stop codon preventing its functional expression. Mice encode TLRs 1 to 13 but cannot express TLR10 (Leulier and Lemaitre, 2008; Roach et al., 2005). Each TLR is specific for distinct ligands. Extracellular TLRs (TLR1, 2, 4, 5, 6 and 10) specialize in recognizing surface-associated ligands of microbes (cell wall components; viral, fungal and parasitic products), whereas endosomal TLRs (TLR3, 7, 8 and 9) bind pathogen-derived DNA and RNA fragments.

**Table IA-1 Human TLRs and microbial ligands from various species**

| | Ligands | Origin |
|---|---|---|
| **TLR1** | Triacyl lipopeptides<br>Soluble factors<br>Outer surface protein A (OspA) | Bacteria, Mycobacteria<br>*Neisseria meningitides*<br>*Borrelia burgdorferi* |
| **TLR2** | Lipoproteins/lipopeptides<br>Peptidoglycan<br>Lipoteichoic acid<br>Lipoarabinomannan<br>Phospholipomannan<br>Zymosan<br>Hemagglutinin | Various pathogens<br>Gram-positive bacteria<br>Gram-positive bacteria<br>Mycobacteria<br>*Candida albicans*<br>*Saccharomyces cerevisiae*<br>Measles virus |
| **TLR3** | dsRNA | Viruses |
| **TLR4** | Lipopolysaccharide<br>Mannan<br>Glycoinositolphospholipids<br>Taxol<br>Envelope proteins | Gram-negative bacteria<br>*Candida albicans*<br>*Trypanosoma cruzi*<br>Plants<br>Mouse mammary tumor virus |
| **TLR5** | Flagellin | Bacteria |
| **TLR6** | Diacyl lipopeptides<br>Peptidoglycan<br>Zymosan | Mycoplasma<br>Gram-positive bacteria<br>*Saccharomyces cerevisiae* |
| **TLR7** | ssRNA | Viruses |
| **TLR8** | ssRNA | Viruses |
| **TLR9** | Unmethylated CpG-rich DNA | Bacteria and viruses |
| **TLR10** | Unknown | Unknown |

Compiled from Akira et al., 2006; Chang, 2010; Gay and Gangloff, 2007; and Kumar et al., 2009.

Table IA-1 illustrates the diversity of ligands from microbial pathogens that induce TLR-based immune responses. Recognition includes lipopeptides by TLR2 in complex

with TLR1 or TLR6 (Takeda et al., 2002; Takeuchi et al., 2001), double-stranded RNA by TLR3 (Alexopoulou et al., 2001), lipopolysaccharides by TLR4 (Poltorak et al., 1998), flagellin by TLR5 (Hayashi et al., 2001), single-stranded RNA by TLR7 and TLR8 (Heil et al., 2004; Hemmi et al., 2002), unmethylated CpG motifs in DNA by TLR9 (Hochrein et al., 2004), and many others. One receptor can recognize several structurally unrelated ligands, and germ-line mutations have demonstrated the participation of additional adaptor proteins such as CD14, CD36, MD-2 and Dectin-1 for full signaling efficacy by TLR2 and TLR4 complexes (Beutler, 2009; Piccinini and Midwood, 2010).

### IA.3.2 Damage-associated molecular patterns (DAMPs)

Alongside microbial derived components, TLRs also recognize damage-associated molecular patterns (DAMPs), host endogenous molecules released and distributed following stress, tissue damage and cellular diseases. DAMPs induce strong inflammatory immune responses and lead to the recruitment of phagocytes. A list of known endogenous ligands are summarized in Table IA-2.

**Table IA-2 Endogenous TLR ligands**

| | **Ligands** |
|---|---|
| **TLR2** | Glycoprotein 96 (gp96, or heat shock protein 96, HSP96)<br>Serum amyloid A<br>HSP60<br>HSP70<br>High-mobility group protein B1 (HMGB1)<br>Biglycan<br>Alzheimer's amyloid β peptide |
| **TLR3** | self dsRNA |
| **TLR4** | Extra domain A (EDA) of fibronectin<br>Oligosaccharides of hyaluronic acid<br>Fibrinogen<br>Tenascin-C<br>HSP22<br>HSP60<br>HSP70<br>High-mobility group protein B1 (HMGB1)<br>Biglycan |
| **TLR7** | self ssRNA |
| **TLR8** | self ssRNA |
| **TLR9** | self DNA<br>Chromatin-IgG complexes |

Compiled from Chang, 2010; Gay and Gangloff, 2007; Huang and Pope, 2010, and Liu *et al.*, 2011.

Loss of immune response dampening and innate immunity down-regulation results in persistent expression of pro-inflammatory cytokines leading to inflammation and autoimmune diseases such as rheumatoid arthritis (RA), systemic lupus erythematosus (SLE), atherosclerosis and ischemia-reperfusion (I/R) injury (Farrar et al., 2011; Huang and Pope, 2010; Kovach and Standiford, 2011).

TLRs are found in a wide range of cell types including cells of the innate immune system (macrophages, dendritic cells, neutrophils and natural killer cells), adaptive immune system (T cells, B cells), tissues (endothelial cells, epithelial cells, skin keratinocytes, fibroblasts), cancer cells, and many others. This variety demonstrates the importance of TLRs in the regulation of innate and adaptive immune responses after pathogen invasions but also in tissue repair and regeneration (Chang, 2010).

### IA.3.3 TLR signaling pathways

Signal initiation by TLR is elicited by the ligand-induced dimerization of two TLR molecules. Extracellular or endosomal ligands induce dimerization of the corresponding TLR domains leading to the dimerization of the cytosolic Toll/interleukin-1 receptor (TIR) domains and conformational changes required to recruit other TIR domain-containing adaptor molecules (O'Neill and Bowie, 2007). Signaling by all TLRs except TLR3 involves one such adaptor molecule “myeloid differentiation primary-response gene 88” (MyD88), whereas TLR3 instead signals through “TIR domain-containing adaptor protein inducing interferon-β” (TRIF). “MyD88-adaptor-like” protein (MAL) is involved in signaling alongside MyD88 in TLR2 and TLR4, whereas TLR4 and TRIF are linked by “TRIF-related adaptor molecule” (TRAM) (O'Neill, 2008). The adaptors trigger a number of signaling cascades through phosphorylation, ubiquitination and protein-protein interactions (Mogensen, 2009) culminating in the translocation of transcription factors into the nucleus where they regulate the expression of interferons and proinflammatory cytokines (Figure IA-3).

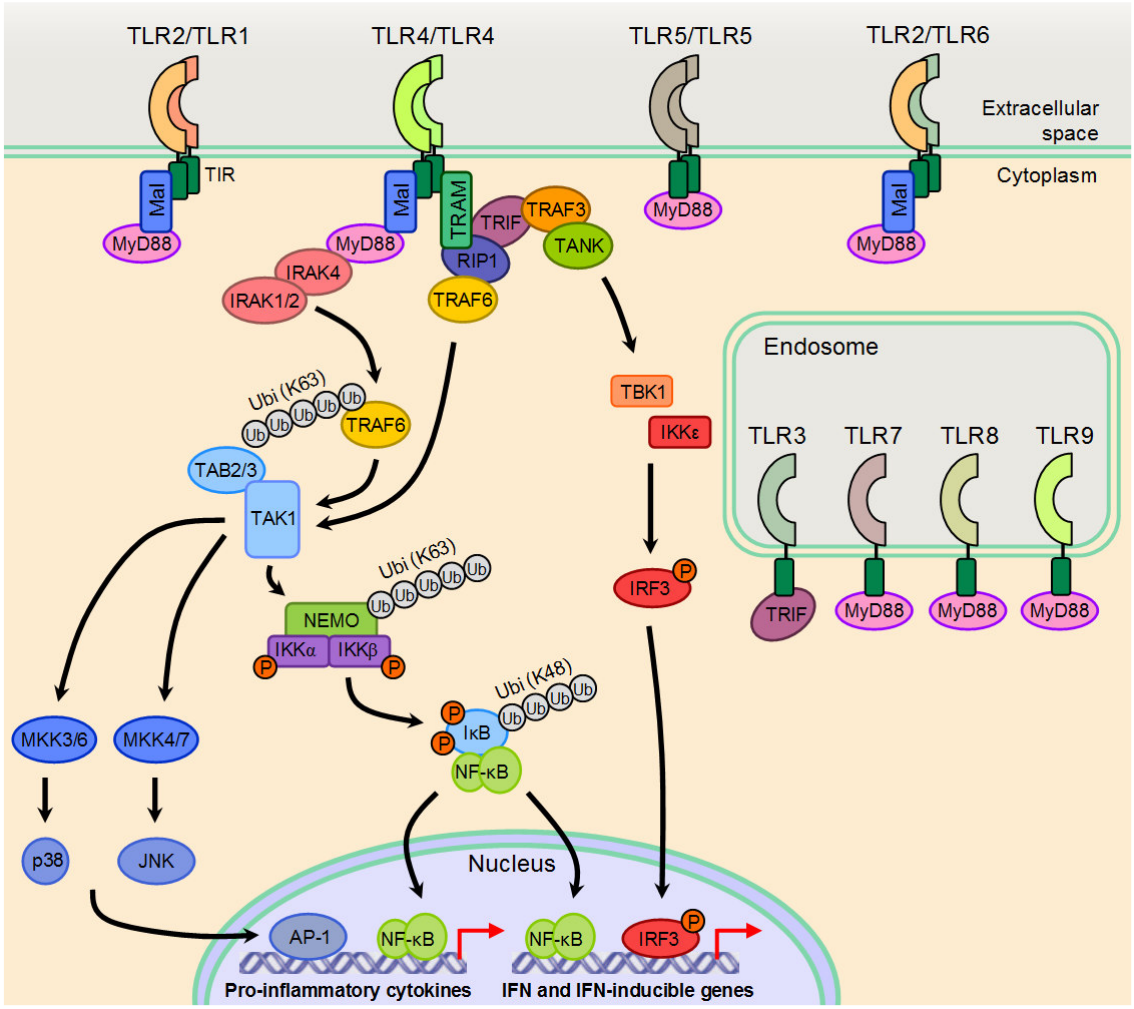


**Figure IA-3 TLR signaling**
Dimerization of TLRs induces the recruitment of TIR domain-containing adaptor molecules MyD88 (TLR5, TLR7, TLR8, TLR9), Mal and MyD88 (TLR2 and TLR4), TRIF (TLR3), or TRAM and TRIF (TLR4). The MyD88-dependent pathway leads to the recruitment of IRAK4, IRAK1 and IRAK2 and the ubiquitination of TRAF6, which activates TAK1. TAK1 in turn activates the IKK complex (NEMO, IKKα, IKKβ), leading to phosphorylation and degradation of the inhibitory IκB. The activated transcription factor NF-κB is translocated into the nucleus and induces the production of pro-inflammatory cytokines. TAK1 also triggers the activation of MKK proteins and the activation of transcription factor AP-1. The TRIF-dependent pathway involves the recruitment of TRAF3 and TANK, following the activation of the IKK-related kinases TBK1 and IKKε. The kinases directly phosphorylate the transcription factors IRF3 and IRF7, which are translocated into the nucleus to activate the expression of type-I interferons. The TRIF-dependent pathway is further linked to NF-κB activation through recruitment and activation of TRAF6. (Adapted from: Mogensen, 2009)

The MyD88-dependent pathway culminates in the activation of NF-κB and the production of pro-inflammatory cytokines. The pathway involves i) “IL-1-receptor-associated kinases” (IRAKs), ii) the ubiquitin-protein ligase “tumour-necrosis-factor-receptor-associated factor 6” (TRAF6), that generates Lys63-linked polyubiquitin chains on itself, iii) the “transforming growth factor-activated protein kinase 1” (TAK1) and iv) “NF-κB-essential modulator” (NEMO) (Mogensen, 2009). NEMO forms part of v) the “ ‘inhibitor of nuclear factor-κB’ (IκB)-kinase” (IKK) complex together with the

proteins IKK-α and IKK-β. IKK is activated and site-specifically phosphorylates vi) IκB releasing vii) NF-κB which translocates to the nucleus (Akira and Takeda, 2004; Hayden and Ghosh, 2008). In a second MyD88-dependent pathway, the activation of members of the " 'mitogen-activated protein kinase' (MAPK) kinase" (MKK) family leads to the phosphorylation and activation of p38 and ultimately to the activation of the "transcription factor activator protein 1" (AP1) (Chang and Karin, 2001).

The MyD88-independent, TRIF-dependent pathway triggers the expression of type I interferons (IFN) and IFN-inducible genes by phosphorylation and activation of the transcription factors "interferon regulatory factor 3" (IRF3) and IRF7 through IKK-related kinases " 'TRAF associated NFκB activator' (TANK)-binding kinase 1" (TBK1) and IKKε (Fitzgerald et al., 2003; Sharma et al., 2003). This pathway also cross-links with the NF-κB signaling by recruitment of TRAF6, which leads to ubiquitination and activation of TAK1 and subsequent activation of the IKK complex (Sato et al., 2003).

In addition to pathways activating the cellular immune response, it appears that at least TLR2, TLR3 and TLR4 can induce apoptosis by activating death signaling pathways (Aliprantis et al., 1999; Gay and Gangloff, 2007; Kaiser and Offermann, 2005).

The complexity of TLR-induced signaling requires precise regulation as the excessive or erroneous activation of pathways can lead to severe disease. TLR4 signaling is correspondingly controlled by the two competing adaptor protein pairs MAL/MyD88 and TRAM/TRIF, involved in two independent but sequentially activated pathways regulated by the endocytosis of the TLR4 complex (Kagan et al., 2008). Apparently TLR4 in the plasma membrane induces MAL/MyD88 signaling while TLR4 endocytosis activates TRAM/TRIF signaling (Kagan et al., 2008).

Negative regulation of TLR-dependent signaling was observed by the TIR adaptor "sterile alpha- and armadillo motif-containing protein" (SARM) that competes with TRIF-dependent signaling in human cells (Carty et al., 2006). "Suppressor of cytokine signaling 1" (SOCS1) mediates the degradation of the TIR adaptor MAL and is thus a negative regulator of TLR2 and TLR4 pathways (Mansell et al., 2006). Further negative regulation by competition, degradation or deubiquitination include the IRF-3-controlling "prolyl isomerase 1" (Pin1), the protein A20 which removes Lys63-linked

polyubiquitin chains from TRAF6, and the formation of heterodimers of MyD88 with the splice variant MyD88s, which can no longer phosphorylate IRAK-1 or interact with IRAK-4 (Wang et al., 2009).

## IA.4 The molecular basis of recognition by TLRs

### IA.4.1 The extracellular LRR domain

TLRs are type-I membrane proteins, in which a single transmembrane α-helix connects the extracellular (endosomal) ligand-binding domain with the cytosolic TIR domain. The extracellular domain (ECD) of TLRs is composed of 16-28 consecutive LRR units forming a curved horseshoe-like shape (Matsushima et al., 2007).

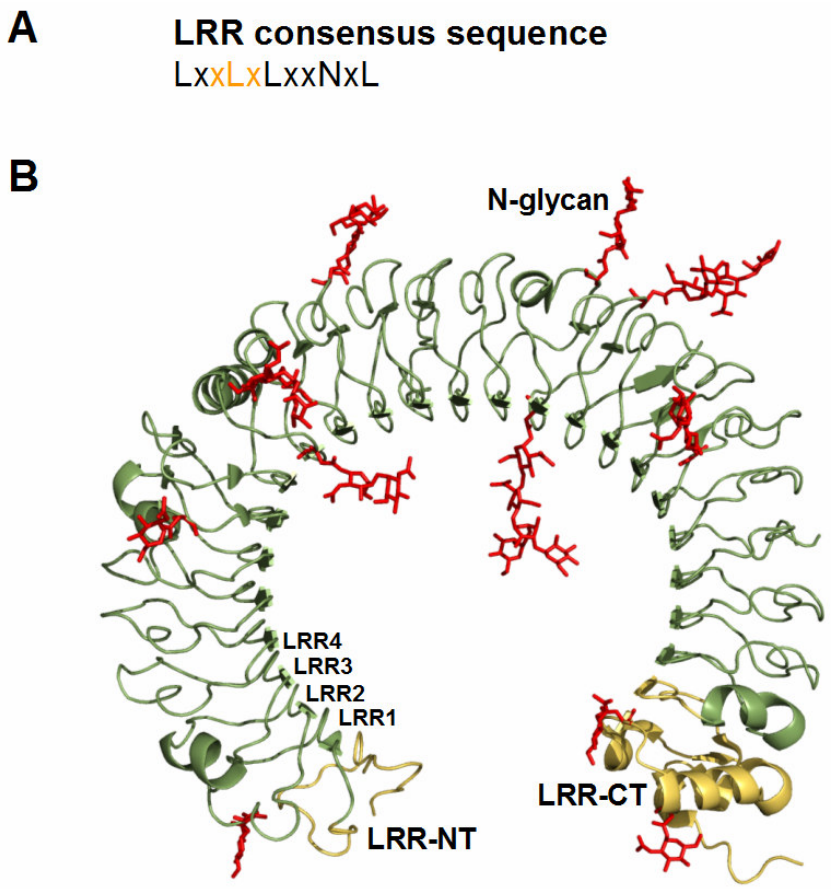


**Figure IA-4 The structure of the extracellular domain of TLRs**
**(A)** The LRR consensus sequence for TLRs. The residues xLx (yellow) form a β-strand that aligns with that of neighboring LRRs. **(B)** Extracellular domain of TLRs using the example of TLR3 (Liu et al., 2008a), with N-linked glycosylation and LRR-NT and LRR-CT capping regions. For a detailed description of structural features, see the text below.

LRRs generally generate right-handed helical or solenoid structures in which each repeat adds one turn to the solenoid. Each LRR may be considered as consisting of a conserved and a variable region, where the conserved elements entail the motif LxxLxLxxNxL (L, hydrophobic aa; N, polar uncharged aa; x any aa), the residues xLx at positions 3 through 5 of which form a β-strand that aligns with that of neighboring repeats to generate a parallel β-sheet (Matsushima et al., 2007) (Figure IA-4, A). The variable parts either form an α-helix, a $3_{10}$-helix or an extended structure (depending on its length) plus loops on either side connecting it with the β-strands. Conserved, hydrophobic (mostly aliphatic) residues as well as conserved asparagines point to the interior forming a stable hydrophobic core, while non-conserved residues face the exterior (Kajava, 1998; Kobe and Kajava, 2001). Because β-strands of each LRR are narrower than the helices, LRR domains adopt a curved conformation, in which the β-sheet forms the concave surface and the non-β portions form the convex surface (Botos et al., 2011; Kajava, 1998) (Figure IA-4, B).

The LRR domain of TLRs is protected N- and C-terminally by two small capping modules denoted LRR-NT and LRR-CT domains. In TLRs these contain disulfide bridges and shield the hydrophobic LRR core from the hydrophilic solvent (Jin and Lee, 2008b) (Figure IA-4, B).

### IA.4.2 TLR crystal structures

The first crystal structure of an TLR-ECD was that of human TLR3 (Bell et al., 2005; Choe et al., 2005). In total, five TLR/ligand complexes have been crystallized and their structures solved to date. Complexes include TLR1/TLR2/$Pam_3CSK_4$ (Jin et al., 2007), TLR4/MD-2/LPS (Kim et al., 2007; Park et al., 2009), TLR3/dsRNA (Liu et al., 2008a), TLR2/TLR6/$Pam_2CSK_4$ (Kang et al., 2009), and TLR5/flagellin (Yoon et al., 2012). All structures reveal the typical horseshoe-like shape. They can, however, not be superimposed due to variations in curvature (Figure IA-5).

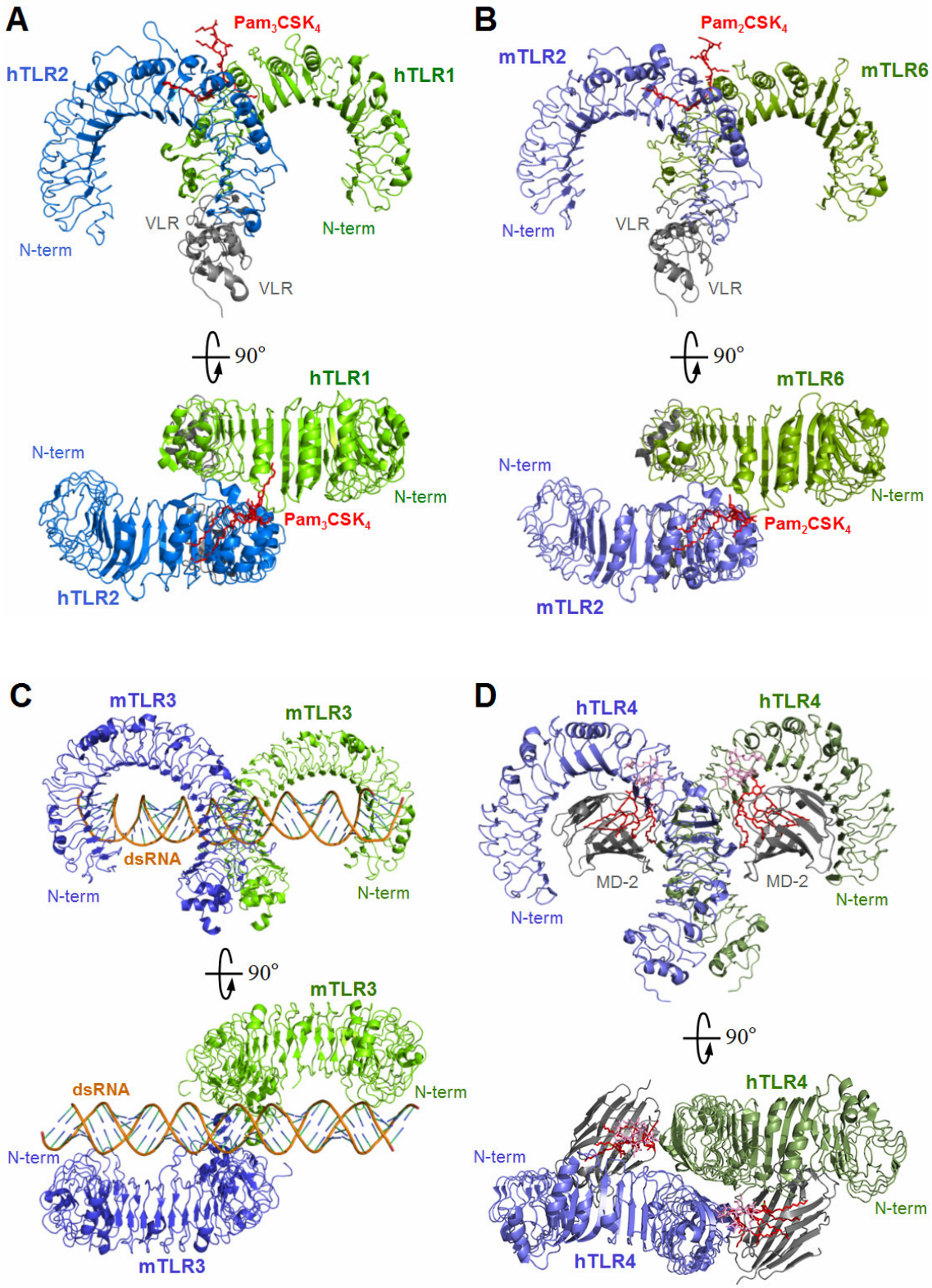
A
Pam3CSK4
hTLR2
hTLR1
VLR
N-term
N-term
VLR
90°
hTLR1
N-term
N-term
Pam3CSK4
hTLR2
B
Pam2CSK4
mTLR2
mTLR6
N-term
VLR
VLR
90°
mTLR6
N-term
N-term
Pam2CSK4
mTLR2
C
mTLR3
mTLR3
dsRNA
N-term
N-term
90°
mTLR3
dsRNA
N-term
N-term
mTLR3
D
hTLR4
hTLR4
MD-2
MD-2
N-term
N-term
90°
hTLR4
N-term
N-term
hTLR4

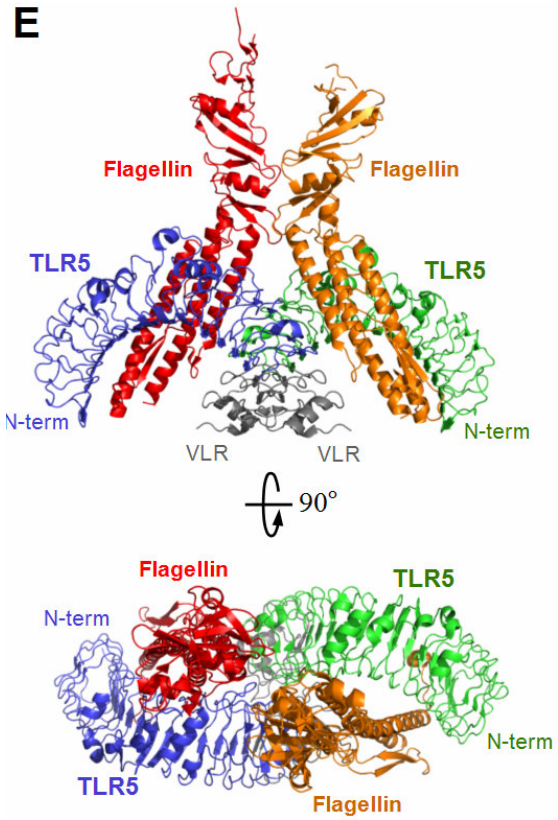


**Figure IA-5 TLR-ligand structures**
Side and top views of **(A)** TLR2/TLR1/$Pam_3CSK_4$ (Jin et al., 2007) and **(B)** TLR2/TLR6/$Pam_2CSK_4$ (Kang et al., 2009). C-terminal domains of TLR1, TLR2 and TLR6 were replaced by hagfish VLR domains (highlighted in grey) to promote crystallization. **(C)** TLR3/dsRNA (Liu et al., 2008a), **(D)** TLR4/MD-2/LPS (Park et al., 2009). The lipid A component of LPS is colored red and the inner core carbohydrates of LPS is colored pink. **(E)** TLR5/flagellin (Yoon et al., 2012). C-terminal domain of TLR5 was replaced by hagfish VLR domain (highlighted in grey) to promote crystallization. In all TLR complexes ligand binding induces TLR dimerization in the C-terminal regions.

The LRR motifs constitute a rigid yet adaptable scaffold for the formation of TLR/ligand interactions. Whereas most LRR proteins bind ligands through their concave surfaces, ligand interaction in TLRs mainly occurs on the ascending lateral surface (Botos et al., 2011), but can involve the concave (TLR4, TLR5) as well as the convex (TLR2/TLR1, TLR2/TLR6, TLR4) surface (Figure IA-5). Hydrophobic (TLR1, TLR2, TLR3 and TLR6) as well as polar interactions (TLR3-dsRNA, TLR5) are developed during ligand interaction (Jin et al., 2007; Liu et al., 2008a).

### IA.4.3 Ligand binding induces dimerization and signal transduction

Ligand binding to the lateral surface of TLRs results in dimerization of the extracellular domains (Figure IA-5). In the TLR2/TLR1 and TLR2/TLR6 complexes, direct protein-protein interactions occur in the central LRRs involving residues immediately adjacent

to the ligand binding pockets. In the TLR3/dsRNA complex, by contrast, TLR3/TLR3 interactions occur only at the LRR-CT (Botos et al., 2011). In the TLR4/MD-2/LPS complex, the adaptor protein together with the LPS mediates the receptor interaction (Park et al., 2009). In the TLR5/flagellin complex, the flagellin domain is located on the lateral side of TLR5, forming a 1:1 heterodimer. Two heterodimers further oligomerize to a symmetric 2:2 complex (Yoon et al., 2012). The fact that ligand interaction involves the lateral surface of the TLRs in all known TLR/ligand structures is corroborated by the observation that this surface is the only part of the molecule that is not N-glycosylated leaving it free for protein-protein and protein-ligand interaction (Botos et al., 2011).

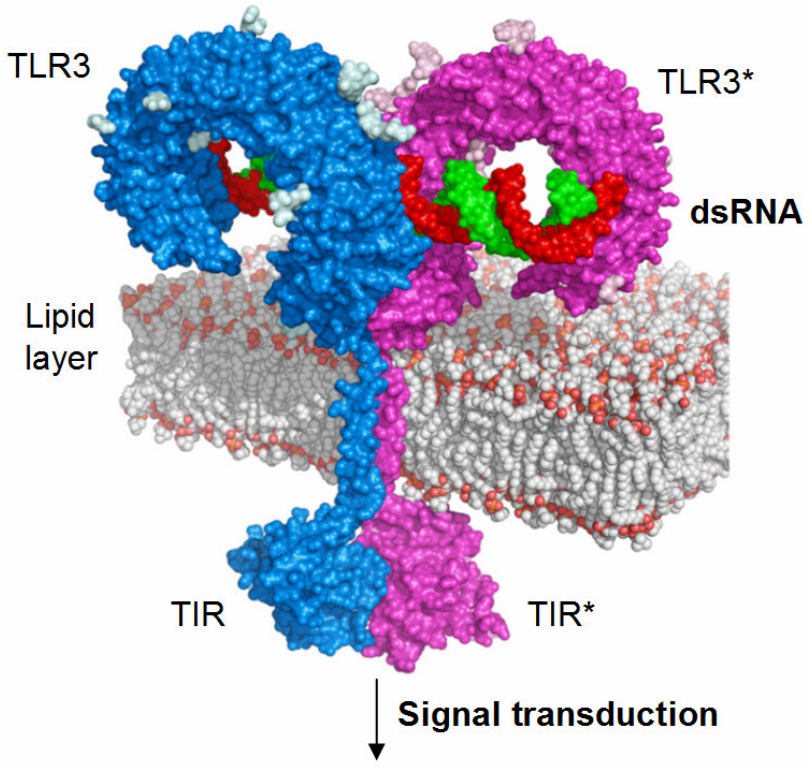


**Figure IA-6 Dimerization triggers signal transduction**
Structural model of full length TLR3/dsRNA complex. The model is based on the TLR3/dsRNA structure (Liu et al., 2008a) and a TLR3 TIR domain homology model based on the TLR10 TIR structure (Nyman et al., 2008). The membrane portions have been modeled as α-helices. (Source: Botos *et al.*, 2011).

Ligand-induced TLR dimerization invariantly results in the C-terminal regions being placed in close physical proximity (Figure IA-5). This then allows for the alignment of the transmembrane α-helices and for the dimerization of the cytoplasmic TIR domains (Figure IA-6). This in turn triggers the activation of the signaling cascades.

## IA.5 Toll-like receptor 2: A promising drug target

All TLRs are potential therapeutic targets in that i) they are overexpressed in certain diseases, ii) corresponding knockout mice are resistant to these diseases, iii) ligands exacerbate inflammation in disease models and iv) genetic differences in TLRs correlate with risk of disease (Hennessy et al., 2010). Furthermore, TLRs operate in an early stage of inflammation signaling and might therefore be preferred for modulation.

TLR2 is by far the most intensively studied member of the family. It is expressed on a large variety of human cell types, and recognizes a wide array of ligands more than any other member of the TLR family and not restricted to diacylated and triacylated lipopeptides for which crystal structures have been solved (Figure IA-5). Ligands include peptidoglycan (PGN) and lipoteichoic acid (LTA) from Gram-positive bacteria (Mitsuzawa et al., 2001), lipoarabinomannan from mycobacteria (Underhill et al., 1999), Zymosan from fungi; lipopolysaccharides (LPS) from spirochetes (Werts et al., 2001), hemagglutinin protein from measles virus (Bieback et al., 2002), and others (Chang, 2010; Gay and Gangloff, 2007). Known endogenous damage signals amongst others are HSP60 (Prakken et al., 1997), HSP70 (Asea et al., 2002), gp96 (Huang et al., 2009), and HMGB1 (Huang and Pope, 2010) (see also Table IA-1 and Table IA-2).

The complexity of ligand recognition and activation and inactivation of signaling pathways presumes a precise regulation, but the mechanisms are not yet fully understood. It is known that uncontrolled or disregulated activation of TLR2 can cause severe diseases in humans. TLR2 antagonists as well as agonists are currently in development to treat various human diseases and especially TLR structures in complex with their ligands can contribute to rationally design TLR drugs (Hennessy et al., 2010).

### IA.5.1 TLR2-related diseases

The detection of microbial and endogenous products by TLR2 and other TLRs induces the release of large amounts of inflammatory cytokines and chemokines, such as TNF-α, IL-1β and IL-6. A corresponding hyperactivation of immune cells by bacteria through TLR2 stimulation can lead to septic shock pathology, clinically characterized by abnormal coagulation, profound hypotension, and organ failure (Cohen, 2002;

Hotchkiss and Karl, 2003; Meng et al., 2004). Ulcerative colitis, a form of inflammatory bowel diseases (IBDs), is associated with a Arg753Gly polymorphism of TLR2 (Pierik et al., 2006) and causes chronic intestinal inflammation induced by the commensal flora (Fukata et al., 2009) (Figure IA-8, C).

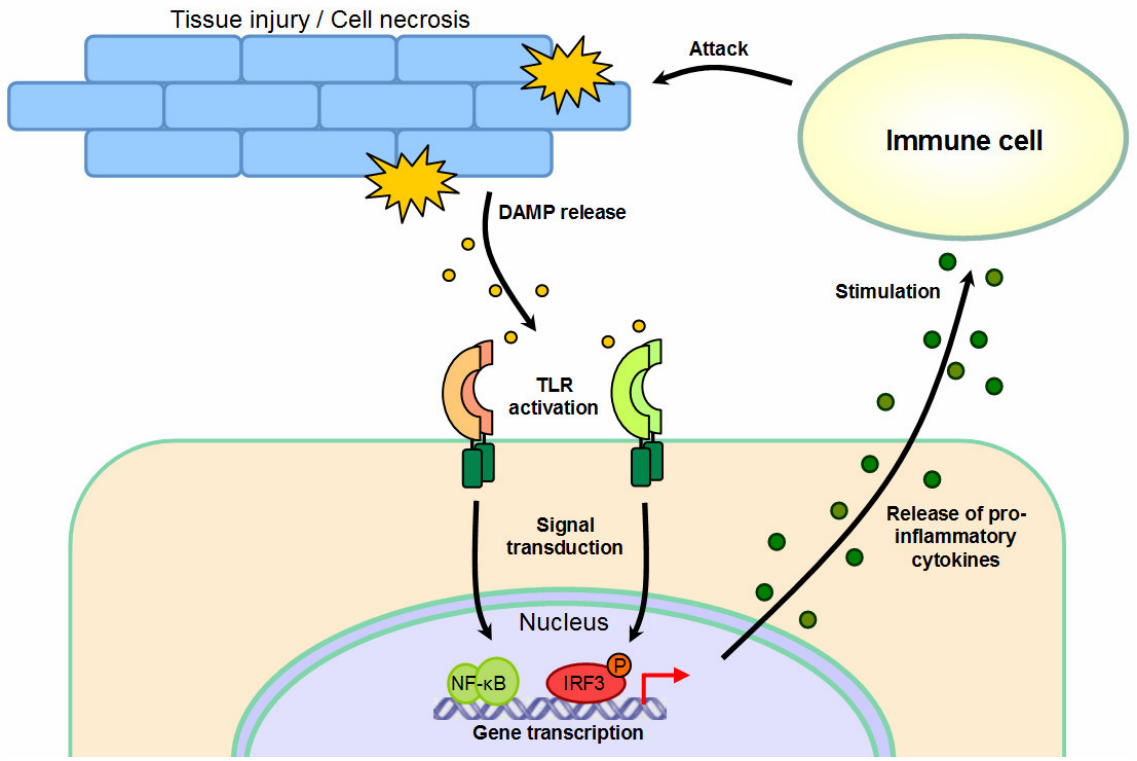


**Figure IA-7 DAMP-mediated vicious inflammation cycle**
DAMPs released from injured tissue activate TLRs and leads to the induction of intracellular signaling cascades, the activation of transcription factors and the production of pro-inflammatory cytokines. The mediators stimulate and recruit more immune cells that lead to further cell necrosis, which in turn releases more DAMPs.

Likewise, the recognition of DAMPs released from inflamed tissues can lead to chronic inflammation, caused by a self-promoting cycle in which more inflammatory mediators are generated, leading to further activation of TLRs (Hennessy et al., 2010) (Figure IA-7). TLR2- and TLR4-derived chronic inflammation can cause rheumatoid arthritis (RA) in synovial joints leading to destruction of cartilage and bone (Goh and Midwood, 2011) (Figure IA-8, B). Potentially an initial microbial infection or trauma induces tissue damage causing the release of endogenous TLR ligands and starting the cycle of inflammation (Santegoets et al., 2011). Examples of identified TLR2-dependent endogenous ligands involved in RA are biglycan and gp96 (Huang and Pope, 2010; Piccinini and Midwood, 2010).

The autoimmune disease systemic lupus erythematosus (SLE) is characterized by the destruction of organ tissue of the human body including skin, kidneys, joints and the central nervous system through autoantibodies (Figure IA-8, A). In SLE patients with impaired apoptotic cell clearance, the release of HMGB1 induces autoantibody production in a TLR2-dependent manner (Urbonaviciute et al., 2008).

TLR2 is also involved in the development of atherosclerosis, a chronic inflammatory disease of arteries that results in the formation of plaque and blood-vessel narrowing (Figure IA-8, D). This can culminate in thrombosis and occlusion, resulting in a myocardial infarction or stroke (Huang and Pope, 2010). Transfection of carotid arteries of rabbits with cDNA encoding TLR2 or TLR4 induced atherosclerosis (Shinohara et al., 2007), and TLR2$^{-/-}$ mice exhibited decreased atherosclerotic plaques and decreased numbers of macrophages (Liu et al., 2008b).

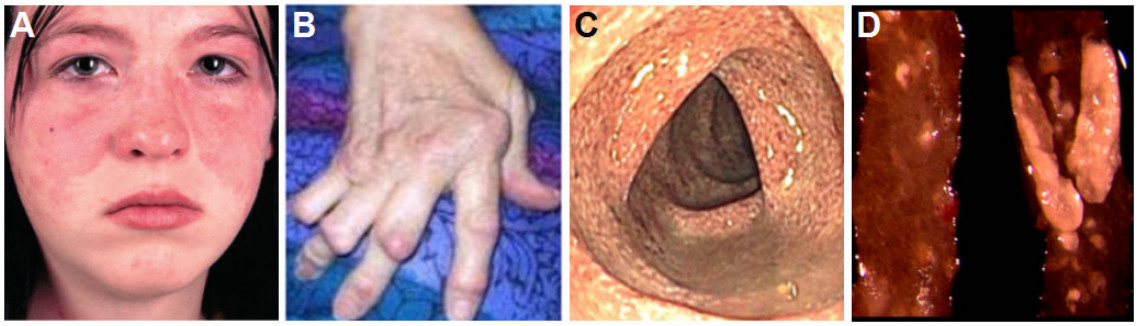


**Figure IA-8 Medical signs associated with TLR2-related diseases**
**(A)** The typical "butterfly rash" found in systemic lupus erythematosus. **(B)** Deformations of the hand caused by rheumatoid arthritis. **(C)** Ulcerative colitis of the transverse colon with granularity and friability of the mucosa. **(D)** Lesions in aorta of murine model of atherosclerosis. (Sources: (A) http://trialx.com/curebyte/2011/06/01/ (B) http://nihseniorhealth.gov/rheumatoidarthritis/toc.html (C) Fukata *et al.*, 2009 (D) http://www.bcm.edu/mcb/?PMID=8876

TLR2 is crucial in the development of ischemia/reperfusion (I/R) injury, a disease characterized by inflammatory tissue damage caused by reperfusion (restoration of blood flow) to a tissue after a period of ischemia (restriction in blood supply). It is associated with trauma, stroke, myocardial infarction, and solid organ transplantation (Arslan et al., 2010a). I/R injury after myocardial infarction increases infarct size (Arslan et al., 2010b) whereas it leads to acute kidney injury after renal transplantation (Farrar et al., 2011). HSP70-dependent TLR2 activation was observed in cardiomyocytes (Mathur et al., 2011) resulting in decreased cardiomyocyte contractility (Boyd et al., 2006). *Ex vivo* experiments with TLR2-knockout (TLR2$^{-/-}$) hearts

increased heart performance in comparison to wild-type hearts after myocardial I/R injury (Sakata et al., 2007). Furthermore TLR2$^{-/-}$ mice are protected against endothelial dysfunction after myocardial I/R injury (Favre et al., 2007). Renal inflammation increases TLR2 and TLR4 expression in epithelium, thin limb and collecting ducts (Wolfs et al., 2002). However, renal I/R injury was reduced in TLR2$^{-/-}$ mice (Leemans et al., 2005). Likewise, the amount of brain damage and neurological deficits caused by a stroke were significantly less in mice deficient in TLR2 or -4 compared with WT control mice (Tang et al., 2007). TLR2 is also involved in lung diseases, such as asthma (Kovach and Standiford, 2011). More recently, TLR2 was identified as a primary receptor triggering neuroinflammation through Alzheimer-associated amyloid β peptide recognition (Liu et al., 2011).

### IA.5.2 TLR2 agonists

Immunostimulatory TLR agonists can be used to induce a strong pro-inflammatory response in treating acute viral and bacterial infection (Hennessy et al., 2010). Several compounds, mainly small DNA or RNA fragments against TLR7, TLR8 and TLR9 are currently in clinical trials. Alternatively, TLR agonists are used to stimulate immune response in advanced stages of cancer to induce apoptosis of chemotherapy-resistant cancer cells. SMP-105, a drug with strong antitumor activities, consists of cell wall skeleton compounds of *Mycobacterium bovis* and was proven to enhance TLR2-dependent immune response, such as the number of interferon-γ-producing cells and cytotoxic T lymphocytes, leading to reduced tumor growth (Murata, 2008). SMP-105 is currently in preclinical trials for the treatment of bladder cancer.

## IA.6 Antagonistic antibody inhibits TLR2 signaling

The development of TLR2 antagonists to inhibit cytokine production during inflammation and autoimmunity diseases has become a major interest. One very promising candidate is the TLR2 specific monoclonal antibody OPN-305, a humanized version of the mouse IgG OPN-301 (also known as T2.5) based on a human IgG framework. The antibody was originally found to inhibit lipopeptide, PGN, LTA and heat inactivated *Bacillus subtilis* induced TNF-α production in HEK293 and murine RAW264.7 and primary macrophages, and thus to suppress septic shock in mice (Meng

G, 2004). The antibody cross-reacts with other TLR2s including human, pig and cynomolgus monkey TLR2, indicating that it is specific for a critical epitope yet conserved (Arslan et al., 2010b).

Several results have shown that TLR2 inhibition with OPN-301 effectively reduces myocardial I/R injury and preserves cardiac function and geometry *in vivo* in mice. It thus has the potential as an effective treatment for patients with acute myocardial infarction (Arslan et al., 2010b). OPN-301 also provides significant protection from I/R injury in a murine model of kidney transplantation (Farrar et al., 2011). The antibody prevents pro-inflammatory cytokine release in RA tissue synovial explant cultures *ex vivo* (Ultaigh et al., 2011) and in a sepsis model in mice (Farrar et al., 2011). OPN-305 was granted orphan status for the prevention of the I/R injury associated with organ transplantation and is currently tested in human trials.

# IB Producing mouse/human Toll-like receptors 2 and 6 in insect cells using the baculovirus expression system

In the past years increasingly more exogenous and endogenous TLR and especially TLR2 ligands have been identified (Table IA-1, Table IA-2). These ligands originate from taxonomically unrelated organisms and differ fundamentally in their structures. The first crystal structures of lipopeptides-bound TLR2/TLR1 and TLR2/TLR6 complexes provide a first detailed structural insight into ligand recognition by TLR2 complexes. However, this milestone is best regarded as a start rather than the end of understanding TLR2 and other TLRs with regard to their ability to distinguish and respond to such a diversity of molecules. The epitopes of other TLR2 ligands and their mode of recognition are still unknown, but there is evidence that further accessory molecules and co-receptors are necessary for PAMP and DAMP recognition, which directly bind to the TLR and/or the ligand.

## IB.1 TLR1/TLR2 and TLR2/TLR6 in complex with lipopeptides

TLR1 and TLR6 share a high degree of sequence similarity and tandem arrangement in the human genome, indicative of a fairly recent gene duplication event (Roach et al., 2005). Together with TLR2 they form a phylogenetically related subfamily (Chang, 2010). TLR2 in complex with TLR1 or TLR6 is essential for the recognition of bacterial lipoproteins and lipopeptides (Figure IB-1). These molecules are embedded with their lipid chains (acyl groups) in cell walls and membranes of a variety of microorganisms and trigger the immune response via TLR2/TLR1 and TLR2/TLR6 heterodimers (Takeda et al., 2002). Lipidated peptides/proteins are mostly triacylated bearing three lipid chains connected to the N-terminal cysteine of an amino acid chain. Mycoplasmal lipopeptides, by contrast, are only diacylated (Takeuchi et al., 2001). In triacylated lipopeptides a diglyceride or diacylated glycerol is bound to the N-terminal cysteine side-chain by a thioether bond while a third fatty acid is bound to the amino group of the same cysteine by an amide link. Diacylated lipopeptides like mycoplasmal “macrophage-activating lipopeptide-2 kDa” (MALP-2) lack the nitrogen bound fatty acid (Mühlradt et al., 1997).

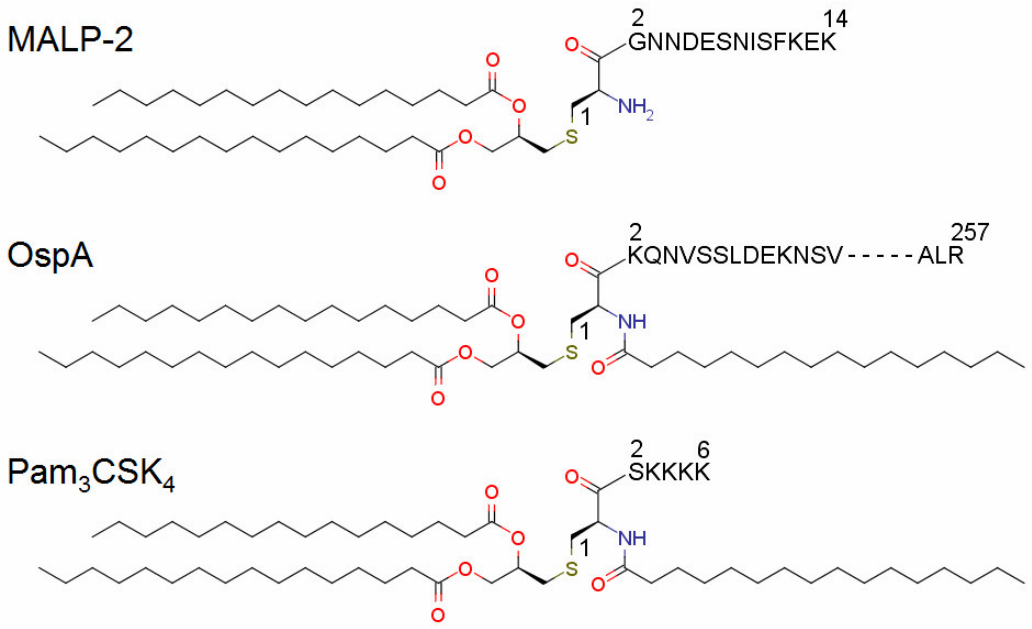


**Figure IB-1 Chemical structures of lipopeptides**
Chemical structures of the diacylated lipopeptide MALP-2, the triacylated lipopeptides "outer surface protein A" (OspA) of *B. burgdorferi* and the synthetic lipopeptide $Pam_3CSK_4$.

Triacylated lipopeptides are recognized by the complex of TLR2/TLR1, diacetylated lipopeptides by TLR2/TLR6 (Botos et al., 2011). TLR1 and TLR6 are therefore crucial in distinguishing tri- and diacylated lipopeptides and lipoproteins. Synthetic lipopeptides from which most amino acid residues have been removed still cause inflammation (Berg et al., 1994; Bessler et al., 1985; Seifert et al., 1990) implying that merely the acylated N-terminal cysteine is critical for recognition by TLRs. This was confirmed by the crystal structures of TLR2/TLR1/$Pam_3CSK_4$ (Jin et al., 2007) and TLR2/TLR6/$Pam_2CSK_4$ (Kang et al., 2009). In TLR6 the lipid channel that accommodates the third aliphatic chain of triacylated lipopeptides in TLR1 is blocked by two phenylalanines restricting TLR6 to diacylated lipopeptides (Figure IB-2).

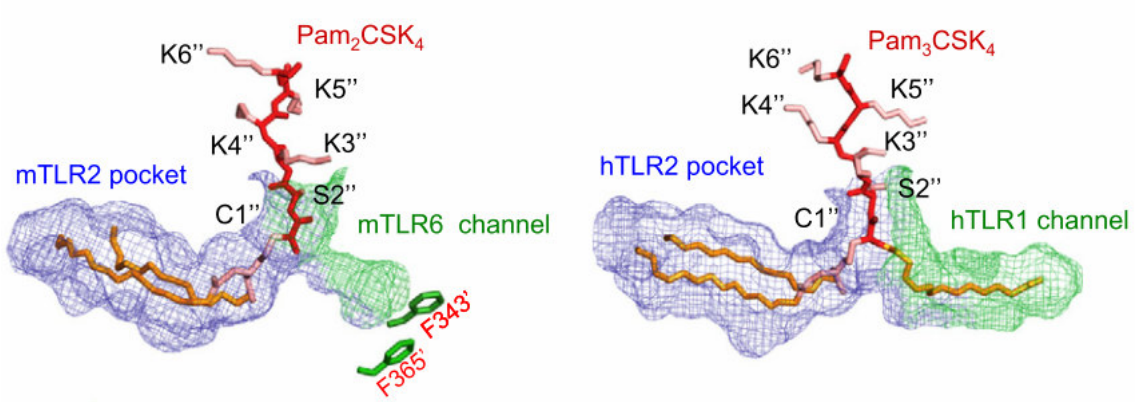


**Figure IB-2 Distinction of di- and triacylated lipopeptides by TLR1 and TLR6**
$Pam_2CSK_4$ binding pocket in the TLR2/TLR6 complex (left) and $Pam_3CSK_4$ binding pocket in the TLR2/TLR1 complex (right). The TLR6 channel is blocked by the two phenylalanines F343 and F365 and therefore inaccessible for a lipid chain. (Source: Kang *et al.*, 2009)

## IB.2 TLR2 accessory molecules and co-receptors

Lipopeptide recognition by TLR2/TLR1 and TLR2/TLR6 complexes is enhanced by accessory molecules. CD14 was identified as a sensor molecule of triacylated lipopeptides (Nakata et al., 2006) whereas CD36 adopts this function for diacylated lipopeptides (Hoebe et al., 2005) facilitating ligand recognition by TLR2/TLR1 and TLR2/TLR6, respectively.

TLR2 appears to require the help of PRR dectin-1 to recognize the fungal component zymosan (Gantner et al., 2003) whereas “macrophage receptor with collagenous structure” (MARCO) and CD14 are essential to bind the cell wall glycolipid TDM from *Mycobacterium tuberculosis* (Bowdish et al., 2009). Similarly, CD14 and MD-2 are essential for DAMP recognition by TLR2 (Piccinini and Midwood, 2010).

# IC Aims of this work

## IC.1 Inhibition of mTLR2 with a monoclonal antibody

The monoclonal antibody OPN-305 has previously been shown to efficiently inhibit the immune receptor TLR2, downstream cytokine release and hence the TLR2-mediated immune response. OPN-305 has successfully been used to treat chronic inflammatory diseases such as RA and I/R injury *in vitro* and *in vivo*, and the antibody is on its way to market authorization as a therapeutic drug. However, the mechanism of TLR2 inhibition by OPN-305 and its epitope is still unknown. The aim of this project was therefore to use structural methods such as crystallography and electron microscopy to provide structural information on the TLR2/OPN-305 complex so as to explain TLR2 silencing by OPN-305. For that purpose protocols for the purification of TLR2 and antibody as well as for the purification of the TLR2/Fab complex had to be established to obtain protein in amounts and degrees of purity suitable for crystallization and EM trials. Prior to antibody purification, antibody Fab fragments had to be generated by proteolytic cleavage. The crystallization conditions had to be modulated to improve crystal growth and quality. Furthermore, as TLR2 is a glycoprotein, the impact of glycosylation on crystallization had to be analyzed. In case of a successful structure determination of the TLR2/Fab structure, functional studies were to be performed to unravel the mechanism of TLR2 inhibition by OPN-305. Furthermore the novel structural information was to be compared to other TLR2 complex structures and published literature on TLR2 to fully analyze the structure.

## IC.2 Producing mouse/human Toll-like Receptors 2 and 6 in insect cells using the Baculoviral Expression System

The only established expression clone of a TLR available in the department at the beginning of the work was a mTLR2 ECD construct with a C-terminal $His_6$-tag previously used for antibody interaction experiments described in part IA. The first aim of this project was to design and generate new recombinant constructs to produce murine and human TLR2 and TLR6 ECDs. An optimized purification strategy with cleavable C-terminally fused, highly specific Fc-tag was to be established to improve

the speed, yield and reproducibility of purification. Furthermore, the signal peptide was to be replaced to increase the secretion rate of the protein. As previous attempts to produce TLR2 and TLR6 in bacterial expression systems had not been successful, protein production was to be planned for eukaryotic expression systems such as insect cells using the baculovirus expression system. For this purpose, gene constructs had to be cloned into the vector pFastbac following the production of the baculovirus-DNA and transfection into Sf21 insect cells to produce virus containing the TLR gene constructs. A virus production protocol had to be established, and the amplified virus was to be used to infect insect cell cultures to start the production of the recombinant target protein. After successful protein production, expression tests had to be performed to analyze the quality and quantity of protein production.

Initially it was planned to use produced and purified TLR2 and TLR6 for crystallization in complex with MALP-2 to get a closer insight into the mechanism of lipopeptide recognition by TLRs. However, this aim was superseded when the crystal structure of the complex of TLR2, TLR6 and the synthetic lipopeptide $Pam_2CSK_4$ was published. However, as TLR2 plays a pivotal role not only in the recognition of bacterial lipopeptides but also of many other ligands such as peptidoglycan and zymosan (see Table IA-1), and as other studies reveal that TLR2 needs other distinct co-receptors and accessory molecules for full efficacy to deal with the breadth of the ligand repertoire, recombinant production of TLR2 and TLR6 and other TLRs still remain an important prerequisite for the investigation of TLR interactions and structural analysis. Moreover, TLR2 and TLR6 can be used in studies to analyze the influence of antibody OPN-305 on complex formation and/or ligand binding.

# II Material and Methods

## IIA Standard materials

### IIA.1 Chemicals, enzymes, kits and standards

If not stated otherwise, all chemicals used in this work were purchased in "*pro analysis*" grade from the following companies: Difco, Fermentas, Fluka, GE-Healthcare, Hampton Research, Invitrogen, Macherey-Nagel, Merck, Millipore, Promega, Qiagen, Roche, Roth, Sigma-Aldrich and Stratagene.

**Table IIA-1 Enzymes**

| Enzyme | Source |
|---|---|
| DNAse I | Roche |
| Lysozyme | Fluka |
| Papain | Roche |
| Platinum Pfx DNA Polymerase | Invitrogen |
| PNGase F | New England Biolabs |
| PreScission protease | UWC |
| Lysozyme | Fluka |
| Restriction endonucleases: BamHI, BglII, HindIII, NdeI, NheI, XhoI | Fermentas |
| T4 DNA Ligase | Roche |
| TEV protease | HZI |

**Table IIA-2 Kits**

| Name | Company |
|---|---|
| GeneJET Gel Extraction Kit | Fermentas |
| GeneJET DNA Purification Kit | Fermentas |
| GeneJET Plasmid Miniprep Kit | Fermentas |
| GeneJET Plasmid Maxiprep Kit | Fermentas |

**Table IIA-3 Molecular weight standards**

| Name | Usage | Company |
|---|---|---|
| PageRuler Unstained Ladder | SDS-PAGE | Fermentas |
| Precision Plus Protein All Blue Standard | SDS-PAGE/Western Blot | BioRad |
| Smart Ladder | Agarose gel electrophoresis | Eurogentec |
| Unstained Protein Molecular Weight Marker | SDS-PAGE | Fermentas |

## IIA.2 Crystallization screens

To screen for crystallization conditions, the following commercial screens were used:

**Table IIA-4 Crystallization screens**

| Name | Company |
|---|---|
| $AmSO_4$ Suite | |
| ComPAS Suite | |
| Cryos Suite | |
| JCSG Core I Suite | |
| JCSG Core II Suite | |
| JCSG Core II Suite | Qiagen |
| JCSG Core IV Suite | |
| JCSG Core+ Suite | |
| MPD Suite | |
| PACT Suite | |
| PEGs Suite | |
| PEGs II Suite | |
| Protein Complex Suite | |
| Additive Screen | Hampton Research Corp. |
| Pre-Crystallization Test | |

## IIA.3 Further reagents

**Table IIA-5 Further reagents**

| Name | Company |
|---|---|
| BugBuster Protein Extraction Reagent | Novagen |
| CytoBuster Protein Extraction Reagent | Novagen |
| “Complete” protease inhibitor tablets | Roche |
| Ni-NTA Agarose | Qiagen |

# IIB Inhibition of Toll-like receptor 2 with a monoclonal antibody

## IIB.1 Expression and purification of $mTLR2_{25\text{-}587}$-$His_6$

The extracellular domain of mTLR2 (aa 1-587) was recombinantly expressed with a C-terminal linked $His_6$-tag in Sf21 insect cells in a 6 L scale, and in CHO lec3.2.8.1 cells (Stanley, 1989; Wilke et al., 2010) in a 35 L scale (Dr. Joop van den Heuvel, HZI, Braunschweig, Germany). The native N-terminal signal peptide (aa 1-24) which led to

the secretion of the protein into the medium was cleaved by the cell own signal peptidase during translocation of the protein through the cell membrane. After 72 h the cells were removed by centrifugation and the supernatant was then filtered, concentrated (Sf21 cells: 10x, CHO cells: 20x) and dialyzed against 50 mM Tris pH 8, 500 mM NaCl, and 5% glycerol. 0.1% sodium azide was added to prevent bacterial and fungal growth. The shipment to South Africa was done at 4 °C and took 3-4 days.

Prior to purification a “Complete” protease inhibitor cocktail tablet, EDTA-free (Roche, Basel, Switzerland) was added to the protein solution and the sample centrifuged for 1 h at 16’500 rpm (Centrifuge RC6, Sorvall/Thermo Fisher Scientific, Massachusetts, USA). Initial purification was achieved by Ni-NTA chromatography (Qiagen, Hilden, Germany). The protein was immobilized and the column was washed with ~400 mL wash-buffer 1 (50 mM Tris pH 8, 300 mM NaCl, 10 mM imidazole) and ~75 mL wash-buffer 2 (50 mM Tris pH 8, 300 mM NaCl, 40 mM imidazole). $mTLR2_{25-587}$ was eluted by stepwise addition of elution buffer (50 mM Tris pH 8, 50 mM NaCl; imidazole steps: 100, 250, 500 mM). After elution, $mTLR2_{25-587}$ was diluted with 25 mM Tris pH 8, 25 mM NaCl to reach an imidazole concentration below 50 mM. The protein was then further purified by anion exchange chromatography (MonoQ HR10/10, GE Healthcare, UK). The protein was eluted using a salt gradient running from 80 to 200 mM NaCl during 25 column volumes. The pure protein (purity > 95 %) was concentrated to 2 mg/mL.

## IIB.2 Deglycosylation

For deglycosylation, 10 units of PNGase F (New England Biolabs, Massachusetts, USA) were utilized per 10 µg of $mTLR2_{25-587}$ and incubated for 15 h at room temperature in 50 mM Tris pH 8, 50 mM NaCl. The protein was either immediately used for complex formation or shock frozen in liquid nitrogen and stored at -80 °C.

## IIB.3 Papain digestion and purification of OPN-305

The antibody OPN-305 was provided by Opsona Therapeutics (Dublin, Ireland) in 10 mg/mL stocks in 25 mM sodium citrate pH 4.5 and 125 mM NaCl. The antibody was shock frozen in liquid $N_2$ and stored at -80 °C until usage. For papain cleavage of the

antibody, the enzyme was first activated by incubation in 100 mM Tris pH 8, 20 mM L-cysteine for 30 min at 37 °C, and the antibody buffer was exchanged by adding 100 mM Tris pH 8. Cleavage was initiated by mixing activated papain and antibody (mass ratio 1:20) and incubation for at least 8 h at 37 °C. Size exclusion chromatography (Superdex 200 16/60, GE Healthcare) with running buffer containing 50 mM Tris pH 8, 50 mM NaCl was performed to separate the fully cleaved antibody from incompletely cleaved molecules. Incompletely cleaved antibody was pooled and used as part of the next digestion. OPN-305 Fab fractions were concentrated and further purified performing a second run of size exclusion chromatography. OPN-305 Fab was stored at -80 °C after shock freezing in liquid $N_2$.

## IIB.4 Purification of the mTLR2$_{25-587}$/Fab complex

mTLR2$_{25-587}$ and OPN-305 Fab were mixed in a molar ratio of 1:2 and subjected to size exclusion chromatography (Superdex 200 16/60, GE Healthcare) using 25 mM Tris pH 8, 25 mM NaCl as running buffer. The complex fractions were diluted to 12 mM Tris pH 8, 12 mM NaCl with water and concentrated to 20 mg/mL prior to crystallization setups.

## IIB.5 SDS-polyacrylamide gel electrophoresis (SDS-PAGE)

Protein samples were analyzed by SDS-PAGE. This method separates proteins by an electric field dependent on their molecular weight. For this purpose proteins are denatured by incubation with a reducing agent and boiling. Proteins are further masked with the strongly negative charged substance sodium dodecyl sulphate (SDS) giving all proteins an almost equal charge to size ratio. This allows the separation by size through a porous, polymer matrix. During this discontinuous system (Laemmli, 1970) protein samples are first concentrated in a stacking gel before they are separated in a separating gel. The two gels differ in pH, ionic strength and pore dimension.

10 µL of protein sample were mixed with 3 µL of SDS-containing 8x sample buffer following incubation of the sample for 5 min at 96 °C to ensure complete denaturing. To prevent breaking of disulfide bridges that link heavy and light chain of antibodies, 8x sample buffer without the reducing agent β-mercaptoethanol was used in case of

samples containing OPN-305 antibody. The samples were applied to the stacking gel and the gel was run at constant 40 mM for 33 min. After the run the gel was stained for 15 min in staining solution and excess stain removed by incubation of the gel in destaining solution. Gels were air dried in framings between cellophane foil (BioRad, California, USA).

**12 % separating gel:**
12 mL acrylamide/bisacrylamide 30 % (w/v)/0.8 % (w/v)
7.6 mL 1.5 M Tris/HCl, pH 8.8
300 µL 10 % (w/v) SDS
10 mL $H_2O$
40 µL TEMED
100 µL 25 % (w/v) APS

**5 % stacking gel:**
1.5 mL acrylamide/bisacrylamide 30 % (w/v)/0.8 % (w/v)
2.5 mL 0.5 M Tris/HCl, pH 6.8
5.9 mL dd$H_2O$
15 µL TEMED
25 µL 25 % (w/v) APS

**8x sample buffer:**
16 mL 10 % SDS
4 mL glycerol
2.2 mL Tris/HCl, pH 6.8
800 µL β-mercaptoethanol
1 spatula tip bromophenol blue

**Staining solution:**
0.25 % (w/v) Coomassie Brilliant Blue R-250
30 % (v/v) ethanol
10 % (v/v) acetic acid

**Destaining solution:**
40 % (v/v) ethanol
10 % (v/v) acetic acid

## IIB.6 Native PAGE

The native PAGE was performed according to standard SDS-PAGE, but no SDS and reducing agent were used in the electrophoresis solutions and the gel to prevent denaturing of the proteins. The run was done on ice using a low voltage of 100 V to avoid overheating of the gel and thus denaturing of the proteins.

## IIB.7 Concentration of protein solutions

Protein samples of OPN-305, TLR2 and TLR2/Fab complex were concentrated by ultracentrifugation using Vivaspin-2, -6- and -20 concentrators (Sartorius, Göttingen, Germany) with a MW cut-off of 10 kDa. The absorption at 280 nm was measured during the process. Centrifugation was terminated once the desired protein concentration was reached (see IIB.8). If reduction of buffer or salt concentration of a sample was required, the concentrated protein solution was diluted with suitable buffer and re-concentrated to desired volume.

## IIB.8 Protein concentration quantification

Amino acids residues with aromatic side chains absorb UV light at a wavelength of 280 nm. The protein concentration in a sample were determined by measurement of the absorption at 280 nm ($A_{280}$) against the sample buffer using a Nanodrop ND-1000 spectrophotometer (peqLab, Erlangen, Germany). For concentration quantification after ultracentrifugation (see IIB.7), the flow through of the Vivaspin concentrators was used as reference solution. The molar extinction coefficient $\varepsilon_{280}$ for each protein was calculated *in silico* with the software VectorNTI (Invitrogen) from its amino acid composition.

According to the Beer-Lambert law

$$c = \frac{A_{280}}{\varepsilon \cdot d} \qquad \textbf{Equation IIB-1}$$

the concentration c can be calculated if the values for A, d, and ε are known. d is the thickness of the measuring chamber and defined by the Nanodrop design. Protein concentration of single proteins was only determined if the target protein was the main protein fraction in a solution with negligible contaminations, as this method cannot distinguish between different proteins in a mixture.

## IIB.9 Mass spectrometry

For electrospray ionization mass spectrometry (ESI-MS) of OPN-305 Fab, the sample buffer was desalted and exchanged to 10 mM ammonium acetate pH 5 using a PD-10

column (GE Healthcare). The sample was concentrated to 10.8 mg/mL (220 µM). Mass spectrometry was performed by Central Analytical Facilities (University of Stellenbosch, Bellville, South Africa).

## IIB.10 Modeling of OPN-305

The OPN-305 Fab heavy chain and light chain variable domains were modeled by 3D structure prediction using SWISS-Model (Arnold et al., 2006; Kiefer et al., 2009; Peitsch et al., 1995). Modeling is based on the comparison of the target sequence with structures in the Protein Data Bank (PDB). The pipeline automatically selects suitable templates based on a Blast (Altschul et al., 1997), the experimental quality of the templates, bound substrate molecules, or different conformational states of the template. Model quality is estimated by calculating global (the whole model) and local (individual residues) scores. The global scoring function QMEAN4 is a linear combination of four structural descriptors using statistical potentials: A torsion angle potential over three consecutive amino acids, two distance-dependent interaction potentials, and a solvation potential to investigate the burial status of the residues (Benkert et al., 2008). The quality estimate ranges between 0 and 1 with higher values for better models. In addition, a Z-score of the QMEAN4 provides a relation to scores obtained for high-resolution X-ray crystallography structures and represents a likelihood that the model is of comparable quality to experimental structures (Benkert et al., 2011). Models of low quality are expected to have strongly negative QMEAN Z-scores. The local score QMEAN is an estimate of the expected structural inaccuracy for each position in the model with small values corresponding to regions in the model being potentially more reliable. The local score ANOLEA calculates the atomic empirical mean force potential and is used to assess packing quality of the models (Melo and Feytmans, 1998). Energy calculations on the amino acid chain are performed to evaluate the "Non-Local Environment" of the atoms in the molecule and are displayed in a plot representing the energy for each amino acid of the protein chain. Negative energy values (in green) represent favorable energy environment whereas positive values (in red) unfavorable energy environment for a given amino acid (see results IIIA.3.1).

The modeled structure of the OPN-305 Fab variable domain was aligned with the crystal structure of b12 (PDB code 2NY7; (Zhou et al., 2007)), an antibody Fab

fragment with identical constant domain sequence to OPN-305, in UCSF Chimera (Goddard et al., 2007; Pettersen et al., 2004). Using b12 as a framework, the variable domain of b12 was replaced by the modeled OPN-305 variable domain.

## IIB.11 Electron microscopy

### IIB.11.1 Specimen preparation and EM of mTLR2$_{25-587}$/Fab

A sample of mTLR2$_{25-587}$/Fab in 25 mM Tris pH 8, 25 mM NaCl was diluted to 39 nM and 3 µL were applied on a charged carbon coated grid. After 30 s the grid was held briefly and successively into two drops of $H_2O$ and two drops of 2 % uranyl acetate (wt/vol) staining solution. Excess solution was carefully soaked up with filter paper. The images were collected on a LEO 912 Omega transmission electron microscope (Zeiss, Oberkochen, Germany) operated at an acceleration voltage of 125 kV at a magnification of x48000 and a defocus value between 0.5 and 1.0 µm. Low dose images were collected with a 2k x 2k Proscan CCD camera using the TCL software (Tietz Video and Image Processing Systems, Gauting, Germany)

### IIB.11.2 Referenced-based single-particle reconstruction

Images were converted to mrc format and individual particles selected using the program sparx (Hohn et al., 2007). Mathematical image analysis were carried out with the software SPIDER (Frank et al., 1981; Frank et al., 1996). The particles were binned by a factor of 2 resulting in 64 x 64 pixel images with 4.48 Å/pixel. The particle stack was reference-free aligned by rotation and translation operations and the images were grouped into 50 classes by K-means classification (Penczek et al., 1992). Because no 3D reference was available for mTLR2$_{25-587}$/Fab, the high quality class averages with sharp particle boundary and flat background were used for 3D modeling of the mTLR2$_{25-587}$/Fab complex in PyMOL (Schrödinger, USA) by arranging the crystal structures of mTLR2 (PDB code 2Z81) (Jin et al. 2007) and an IgG4 antibody Fab fragment (PDB code 2NY7) (Zhou et al., 2007) to match the particle shape seen in the averages. The resolution of the model was truncated to 30 Å and used as a first reference for single-particle reconstruction using the reference-based alignment method in SPIDER (Shaikh et al., 2008a). Reference projections were created from the 3D

reference, and the obtained alignment parameters (shifts and rotations) were applied on the particle stack by alignment of the particles against the 2D references. An initial 3D reconstruction was computed from the aligned particle images. 39 iterations of back-projections and angular refinement were performed in SPIDER to improve the density map. The aligned particles of a given reference view were displayed to control the distribution of particles among projections. The 3D reconstruction resolution was calculated by splitting the particle data into two equal sets prior to the back-projection procedure and comparison of the two resulting half-reconstructions. Using the Fourier shell correlation (FSC) = 0.5 criteria (Shaikh et al., 2008b), the resolution was calculated from the FSC curve of the final density map. Density map visualization, docking of the crystal structures and the Fab 3D model, and image preparation were performed using the Chimera software (Goddard et al., 2007; Pettersen et al., 2004).

## IIB.12 Crystallization of mTLR2$_{25-587}$/Fab

### IIB.12.1 Screening for suitable crystallization conditions

Initial crystallization setups were carried out using commercial screens (Qiagen, Hilden, Germany) in 96-well sitting-drop plates. 400 nL drops composed of equal amounts of protein- and crystallization solution were pipetted using a Mosquito 4B nanolitre pipetting robot (TTP LabTech, UK). Plates were incubated at constant temperatures (4 °C, 16 °C and 20 °C). To produce crystals suitable for X-ray diffraction experiments, extensive optimization of initial hit conditions was performed manually in 24-well hanging drop formats using drop volumes of 2 µL by varying the physico-chemical parameters such as precipitant and protein concentration, ionic strength and temperature. Also, additive screening (Hampton Research, California, USA), variation of protein/reservoir ratio and adding of 1.5 % - 3 % glycerol was performed.

### IIB.12.2 Data collection and evaluation

Single protein crystals were harvested from their mother liquor, briefly transferred to 30 % glycerol cryoprotectant solution and flash-cooled in liquid $N_2$. X-ray diffraction data set for mTLR2/Fab was collected at $\lambda$ = 1.54 Å on a home source rotating anode (MicroMax-007HF generator; Rigaku, Japan) using a Saturn 944HG CCD detector

(Rigaku, Japan). Denzo and Scalepack of HKL3000beta suite (Minor et al., 2006; Otwinowski and Minor, 1997) and the CCP4 software suite (Collaborative Computational Project Number 4, 1994) were used for data processing. Molecular replacement trials were done with PHASER (McCoy et al., 2007) and MOLREP (Vagin and Teplyakov, 2010) using search models from OPN-305 Fab (with and without CDRs, see IIB.10) and mTLR2 ECD (Jin et al. 2007) (with and without hagfish domain).

# IIC Producing mouse/human Toll-like receptors 2 and 6 in insect cells using the baculovirus expression system

## IIC.1 Cloning

The Fc gene was amplified by polymerase chain reaction (PCR) from the plasmid pCMV-hFc-XP (in-house plasmid) using primers with BglII, NdeI, NheI and HindIII restriction sites, and a TEV site N-terminal to the Fc fragment (Figure IIC-1, A):

Forward Primer:

BglII NdeI NheI TEV Fc
5′ AAGGAGATCTCATATGACCATGGATGATGCTAGCGAGAATCTTTATTTTCAGGGCCCCAAATCTTGT GACAAAACTCAC 3′

Reverse Primer:

HindIII Fc
5′ AGGAGAAGCTTGCGGCCGCTCATTATCTAGATCATTTACCCGGGGACAGGGAGAGGC 3′

The amplified fragment was digested with BglII/HindIII and cloned into the expression vector pFastbac1 (pFB, Invitrogen) between BamHI and HindIII (BglII and BamHI have compatible cohesive ends) yielding the plasmid pFB-TEV-hFc. The gene construct gp67-hTLR6$_{32\text{-}585}$-His$_8$ (synthesized by Geneart, Regensburg, Germany) was then cloned into pFB-TEV-hFc between the restriction sites NdeI and NheI resulting in the final plasmid pFB-gp67-hTLR6$_{32\text{-}585}$-His$_8$-TEV-hFc. BamHI and XhoI restriction sites allow the facile removal of hTLR6 ECD from the construct to be replaced by gene constructs for hTLR2$_{19\text{-}588}$, mTLR2$_{25\text{-}587}$ and mTLR6$_{28\text{-}584}$ amplified from cDNA (purchased from ImaGenes, Nottingham, UK). The following PCR primers were used:

hTLR2$_{19\text{-}588}$:

BamHI
Forward Primer: GAGGAGGATCCAAGGAAGAATCCTCCAATCAGGC

XhoI
Reverse Primer: AAGGTCACTCGAGTGTCCTGTGACATTCCGACACCGAG

mTLR2$_{25\text{-}587}$:

BglII
Forward Primer: GAGGAGAGATCTCAGGAGTCTCTGTCATGTGATGCTTCTG

XhoI
Reverse Primer: AAGGTCACTCGAGCTGGTGACATTCCAAGACGGAGGG

mTLR6$_{28\text{-}584}$:

BamHI
Forward Primer: GAGGAGGATCCTCCTCTAATGAACTTGAGTCTATGGTAGA

XhoI
Reverse Primer: AAGGTCACTCGAGAGTATCACAGGACAGTGGAGACATGTG

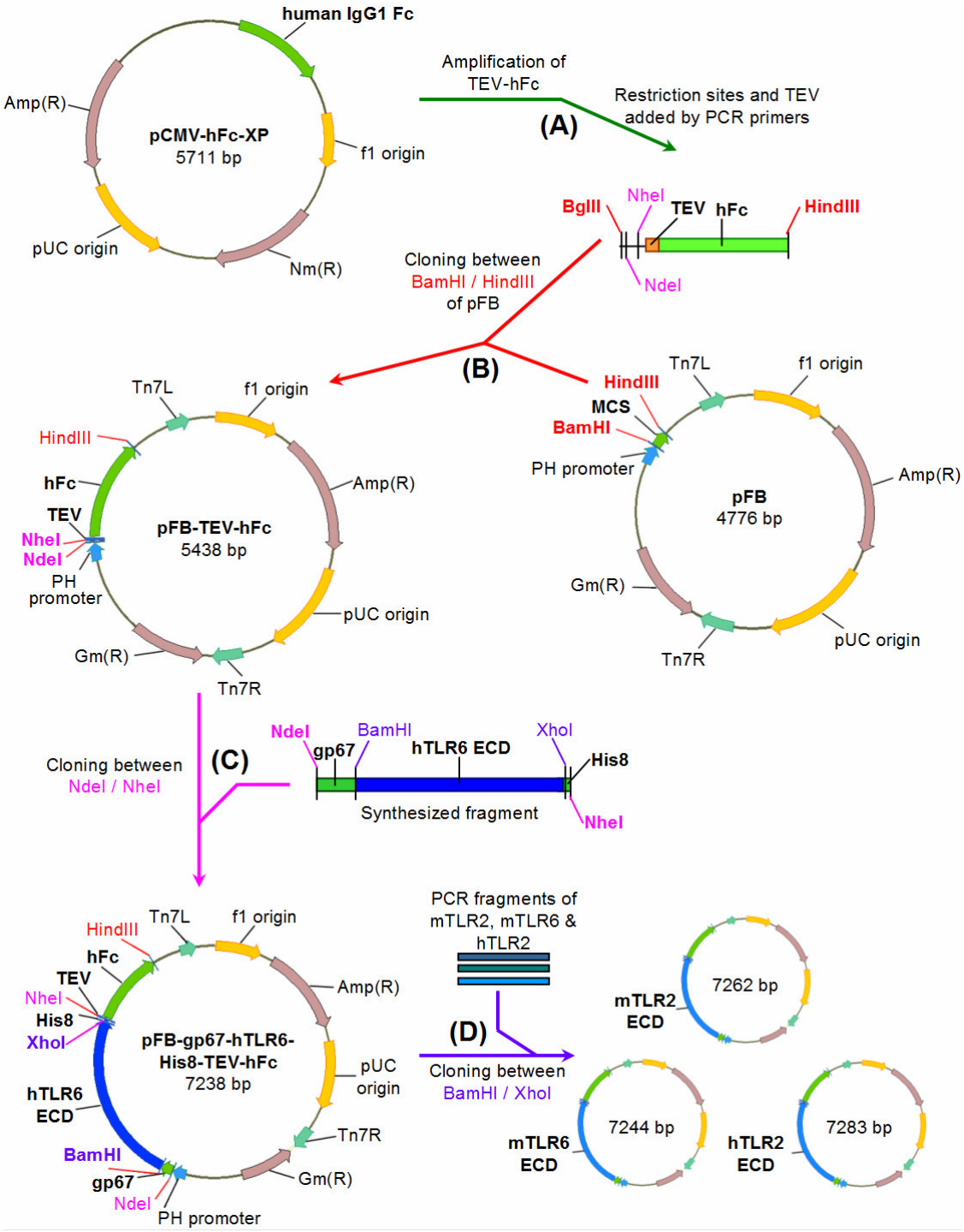


**Figure IIC-1 Cloning strategy to create the four pFB TLR plasmids**
**(A)** PCR from the plasmid pCMV-hFc-XP using primers with flanked BglII and HindIII restriction sites (red), the restriction sites NheI and NdeI (pink), and the TEV cleavage site yields the fragment TEV-hFc. **(B)** TEV-hFc was cloned into the vector pFB between BamHI and HindIII. BglII and BamHI are compatible restriction sites. This yields the plasmid pFB-TEV-hFc with introduced NdeI / NheI sites. **(C)** The synthesized DNA fragment gp67-hTLR6 ECD was cloned into pFB-TEV-hFc between NdeI and NheI yielding the first of the four final pFB-TLR plasmids. The introduced BamHI and XhoI restriction sites further allows a replacement of the hTLR6 ECD. **(D)** PCR fragments from genomic cDNA of mTLR2, mTLR6 and hTLR2 were cloned between BamHI and XhoI to form the other three pFB-TLR plasmids. Amp(R) / Gm(R) / Nm(R) = ampicillin/gentamicin/neomycin resistance; PH promoter = polyhedrin promoter for baculovirus expression; Tn7L / Tn7R = sites for site-specific transposition into baculovirus DNA.

The PCR products were cloned into pFB-gp67-hTLR6$_{32-585}$-His$_8$-TEV-hFc replacing hTLR6$_{32-585}$ by using the restriction enzyme combinations BglII/XhoI and BamHI/XhoI.

All DNA samples were purified using the GeneJET DNA Purification Kit or GeneJET Gel Extraction Kit (Fermentas) prior to ligation and the products of individual cloning steps were analyzed by agarose gel electrophoresis. The recombinant plasmids were verified by sequencing (Eurofins MWG Operon, Ebersberg, Germany).

## IIC.2 Baculovirus expression system

### IIC.2.1 Generation of recombinant Bacmid-DNA

1 ng DNA of each recombinant pFastbac plasmid was transformed into chemical competent DH$_{10}$Bac cells (Invitrogen, Carlsbad, USA). Within these cells the gene construct was to be integrated into the baculovirus mini-*att*Tn7 site by site-specific transposition. The cells were plated on LB$_{Bac}$ agar plates containing 100 µg/mL ampicillin, 50 µg/ml kanamycin, 7 µg/ml gentamicin, 10 µg/ml tetracycline, 100 µg/ml Bluo-gal, and 40 µg/mL IPTG. After incubating for 24 h at 37 °C and 24 h at room temperature (RT), large white colonies were picked and restreaked on fresh LB$_{Bac}$ plates to confirm the white phenotype. The recombinant bacmid DNA was isolated according to the protocol in the BAC-TO-BAC® System manual (Invitrogen) and the gene inserts identified by PCR using the primers M13 Forward and M13 Reverse (Invitrogen) flanking the mini-*att*Tn7 site following agarose gel electrophoresis of the PCR products.

### IIC.2.2 Cell counting

Prior to cell seeding, the cell density of Sf21 cells per mL cell culture was calculated using a hemocytometer by counting the number of cells of four 1mm$^2$ squares. To monitor the cell progeny and vitality during virus and protein production, manual counting with a hemocytometer as well as automated cell counting using a CASY counter (Roche Innovatis, Basel, Switzerland) was utilized to promote maximum accuracy. CASY counter further allowed the determination of cell diameters, an indirect measure for the virus concentration in the cells.

### IIC.2.3 Transfection of bacmid DNA and virus production

5 µL bacmid DNA (~400 ng/µL) were transfected into $1x10^6$ seeded Sf21 cells grown in 2 mL ExCell medium using 5.5 µg Superfectin (Invitrogen). After 3 days of incubation in a 27 °C humidified incubator the supernatant containing the replicated virus was harvested. 2 mL of fresh ExCell medium was added and the cells incubated for another 48 h. The supernatant was pooled with the first harvest and the virus titer determined performing viral plaque assays.

### IIC.2.4 Plaque assay

$1.25x10^6$ cells in 2 mL ExCell medium were seeded per well. After adhesion, the medium was removed and 500 µL of virus dilution ($10^{-4}$, $10^{-5}$, $10^{-6}$) were immediately added to the cells. After 2 h incubation at 27 °C the virus supernatant was removed and the cells overlaid with 4 % agarose. The cells were incubated for 5 days upside down in a 27 °C humidified incubator. The cells were stained with neutral red solution for 4 h at 27 °C, the solution was removed and the cells further incubated over night at RT in dark environment. The next day the white plaques were counted and the pfu/mL (plaque forming units per mL = viruses per mL) were calculated by including plaque number, virus volume and dilution factor. As positive control a commercial virus (Toshi virus) with known virus titer was used.

### IIC.2.5 Virus amplification

The virus was amplified in several cycles repeating cell infection with virus (MOI = 0.1-0.5), incubation, harvest of viruses, and plaque assay, to a volume of 800 mL virus solution with a virus concentration of $1x10^7$ pfu/mL. The cell density and vitality was monitored in all steps by cell counting using a hemocytometer under the light microscope and by using a CASY Cell Counter.

## IIC.3 Expression and purification of (m/h)TLR(2/6)-His-Fc

Protein expression was performed by infection of insect cells ($1 \times 10^6$ cells/mL culture) with TLR-containing baculovirus using a MOI of 2. After 72 h the cells were harvested.

Determination of intracellular and extracellular protein portions was achieved using the Cytobuster protein extraction reagent (Merck, Darmstadt, Germany). The insect cells were centrifuged and the supernatant was collected. The protein supernatant was dialyzed against equilibration buffer (50 mM Tris pH 8, 150 mM NaCl, 1 mM DTT, 0.5 mM EDTA) for 24 h and then coupled to Protein A sepharose matrix (GE Healthcare). The column was washed with equilibration buffer and the protein-coupled matrix was incubated with TEV protease at 4 °C over night, following incubation at room temperature for 4 h. To elute the protein prior to protease digestion, the protein was rapidly eluted with glycine buffer pH 3 and the drops were immediately collected in 100 mM Tris pH 8.0, 100 mM NaCl, but which could not successfully refold the protein.

## IIC.4 Western blotting

Protein bands from SDS-PAGE gels were transferred to PVDF membrane (immobilon-P, Millipore, Massachusetts, USA) for subsequent immunodetection using a Semi-Dry Transfer Cell (BioRad, California, USA). Freshly run SDS-PAGE gel and blotting paper were equilibrated for 15 in transfer buffer. The PVDF membrane was equilibrated in 100 % methanol for 5 sec following washing in $H_2O$ for 5 min and in transfer buffer for 10 min. For the transfer the gel was placed onto the membrane and both was placed between two layers of blotting paper onto the anode of the semi-dry transfer cell. The Western blot was run with 15 V for 30 min. To prevent non-specific binding blocking of the membrane was achieved by incubation for 1 h with 50 mL of TBST buffer following washing for 3 x 5 min in TBST buffer. The primary antibody was incubated with the membrane for 1 h at RT. The membrane was again washed 3 x 5 min with TBST buffer. The membrane was then incubated with an alkaline phosphatase (AP)-conjugated antibody for 1 h at RT and washed 2 x 5 min in TBST buffer. For immunoblotting of (m/h)TLR(2/6)-His-Fc, a mouse anti-His-tag antibody was used as primary antibody and an AP-conjugated anti-mouse antibody as secondary antibody. To label the Fc-tag within the TLR constructs, a primary AP-conjugated goat anti-human antibody was used, which detects the heavy chain as well as the light chain of human IgG antibodies. Prior to staining reaction, the membranes were equilibrated for 5 min in AP buffer. The enzymatic staining reaction was started by incubation for 1 to 5 min with a mixture of 10 mL AP buffer, 66 µL NBT and 33 µL BCIP. The staining was

stopped with several solution changes with deionized water and drying of the membrane.

**Transfer buffer:**
6 g Tris-Base
72 g glycine
300 mL methanol
Filling up to 2 L with $H_2O$

**TBST wash buffer:**
20 mL of 1 M Tris, pH 8
37.5 mL of 4 M NaCl
0.5 mL Tween-20
Filling up to 1 L with $H_2O$

**AP buffer:**
100 mL of 1 M Tris, pH 9.5
25 mL of 4 M NaCl
10 mL of 0.5 M $MgCl_2$
Filling up to 1 L with $H_2O$

# III Results

## IIIA Inhibition of mTLR2 with a monoclonal antibody

The antibody used in these studies, the monoclonal anti-human/mouse TLR2 antibody OPN-305 (Opsona Therapeutics, Dublin, Ireland) is a humanized version of the murine anti-human/mouse TLR2 antibody OPN-301, first developed by Prof. Dr. Carsten Kirschning (Universitätsklinikum Essen, Germany) as antibody T2.5. OPN-305 was provided by Opsona in 10 mg/mL stocks in 25 mM sodium citrate pH 4.5 and 125 mM NaCl. The antibody was shock frozen in liquid $N_2$ and stored at -80 °C until usage.

The mTLR2 clone was initially isolated by Prof. Dr. Carsten Kirschning for expression of mTLR2 in HEK293 cells (Meng et al., 2004), and later recloned into a pFastbac vector by Ute Widow (HZI, Braunschweig, Germany) for the expression in insect cells. A $His_6$-tag was added to the C-terminus. The protein production was performed by the group of Dr. Joop van den Heuvel (HZI, Braunschweig, Germany) and shipped on ice to South Africa. The protein was produced in 6 L Sf21 insect cell cultures as well as in a 35 L fermenter in CHO lec3.2.8.1 cells, optimized for the production of glycoproteins for structural analysis (Stanley, 1989; Wilke et al., 2010).

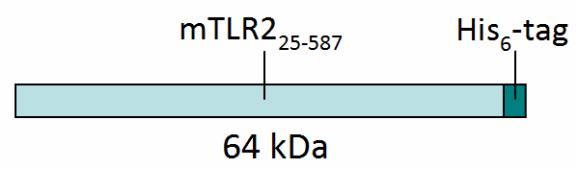


**Figure IIIA-1 Schematic representation of $mTLR2_{25-587}$-$His_6$**
The ECD $mTLR2_{25-587}$ is C-terminally linked to a $His_6$-tag. The molecular weight of the recombinant protein is 64 kDa.

### IIIA.1 Complexation of TLR2 and OPN-305

#### IIIA.1.1 Purification of $mTLR2_{25-587}$-$His_6$

For simplicity, the $His_6$-tagged ECD of murine TLR2, $mTLR2_{25-587}$-His, will henceforth be referred to as TLR2 or mTLR2 in all sections of chapter IIIA.

The C-terminal $His_6$-tag attached to TLR2 allows initial purification by Ni-NTA affinity chromatography (AC), followed by anion exchange chromatography (AEC). TLR2 protein charges from insect cells and CHO cells were indistinguishable in all

chromatographic purification steps. The quality of the purification was analyzed by SDS-PAGE (Figure IIIA-2).

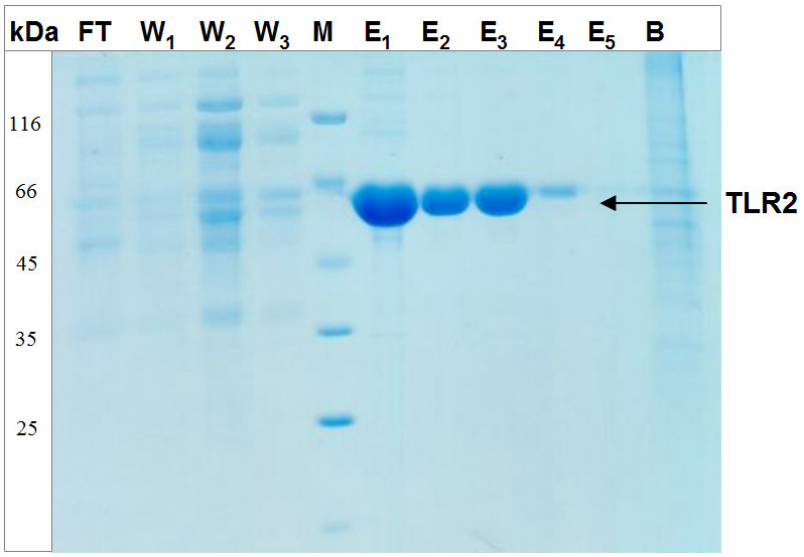


**Figure IIIA-2 Purification of TLR2 by Ni-NTA affinity chromatography**
SDS-PAGE of samples of the flow through (FT); wash fractions $W_1$ (10 mM imidazole), $W_2$ + $W_3$ (40 mM imidazole); elution fractions $E_1$ + $E_2$ (100 mM imidazole), $E_3$ + $E_4$ (250 mM imidazole), $E_5$ (500 mM imidazole), and matrix beads after elution (B). TLR2 eluted with buffers containing 100 mM and 250 mM imidazole. Gel marker: Unstained Protein Molecular Weight Marker (Fermentas).

Coupling TLR2 to the Ni-NTA matrix allowed for the majority of impurities to be removed by washing with buffers containing 10 - 40 mM imidazole (Figure IIIA-2, lanes $W_1$ – $W_3$). TLR2 was eluted with buffer containing 100 - 500 mM imidazole (Figure IIIA-2, lanes $E_1$ – $E_5$). Only insignificant amounts of protein remained bound to the matrix (Figure IIIA-2, lane B). The yield after Ni-NTA AC was generally 0.4 – 0.5 mg TLR2 per L of insect cell culture and 0.6 mg per L CHO cell culture.

The second step in purifying TLR2 involved AEC to remove remaining impurities (Figure IIIA-2, lane $E_1$).

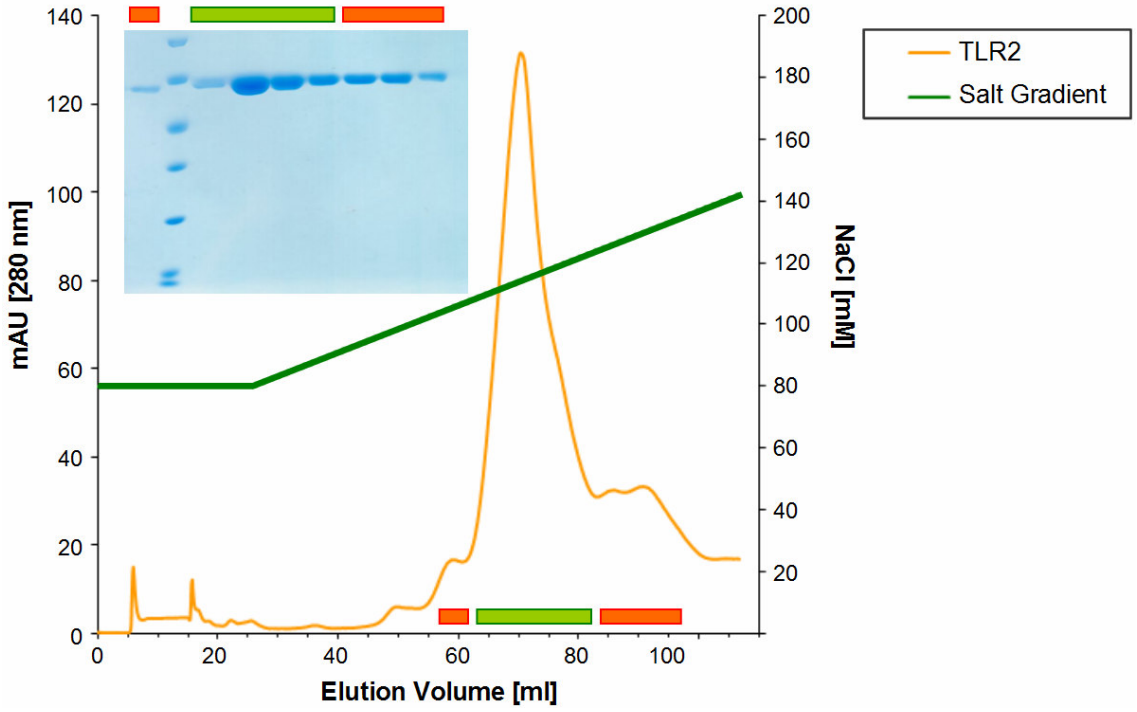


**Figure IIIA-3 Purification of TLR2 by anion exchange chromatography**
Partially pure TLR2 from Ni-NTA AC was further purified by AEC. The proteins were eluted from the column according to their negative charge by applying a salt gradient from 8 mM to 200 mM NaCl (green line) and were monitored by measuring the absorption at 280 nm (orange curve). Elution fractions were analyzed by SDS-PAGE. Fractions from the main peak (green bar) were used for complexation with the OPN-305 Fab fragments. Gel marker: Unstained Protein Molecular Weight Marker (Fermentas).

Applying a salt gradient to the AEC column resulted in TLR2 elution in the range of 100 - 140 mM NaCl, reaching a maximum at 115 mM NaCl (Figure IIIA-3). Elution occurs as one major and several smaller peaks of absorbance at 280 nm. Corresponding elution fractions were analyzed by SDS-PAGE identifying all fractions as TLR2. Impurities were not detectable. As the distinct peaks in the AEC may be due to different glycosylation states of TLR2, only the central fractions of the main peak (Figure IIIA-3, green bar) were pooled and used for further experiments.

### IIIA.1.2 Deglycosylation of TLR2

The ECD of mTLR2 is known to be glycosylated in three sites. Although glycosylation is already minimized in Sf21 insect cells and especially in the CHO strain used here resulting in shorter and more homogeneous sugar chains, glycosylation variability can still introduce protein heterogeneity interfering with crystallization.

We therefore chose to deglycosylate TLR2 with PNGase F (New England Biolabs, Massachusetts, USA), an amidase that cleaves the bond between the asparagine residues and the first GlcNAc in N-linked glycoproteins (Maley et al., 1989).

The following SDS gel documents TLR2 deglycosylation using two enzyme concentrations and a range of incubation times (Figure IIIA-4).

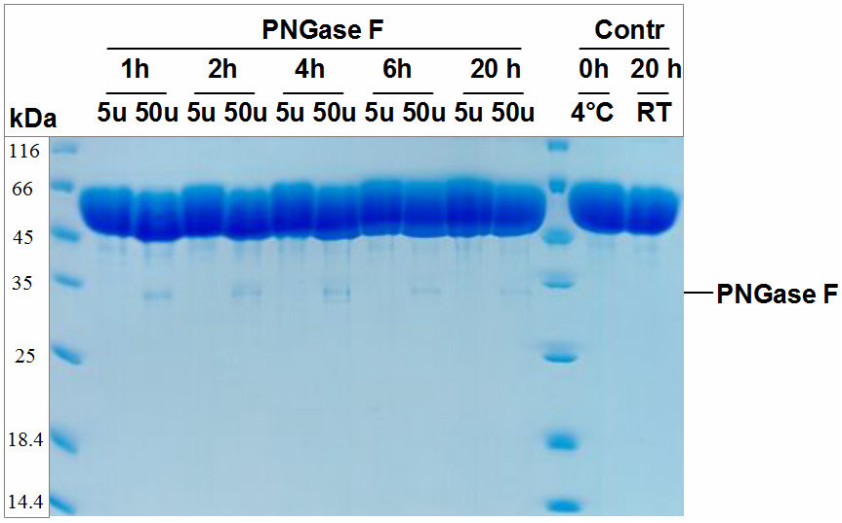


**Figure IIIA-4 Deglycosylation of TLR2**
11 µg of TLR2 were incubated with 5 u and 50 u PNGase F for 1 h, 2 h, 4 h, 6 h, and 20 h at RT. The reaction was stopped by adding SDS buffer and denaturation of the samples at 95 °C. The samples were analyzed by SDS-PAGE. Controls without enzyme were analyzed before start (0 h) at 4 °C and after 20 h at RT. Gel marker: Unstained Protein Molecular Weight Marker (Fermentas).

11 µg of TLR2 was fully deglycosylated after 1 h incubation with 50 u PNGase F. However, 6 h to 20 h were necessary to deglycosylate TLR2 using only 5 u PNGase F. No degradation of TLR2 is apparent after 20 h at room temperature (RT).

Deglycosylating TLR2 from both insect as well CHO cells indicate that actual deglycosylation in the form of changed mass as judged by SDS-PAGE (Figure IIIA-4) is only apparent in TLR2 from insect cells. The mass difference between glycoproteins from CHO cells and their deglycosylated counterparts is too small to see in SDS-PAGE. Surprisingly, glycosylated and deglycosylated TLR2 are indistinguishable in AEC.

Following the analysis in Figure IIIA-4, 10 u of PNGase F were used per 10 µg of TLR2 protein and incubation was extended to 15 h at RT in preparative deglycosylation. Glycosylated as well as deglycosylated TLR2 was used for Fab complex formation and crystallization studies.

### IIIA.1.3 Generation and purification of OPN-305 Fab fragments

The two heavy and two light chains constituting an antibody come together to create three roughly similarly sized protein domains: two identical Fab and one Fc domain. Only the Fab fragments bear the variable regions consisting of the CDRs responsible for antigen recognition. Hence the antibody OPN-305 was digested with the enzyme papain, a cysteine protease to cleave the antibody N-terminally of the two disulfide bridges connecting the two heavy chains. This yields two Fab and one Fc domains (Figure IIIA-5). The smaller Fab fragment is preferred over the full length antibody for structural studies. This is because it potentially forms a rigid 1:1 complex with TLR2 whereas the uncleaved antibody would bind two TLR molecules and be highly flexible due to flexible linkers between the three domains. The flexibility could introduce protein heterogeneity, a major obstacle to crystallization and EM.

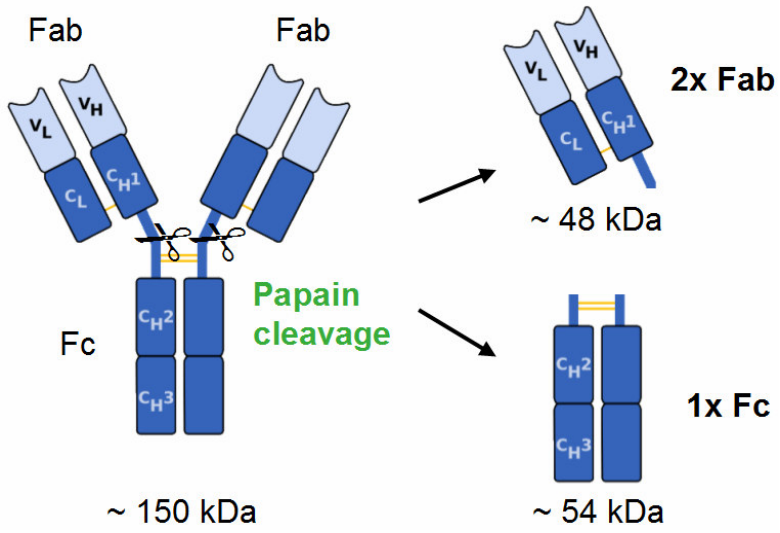


**Figure IIIA-5 Papain cleavage of antibodies**
Antibody OPN-305 has two papain cleavage sites, one in each of the equivalent heavy chain (scissor symbols). Digestion releases two Fab fragments (48 kDa each) and one Fc fragment (54 kDa).

After proteolytic cleavage, size-exclusion chromatography (SEC) was used to separate the Fab and Fc fragments (~50 kDa) from the uncleaved (~150 kDa) and incompletely cleaved (~100 kDa) antibody molecules (Figure IIIA-6 A). Protein fractions from the SEC (Figure IIIA-6 A, green and red bars) were analyzed by SDS-PAGE to confirm the purity of the samples (Figure IIIA-6 B).

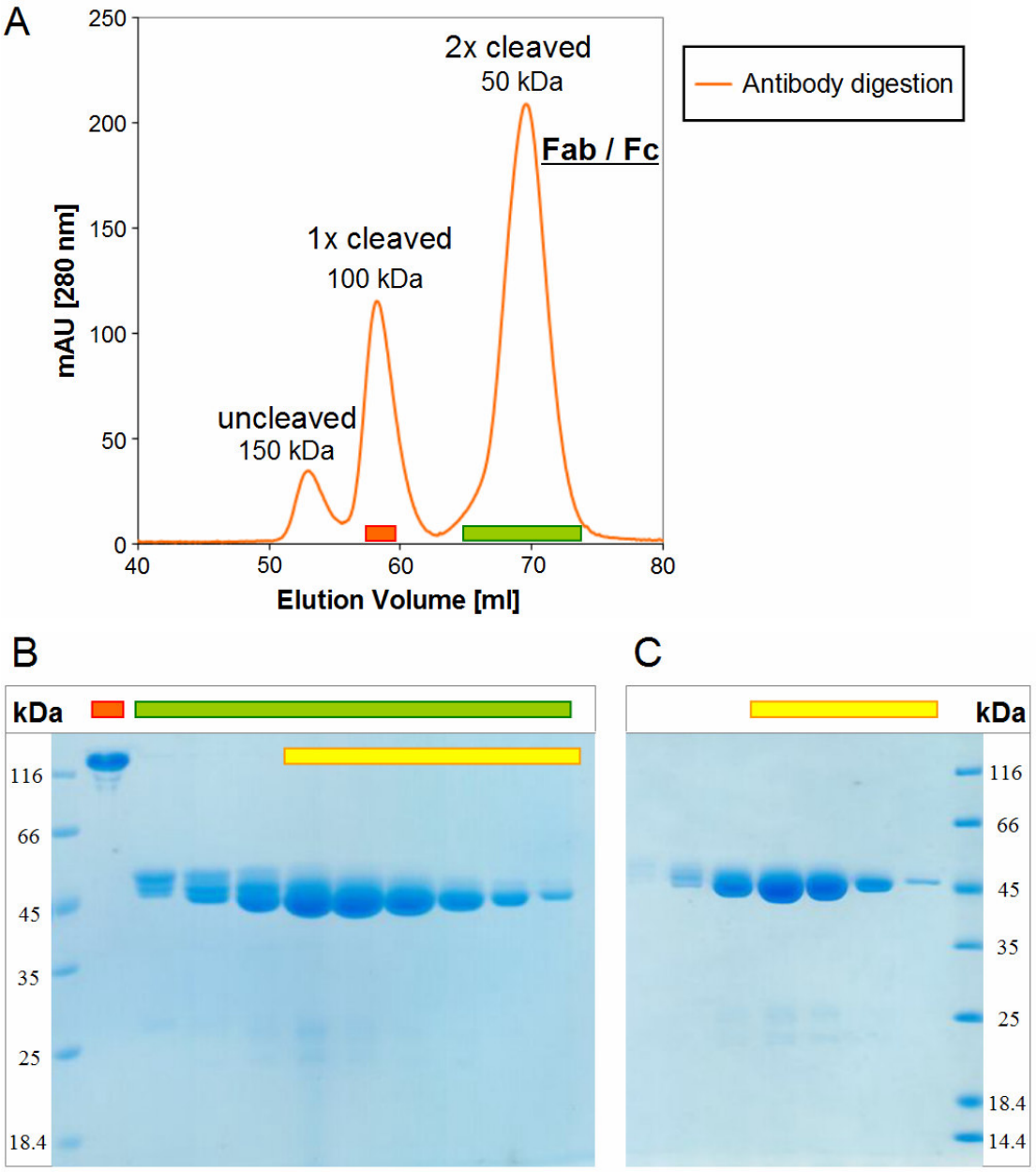


**Figure IIIA-6 Separation and analysis of antibody fragments after papain cleavage**
**(A)** OPN-305 was digested with papain and the products separated by SEC. Fractions marked by bars were analyzed by SDS-PAGE. **(B)** SDS gel of completely (green bar) and incompletely cleaved antibodies (orange bar). Fractions marked by a yellow bar were pooled and separated in a second SEC. **(C)** SDS-PAGE analysis of fractions of the second SEC. The marked samples (yellow bar) were pooled and used for further experiments. Gel marker: Unstained Protein Molecular Weight Marker (Fermentas).

Non-reducing sample conditions were used to avoid breaking disulfide bridges linking heavy and light chains allowing the full size of fragments to be analyzed. The singly or incompletely cleaved antibody retains a mass of ~100 kDa and runs on the SDS gel above the 116 kDa marker band (Figure IIIA-6 B, red bar) presumably due to its elongated shape. For Fab/Fc mixtures SDS-PAGE should, in principle, reveal two closely positioned bands of ~50 kDa, with the Fc fragment (54 kDa) running slightly

higher than the Fab fraction (48 kDa). Instead four bands are observed (Figure IIIA-6 B, green bar), suggesting that papain cleaves the antibody at two distinct positions. As protein crystallization requires homogenous Fab fragments, the SEC fractions bearing the two Fab variants (the two lower bands in Figure IIIA-6 B, yellow bar) were pooled and run on a second SEC. Its fractions were again analyzed by SDS-PAGE (Figure IIIA-6 C). Only those fractions predominantly composed of the smaller Fab variant were pooled and used for further experiments (Figure IIIA-6 C, yellow bar). Around 80 % of the larger Fab variant could be removed.

Mass spectrometry was used to determine the precise mass of the two Fab variants.

### IIIA.1.4 Identification of Fab fragments by mass spectrometry

Peptide mass fingerprinting was used on SDS gel samples of the larger and smaller Fab fragment. In both cases, peptides of the constant Fab region of light chain (Ig kappa chain C, Uniprot entry: P01834) and heavy chain (Ig gamma-4 chain C, Uniprot entry: P01861) of human IgG4 antibodies were identified (Figure IIIA-7).

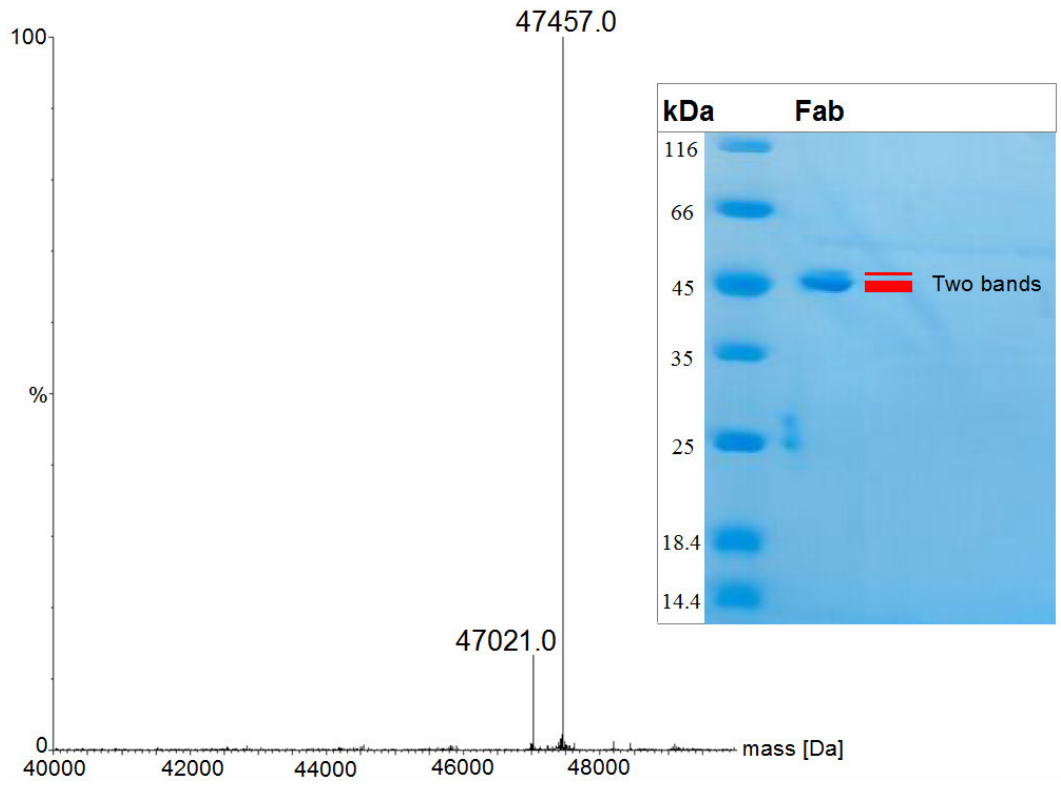


**Figure IIIA-7 Mass spectrometry of Fab**
Electrospray ionization mass spectrometry of Fab in solution: two Fab variants of different sizes (47021 Da and 47457 Da) were identified. Insert: The sample was analyzed by SDS-PAGE prior to MS, confirming two distinct Fab sizes. Gel marker: Unstained Protein Molecular Weight Marker (Fermentas).

Electrospray ionization mass spectrometry (ESI-MS) was used to determine the exact molecular mass of the fragments in solution. Two proteins of mass 47021 and 47457 Da were identified (Figure IIIA-7). Employing the known amino acid sequences of light chain ($Fab_{light}$) and heavy chain ($Fab_{heavy}$) of OPN-305 the two papain cleavage sites in the heavy chain were calculated. A mass of 47457 Da corresponds to $Fab_{light}$ + $Fab_{heavy}$ $Q^{1}$-$G^{221}$, whereas the 436 Da shorter variant matches with $Fab_{light}$ + $Fab_{heavy}$ $Q^{1}$-$G^{217}$. The calculation and heavy chain sequence is shown in Figure IIIA-8.

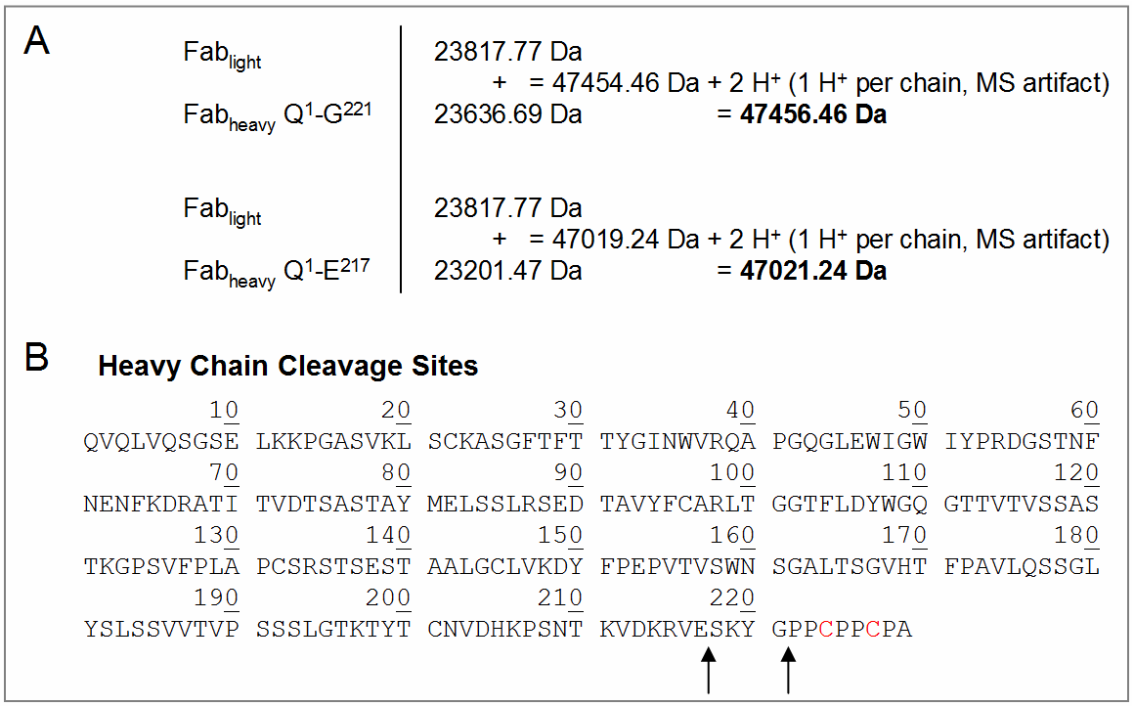


**Figure IIIA-8 Fab heavy chain C-termini**
**(A)** Calculation of molecular weights of the two possible Fab variants according to their masses determined by MS. **(B)** Amino acid sequence of Fab heavy chain. The two papain-derived C-termini are marked by arrows. The two disulfide bridges downstream of the cleavage sites are highlighted in red.

The peak heights or signal intensities of the ESI-MS experiment (Figure IIIA-7) indicates the shorter Fab fragment ($Fab_{light}$/$Fab_{heavy}$ $Q^{1}$-$E^{217}$) constitutes ~15 % and the larger ($Fab_{light}$/$Fab_{heavy}$ $Q^{1}$-$G^{221}$) ~85 % of the sample.

### IIIA.1.5 Generation and purification of the TLR2/Fab complex

Purified TLR2 and Fab were incubated in a molar ratio of 1:2 and analyzed by SEC (Figure IIIA-9).

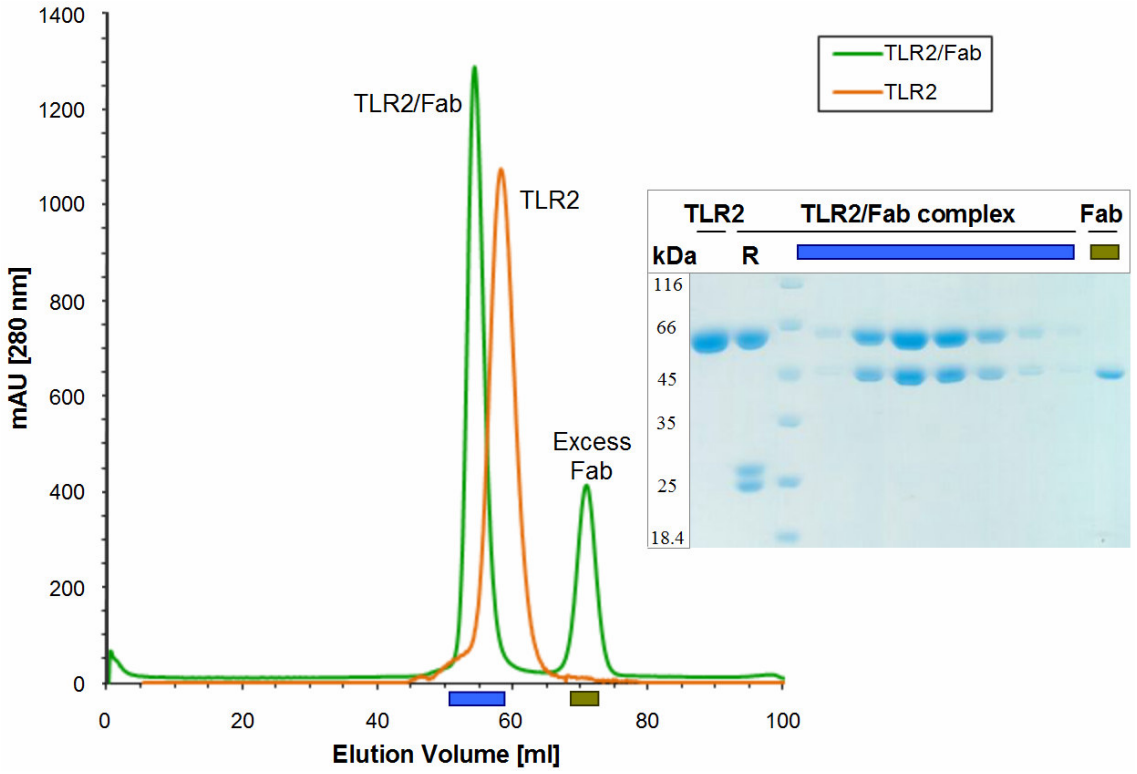


**Figure IIIA-9 Peak shift during SEC between TLR2 and TLR2/Fab**
Overlay of size exclusion chromatographs of TLR2/Fab (green) and TLR2 (orange). Peak shift indicates complex formation. Fractions of the green curve were analyzed by SDS-PAGE. TLR2/Fab complex fractions (blue bar) and excess Fab (ochre bar) are marked. Sample of TLR2 and non-reduced sample of TLR2/Fab (R) are shown for comparison. Gel marker: Unstained Protein Molecular Weight Marker (Fermentas).

The overlay of TLR2/Fab SEC (Figure IIIA-9, green curve) with a curve of TLR2 without Fab (Figure IIIA-9, orange curve) shows a clear peak shift indicating the generation of the complex, which has a higher molecular weight than TLR2 alone. The applied TLR2 was completely bound to Fab molecules in a 1:1 complex, excess Fab fragments and residual Fc fragments could be separated. The SEC fractions were analyzed by SDS-PAGE. Fractions of the complex peak (Figure IIIA-9, blue bar) show two peaks on the gel (upper band is TLR2, lower band is Fab under non-reduced conditions), whereas the excess Fab peak (Figure IIIA-9, ochre bar) resulted in a single band. For comparison, the SDS-gel also shows a sample of TLR2 (first lane) and of the complex under reduced conditions (second lane), leading to the separation of Fab into two chains about 25 kDa.

### IIIA.1.6 Native PAGE of the complex

To verify the complex formation, native PAGE was performed, which allows the analysis of proteins in their folded, non-denatured form. In native PAGE, the gel mobility depends on the ratio of electric charge to hydrodynamic friction (Arakawa et al., 2006). Thus, two proteins with different sizes and shapes like TLR2 and TLR2/Fab are expected to migrate differently through the gel.

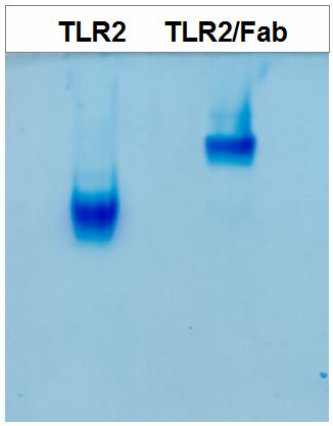


**Figure IIIA-10 Native PAGE analysis of TLR2/Fab**
Comparison of TLR2 monomer with TLR2/Fab under native conditions. The complex migrated slower through the pores of the gel due to its size.

As seen in Figure IIIA-10, the migration path of the complex is shorter than that of the TLR2 monomer, which confirms that the TLR2/Fab complex was successfully generated. The fact that the complex remains stable during the PAGE run is an indication of high affinity of Fab towards TLR2.

### IIIA.1.7 Stability of TLR2/Fab

The quality of the TLR2/Fab complex was further analyzed by anion exchange chromatography (AEC). The aim was to establish whether the complex binds uniformly to the AEC column or if a distribution of peaks would be observed, indicating an instable or flexible protein complex.

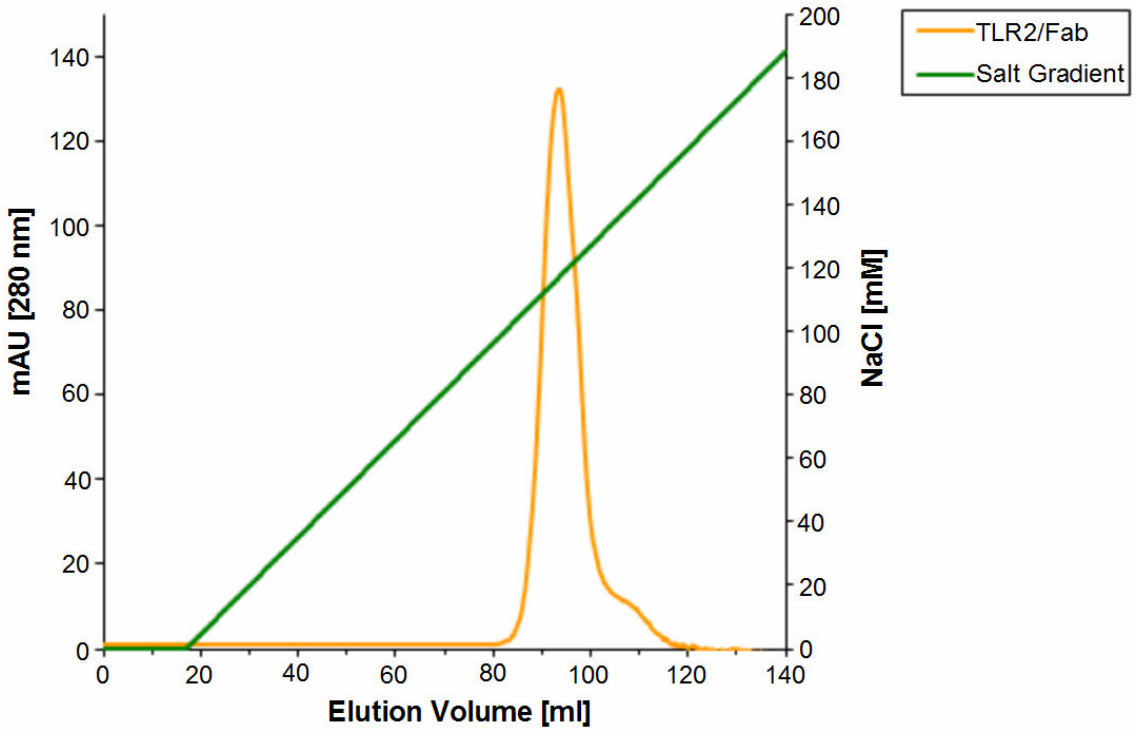


**Figure IIIA-11 Anion exchange chromatography of TLR2/Fab**
TLR2/Fab from the SEC was separated by AEC. The proteins were eluted from column dependent by their negative charge by applying a salt gradient from 0 mM to 200 mM NaCl (green line) and were monitored by measuring the absorption at 280 nm (orange curve).

The chromatogram in Figure IIIA-11 shows a homogeneous and sharp peak eluting with buffer containing 120 mM NaCl. Only a small shoulder can be observed at 140 mM salt. The elution time of the main peak and the shoulder is similar to that of the AEC of the TLR2 monomer (Figure IIIA-3), indicating that TLR2/Fab and the TLR2 from the fractions which were chosen initially in IIIA.1.1 show a similar binding behavior to the chromatographic column, and that the protein has not changed in terms of stability and folding. For further experiments, the purified complex after SEC was used. Selecting the correct TLR2 fractions after AEC (Figure IIIA-3) while excluding neighboring peaks proved critical in obtaining homogenous TLR2, and thus, TLR2/Fab.

## IIIA.2 Negative stain electron microscopy

Electron microscopy (EM) is a commonly used technique to visualize a wide range of biological and inorganic specimens including macromolecules like proteins and protein complexes. In contrast to crystallography, EM is a “direct” method of observing molecules. In negative stain EM, the sample is deposited on a carbon coated grid and then covered with a small drop of an electron-opaque staining solution. The stain fixes

the specimen on the grid in random orientations and produces high contrast ‘electron micrographs’, images of a field of the specimen. By collecting thousands of particle images, a single-particle reconstruction may be attempted to obtain a representation of the outer surface of the molecule. If, as in this case, crystal structures of the individual molecules of a complex have been solved, it may be possible to dock these structures into the EM density map allowing their mode of interaction to be studied.

### IIIA.2.1 Visualization of TLR2/Fab by negative stain EM

After the TLR2/Fab complex was formed and purified as described above, the sample was directly used in negative stain EM experiments. A sample with a concentration of 39 nM was deposited on carbon-coated glow-discharged grids and stained with uranyl acetate solution (see Material and Methods, IIB.11.1.).

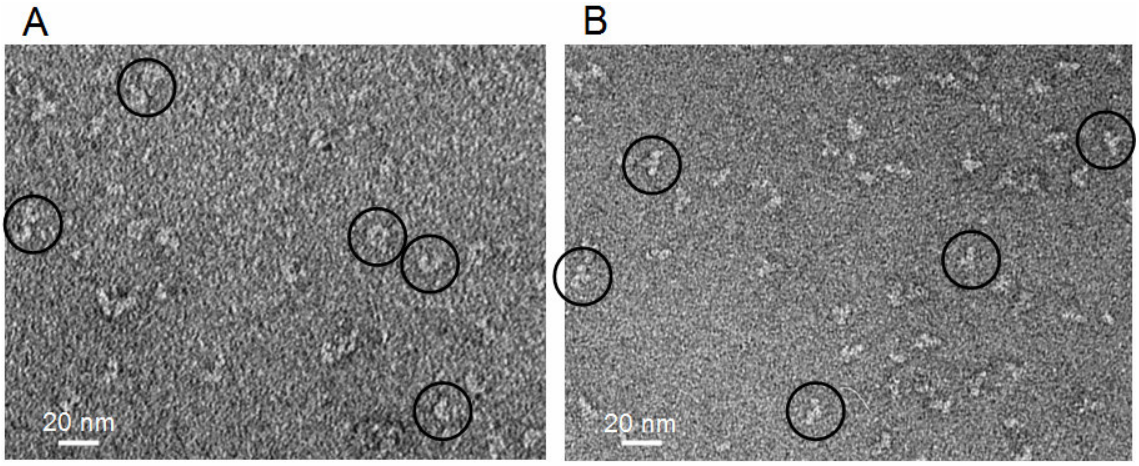


**Figure IIIA-12 Negative stain EM imaging of TLR2 and TLR2/Fab**
Visualization of **(A)** TLR2 and **(B)** TLR2/Fab complex by negative stain EM. Representative particles are highlighted by circles. TLR2 particles (A) have the characteristic horseshoe-like shape, clearly distinguishable from the TLR2/Fab particles (B). Scale bar is 20 nm.

The particles on the negative stain EM images have a homogenous shape with a length of ~150 Å and a width of ~100 Å (Figure IIIA-12, B). The TLR2/Fab particles can be clearly distinguished from EM particles of TLR2, which reveal the characteristic horseshoe-like shape (Figure IIIA-12, A).

In addition to negative stain EM, attempts were made to collect images of TLR2/Fab by cryo-EM. For that purpose different dilutions of protein sample (614 nM, 245 nM, 123 nM and 61 nm) were deposited on carbon coated as well as non-carbon grids.

Several images were collected from different areas of the grids. However, the size of TLR2/Fab of 117 kDa was below the visible limit of cryo-EM and no particles could be observed on the images.

### IIIA.2.2 Particle classification and averaging

Reconstructing a 3D density map involves a number of steps. First, a large stack of particle images need to be collected representing random orientations of the target molecule. Here, a total of 5174 such “particles” were picked from many hundred EM images using the sparx engine (Hohn et al., 2007). Mathematical operations were carried out with the software SPIDER (Frank et al., 1981; Frank et al., 1996) to align the particles by reference-free alignment (Penczek et al., 1992) and to classify the particles into 50 classes with largely identical views. Averages of these classes were then computed to generate high-contrast particle representations. The class averages are shown in Figure IIIA-13.

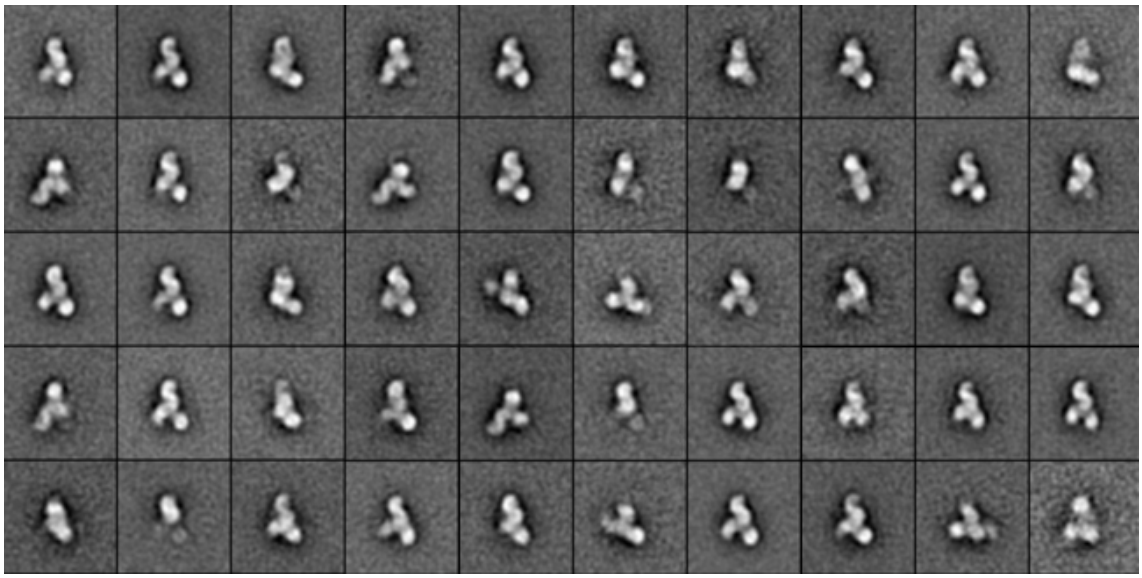

**Figure IIIA-13 Class averages**
5174 particles were classified into 50 classes with largely identical views by mathematical operations using the software SPIDER. The classes were averaged to obtain high quality particle representations.

The averages depict the TLR2/Fab complex in different orientations. Many averages appear similar indicating a majority of particles to have been fixed to the grids in a preferred orientation. Nevertheless, distinct variation is apparent, a prerequisite for a

successful 3D reconstruction. Most averages have a sharp particle boundary and flat background indicating high consistency of particles within the class.

### IIIA.2.3 Reconstruction of the 3D density map

The best class averages were used to manually construct a first 3D model of TLR2/Fab in PyMOL (Schrödinger, USA) by placing the crystal structures of mTLR2 (PDB code 2Z81) (Jin et al., 2007) and an IgG4 antibody Fab fragment (PDB code 2NY7) (Zhou et al., 2007) in contact with each other according indicated by the particle shape in the averages. This model was used as a reference for single-particle reconstruction using the reference-based alignment method (Shaikh et al., 2008a). First, a set of 86 2D reference projections was generated from the 3D reference model. The particle stack was then assigned to the 2D projections applying rotations and translations as required. The aligned particle images were used to create an initial 3D reconstruction, of which 86 reference projections were again generated. In total 39 iterations of back-projections were performed to refine all alignment parameters (Figure IIIA-14).

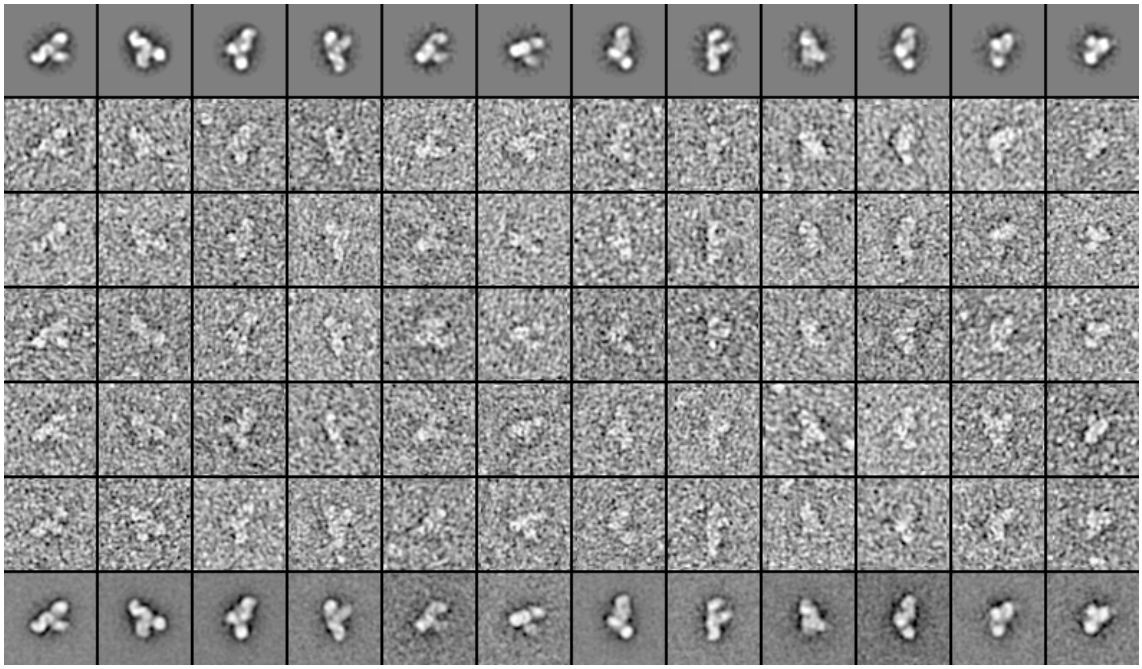

**Figure IIIA-14 Reference-based alignment method**
Reference-projections and particle alignment corresponding to the 39$^{th}$ round of back-projection. The first row depicts 12 of the 86 2D reference projections generated from the previous iteration. Rows 2-6 are individual particles of this class aligned to their reference in the first line. After alignment, each particle set of a reference was averaged, as shown in the last row.

Comparing the reference-projections with the particle averages reveals a high degree of consistency supporting the correctness of the projections and the high quality of alignment.

The back-projection method resulted in the 3D density map presented in Figure IIIA-15.

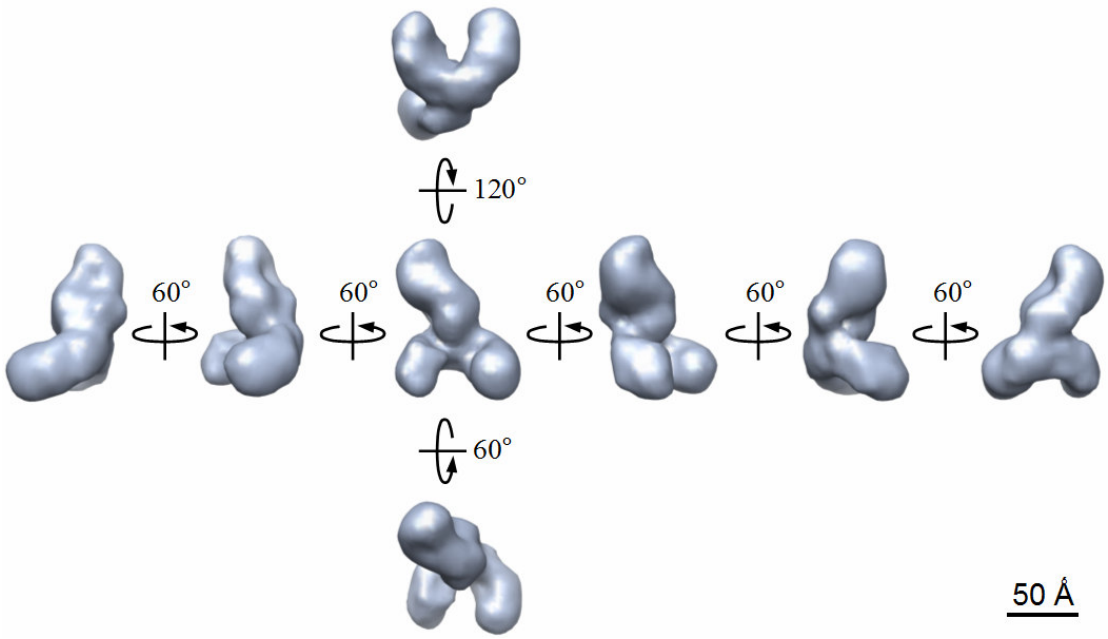


**Figure IIIA-15 3D density map of TLR2/Fab filtered to 21.7 Å**
The density map is rotated about the vertical axis in 60° steps or about 120° and 60° around the horizontal axis relative to the central representation, with rotations indicated around the axis of rotation (circular arrows). The complex structure consists of a horseshoe-like domain and an elongated domain attached laterally to the center of the "horseshoe" extending away from the latter. Scale bar is 50 Å.

To calculate the resolution of the 3D reconstruction, the particle data was split into two equal sets prior to the back-projection procedure and the two resulting half-reconstruction compared. Using the Fourier shell correlation (FSC) = 0.5 criteria, a resolution of 21.7 Å was calculated from the FSC curve of the final density map (Shaikh et al., 2008b).

The structure of the complex is ~130 Å x 90 Å x 70 Å in size and composed of a nearly planar horseshoe-like domain on which a second domain is laterally positioned near its central region. The latter forms angles of 15° and 40° relative to the perpendicular bisector of the horseshoe when respectively projected onto the horseshoe plane or the perpendicular plane sharing the bisector.

## IIIA.3 Analysis of TLR2/OPN-305 interaction

### IIIA.3.1 Modeling of the Fab domain

Antibody Fab fragments are composed of two polypeptide chains, a partial “heavy” and the complete “light” chain of its parent antibody. Each chain bears a constant and a variable part. Although the crystal structure of OPN-305 has not previously been solved, antibodies are mostly largely identical in structure, except for the 6 complementarity determining regions (CDRs) responsible for antigen recognition. Structure-based modeling using the online server Swiss-Model was used to generate the variable domain of OPN-305 (see Material and Methods, IIB.10), in particular so as to obtain a structure with correct CDR sequences and lengths. Quality estimation indicates a model of high reliability giving global QMEAN4 scores of 0.685 for Fab light chain and of 0.818 for Fab heavy chain (quality estimate ranges between 0 and 1 with higher values for better models). The QMEAN4 Z-scores comparing the model with the scores of reference X-ray structures resulted in values close to zero, with -1.19 for Fab light chain and 0.14 for Fab heavy chain, respectively (in theory, models of low quality are expected to have strongly negative QMEAN4 Z-scores).

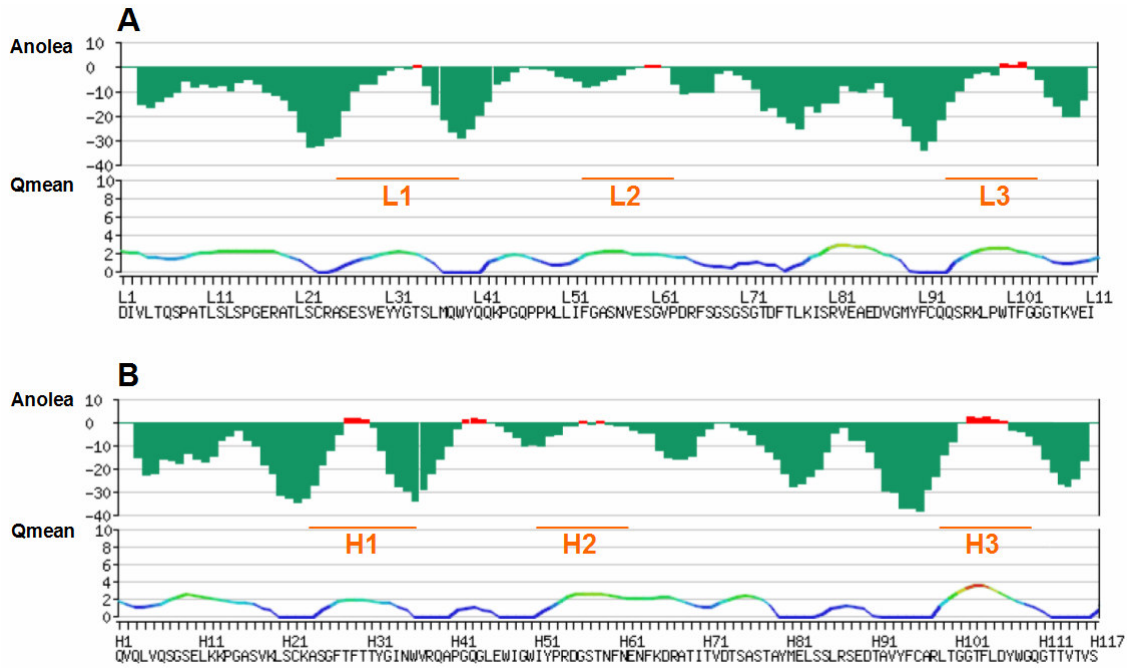


**Figure IIIA-16 Local model quality estimation of Fab variable domain**
Anolea and Qmean scores of **(A)** the light chain and **(B)** heavy chain of OPN-305 Fab variable domain. The CDRs are indicated by orange lines and named L1-L3 for the three CDRs of the light chain and H1-H3 for the three CDRs of the heavy chain. For a detailed description see the text below.

As expected the local scores for individual amino acid residues reveal the highest structural uncertainty in areas of the CDRs (Figure IIIA-16). Within the light chain the Anolea score shows three regions with slightly positive values (in red), all of which belong to the CDRs (Figure IIIA-16, A). The Anolea score of the heavy chain exhibit four regions with modest positive values, of which three belong to the CDRs (Figure IIIA-16, B). Negative energy values (in green) represent a favorable energy environment whereas positive values (in red) an unfavorable energy environment for a given amino acid. The $Q_{mean}$ score is an estimate of the expected structural inaccuracy at a given position with small values corresponding to regions in the model being potentially more reliable. The local scores show modest higher values in particular within the CDR regions. The weakest model reliability is expected for CDR H3 of the heavy chain.

The crystal structure of an IgG4 antibody with identical constant domain sequence as OPN-305 was used as a framework (PDB code 2NY7) (Zhou et al., 2007) and its variable domain replaced by that of the modeled OPN-305 variable domain.

### IIIA.3.2 Docking of TLR2/Fab into the EM density

To identify the interaction area between TLR2 and OPN-305 Fab, crystal structures of mTLR2 and antibody were fitted into the EM density map using the automated “Fit into map” feature of modeling software Chimera (Figure IIIA-17).

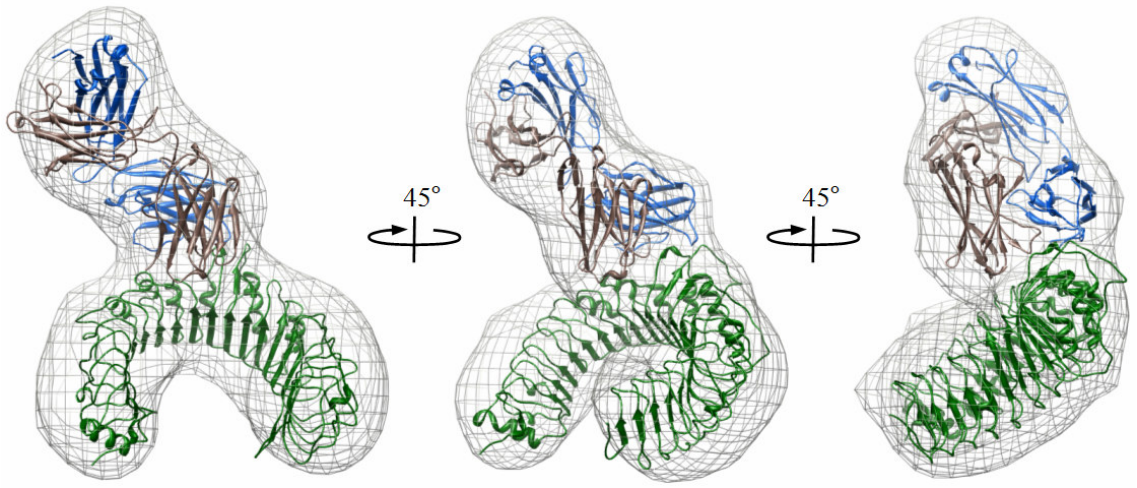


**Figure IIIA-17 Representation of the complex molecules within the EM density map.**
The structure is rotated about the vertical axis in 45° steps. TLR2 is shown in green, Fab heavy chain in brown, and Fab light chain in blue.

The Fab domain model was placed into the EM map to match the lateral density structure emanating from the center of TLR2. The variable domain and its antigen binding site were oriented towards the TLR2 surface (Figure IIIA-18, blue: light chain; brown: heavy chain).

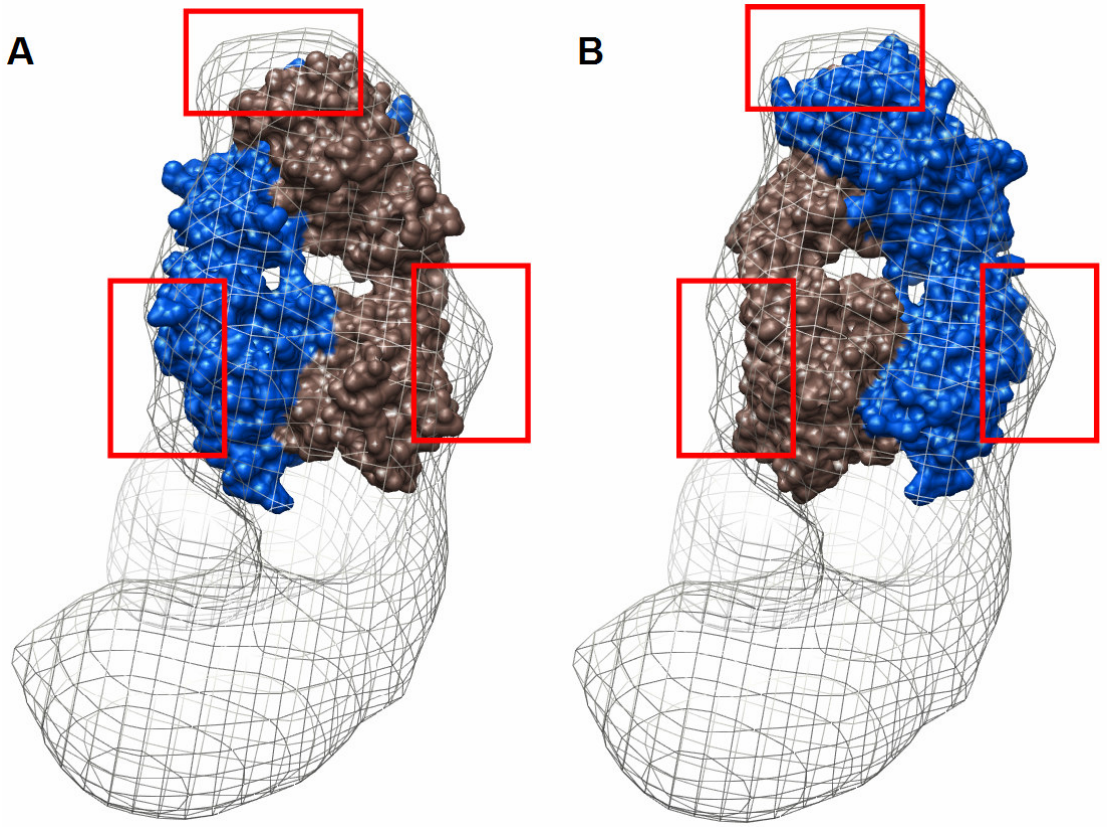


**Figure IIIA-18 Modeling OPN-305 Fab fragment into the EM-derived molecular surface**
The evolutionary homology of the Fab light and heavy chains results in an approximate two-fold rotational symmetry for all Fab fragments along their longest molecular axis. Fitting the generated Fab model structure into the EM-derived molecular surface therefore results in two orientations of Fab related by a 180° rotation around the vertical axis. The two orientations are here denoted Fab#1 **(A)** and Fab#2 **(B)**. The Fab heavy and light chains are respectively rendered in brown and blue. Comparing the two orientations reveals a better agreement between structural model and EM molecular surface for Fab#2 (B) as compared to Fab#1. The latter results in more clashes (red squares) between model and EM surface, implying Fab#2 to be the more likely orientation for the OPN-305 Fab fragment.

Heavy and light chains of Fab fragments are comparable in length and structure resulting in an approximate 2-fold rotational symmetry around the longest axis of the domain. Correspondingly, the OPN-305 Fab structural model has been modelled in two possible orientations (denoted Fab#1 and Fab#2) into the EM derived molecular surface. Comparing the two resulting models (Figure IIIA-18) reveals that Fab#2 (Figure IIIA-18, B) conforms more closely with fine structure of the experimental

molecular surface than Fab#1 (Figure IIIA-18, A). We therefore proposed that the orientation described by Fab#2 constitutes the more probable orientation.

Like all TLRs, the ECD of mTLR2 is composed of multiple consecutive LRRs forming a solenoid structure, which is forced into a curved configuration because of closely packed β sheets on the concave surface and the larger helices on the convex side - generating a horseshoe-like shape (Botos et al., 2011; Kajava, 1998). Our 3D reconstruction shows a similar structural feature allowing the crystal structure of mTLR2 ECD (PDB code 2Z81) (Jin et al., 2007) to be placed into the curved structure of the EM map with a high degree of reliability. As TLR-ECDs are bent yet almost planar in shape, the N- and C-terminal halves of the domain are related to each other by an approximate two-fold rotational symmetry. Correspondingly, mTLR2 may be placed into the EM molecular surface in two essentially equivalent orientations here termed TLR#1 and TLR#2 (Figure IIIA-19).

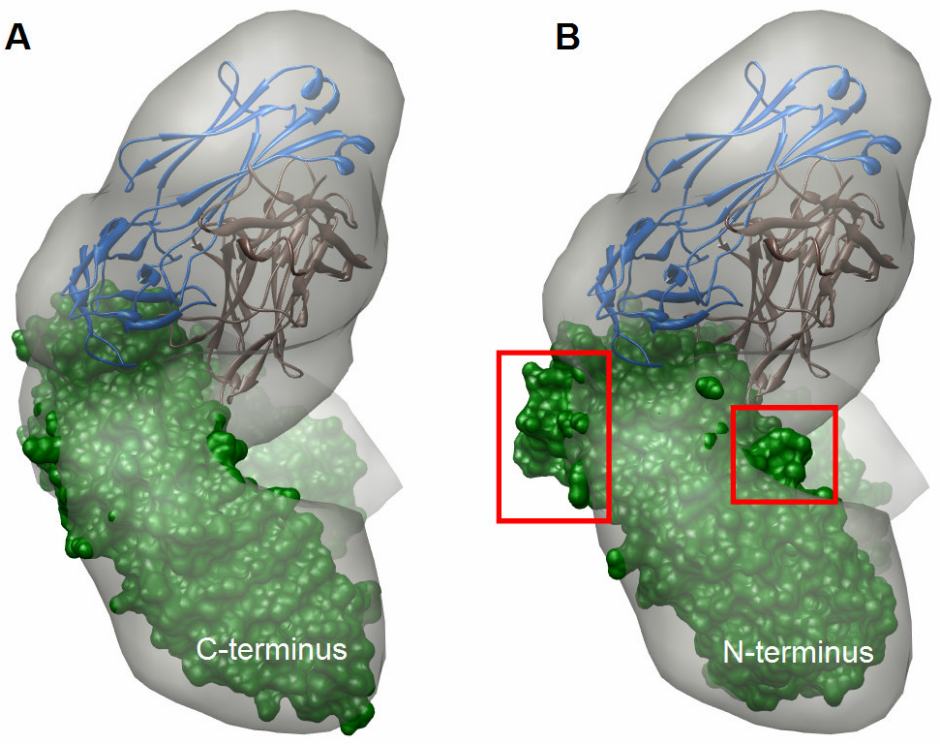


**Figure IIIA-19 Modeling TLR2 into the EM-derived molecular surface**
The N- and C-terminal halves of the TLR2 ECD are related to each other by an approximate two-fold rotational symmetry, allowing the placement of the domain into the EM surface in two orientations. They are here denoted TLR#1 **(A)** and TLR#2 **(B)**. Major clashes of the TLR2 surface with the volume surface can be observed in orientation #2 (B) in comparison to orientation #1 (A), highlighted by red squares, implying TLR#1 to be the more likely orientation for the TLR2 ECD.

In TLR#1, the surface area involved in dimerization with TLR1 and TLR6 faces the OPN-305 Fab fragment, whereas the dimerization site would face away from the Fab in TLR#2. Overall TLR#1 is found to result in fewer and less dramatic clashes between molecular model and the EM molecular surface (Figure IIIA-19, A), whereas TLR#2 reveals some major clashes as indicated by red squares (Figure IIIA-19, B). Therefore, TLR#1 could be identified as the correct orientation in the TLR2/Fab complex.

### IIIA.3.3 OPN-305 blocks the TLR2 dimerization site

After docking both TLR2 and Fab model structures into the EM density, the TLR2 part was superimposed on the TLR2 parts of the TLR2/TLR1 and TLR2/TLR6 complex crystal structures (Figure IIIA-20).

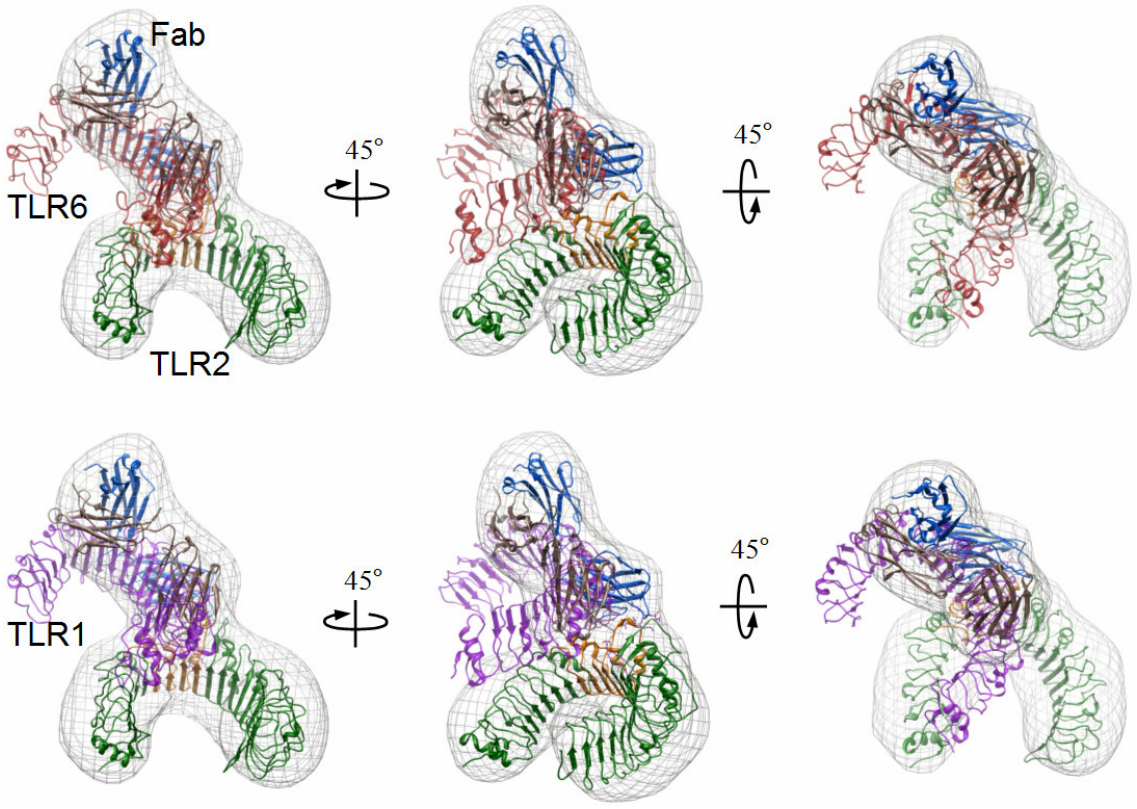


**Figure IIIA-20 TLR2 dimerization is blocked by OPN-305**
Superpositioning TLR2 of TLR2/OPN-305-Fab onto TLR2 parts of TLR2/TLR1 and TLR2/TLR6. The structure is rotated by 45° around the vertical and horizontal axes (relative to the structure on the left). TLR2 is shown in green, Fab heavy chain in brown, and Fab light chain in blue, TLR1 in violet, and TLR6 in red.

The superpositioning clearly illustrates that OPN-305 covers a comparable epitope on TLR2 as TLR1 and TLR6 do. Clearly, OPN-305 blocks the TLR-TLR dimerization

interface on TLR2, preventing TLR1 and TLR6 from binding to TLR2 to generate an intracellular signal.

### IIIA.3.4 Analysis of the epitope

The structural similarity of the Fab light and heavy chains results in an approximate 2-fold rotational symmetry along the Fab longest axis and this symmetry is discernible in the EM-determined molecular surface.

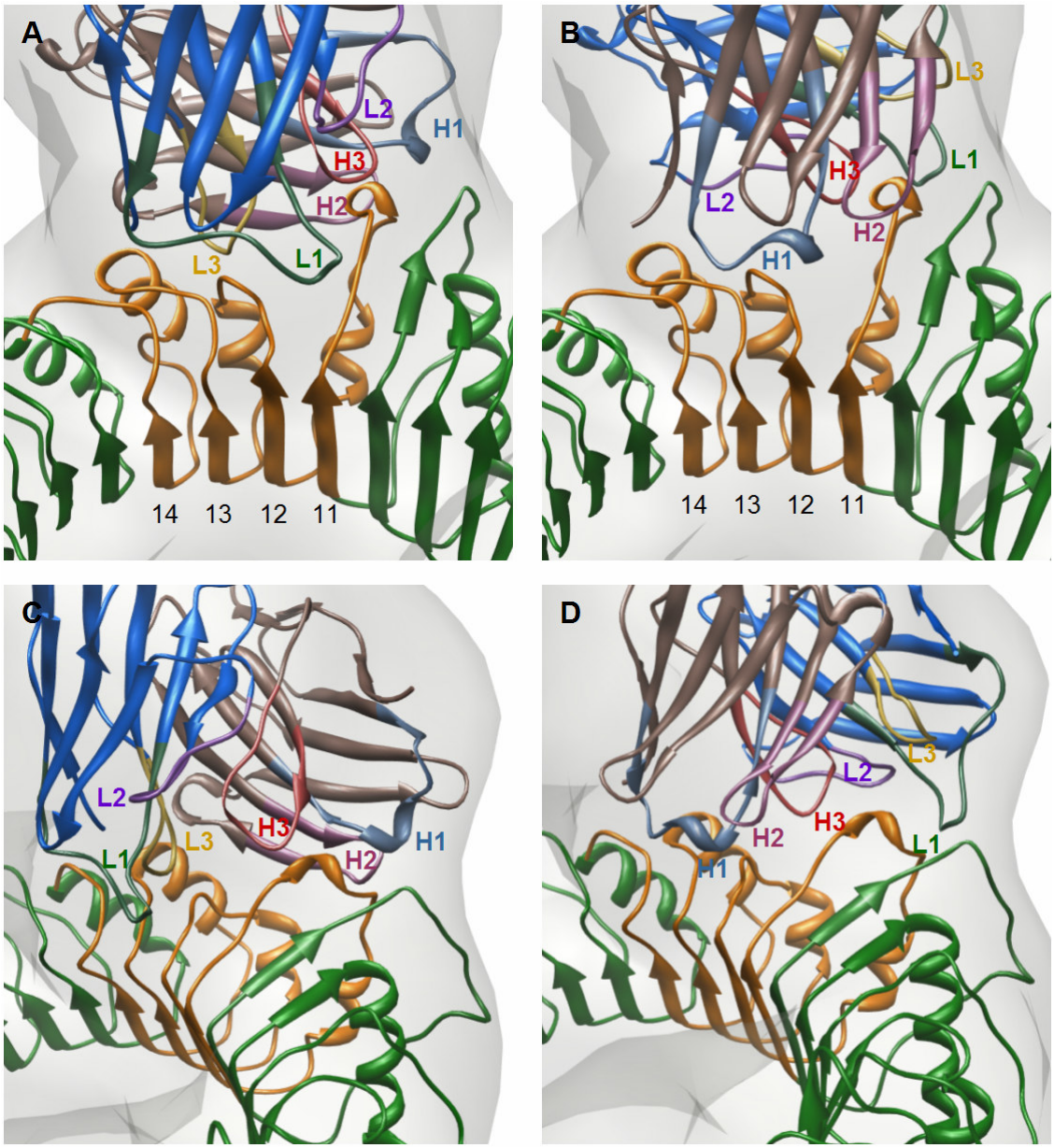


**Figure IIIA-21 Binding of Fab to TLR2 in two theoretical orientations**
Fab orientation #1 (**A and C**) and #2 (**B and D**) in two views. TLR2 is highlighted in green, the leucine rich repeats 11 to 14 of TLR2 in orange, the Fab heavy chain in brown, and the Fab light chain in blue. The six CDRs are coloured individually and are termed H1 – H3 (CDRs of the heavy chain) and L1 – L3 (CDRs of the light chain).

The largest differences between light and heavy chain of a Fab fragment involves the six variable region CDRs, due to the unique sequence, length and conformation of each CDR.

Although one of the two possible orientations of the Fab molecular model results in a better fit to the density (Figure IIIA-18), both orientations were analyzed and compared to comprehensively analyze all possible molecular interactions (Figure IIIA-21). Comparing the binding interface for both Fab rotations indicates that in both cases the CDRs of OPN-305 interact primarily with the lateral surface loops of LRRs 11-14. In particular, the extended loop of LLR11 is crucial for recognition, due to its proximity to at least 3 CDRs of heavy and light chain (Figure IIIA-21).

### IIIA.3.5 TLR2 surface residues involved in Fab interaction

The optimal molecular model derived from the EM molecular surface and the molecular models of the constituent proteins clearly identifies LRRs 11-14 as the dominant site of interaction between TLR2 and the antibody Fab fragment. Despite limitations imposed by the resolution (inherent to the EM method employed) in identifying residues involved in recognition, these residues additionally need to conform to two additional criteria allowing their identity to be narrowed down: 1) Their side chains must face the antibody and 2) the recognition residues of TLR2 should be (partly) conserved in TLR2s from different organisms with which the antibody is known to cross-react.

In total, 10 amino acids on the surface of LRRs 11-14 fulfill the first requirement outlined above, based on the structure of mTLR2 (PDB code 2Z81). They include histidine 318, proline 320, glutamine 321 and tyrosine 323 in LRR11; lysine 347 and phenylalanine 349 in LRR12; leucine 371, glutamate 375 and tyrosine 376 in LRR13; and histidine 398 in LRR14 (Figure IIIA-22).

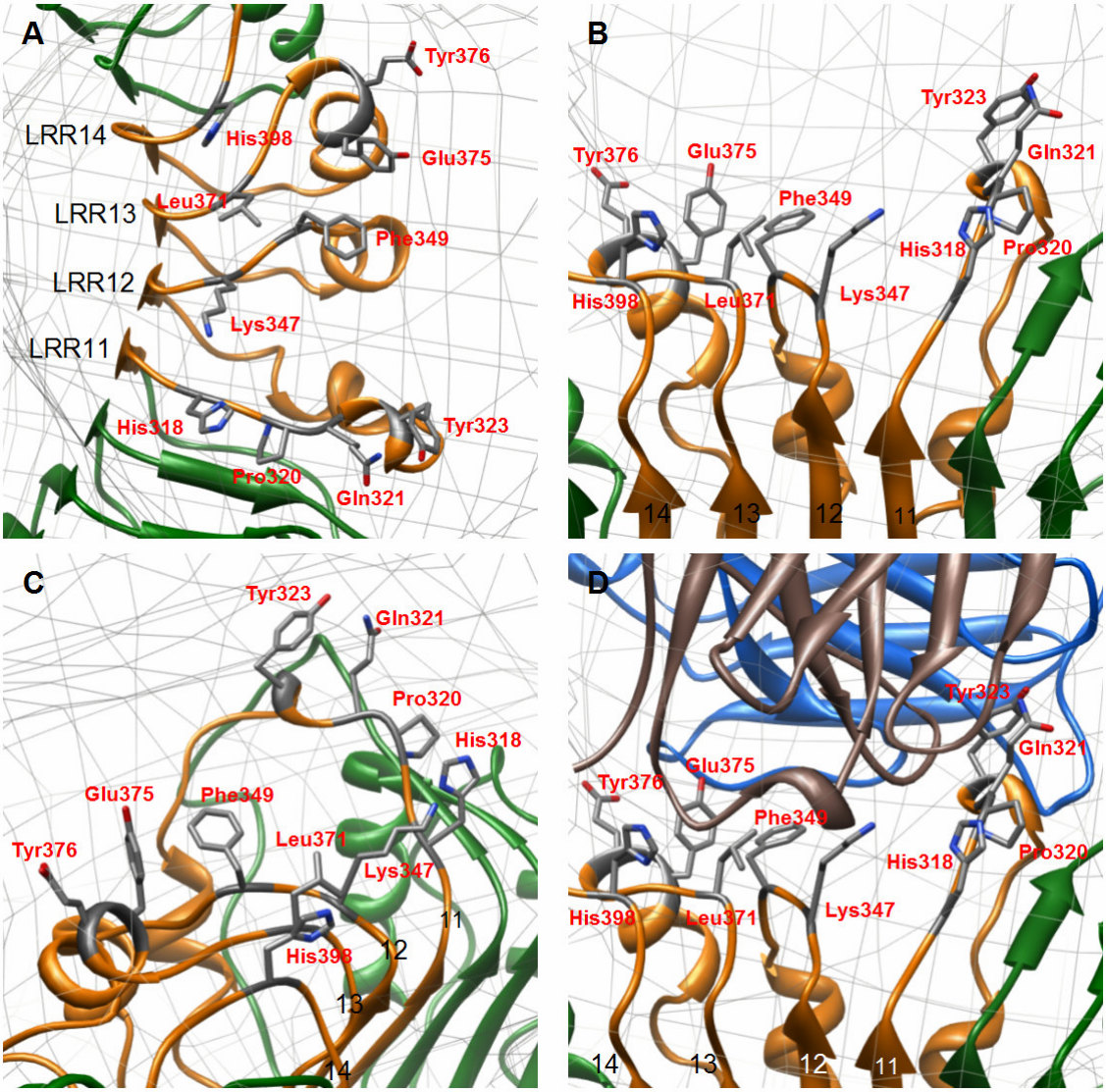


**Figure IIIA-22 Exposed surface residues of mTLR2 involved in recognition by OPN-305**
Surface-exposed residues in LRRs 11-14 of TLR2 are rendered in grey and labeled in red. Ten residues were identified having the highest probability of being involved in antibody interaction. **(A)** Top view, **(B)** front view, **(C)** side view and **(D)** front view with Fab heavy chain (brown) and light chain (blue).

Compliance of the second requirement outlined above, involving residues being conserved in TLR2s from different organisms, was investigated by multi-sequence alignment using the amino acid sequences of LRRs 11-14 from human, murine, apish and porcine TLR2. This analysis reveals that all residues listed above are perfectly conserved in all of these molecules, except glutamine 321 and tyrosine 323 (Figure IIIA-23). Glutamine 321 is replaced by arginine in human TLR2 whereas tyrosine 323 is replaced by phenylalanine in porcine TLR2.

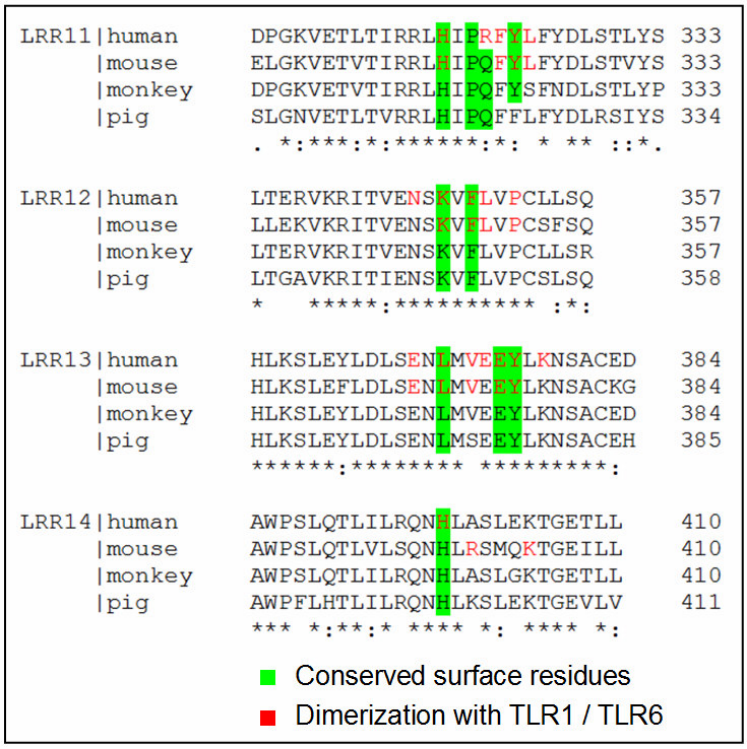


**Figure IIIA-23 Multi-sequence alignment of LRRs 11-14 from different species**
OPN-305 neutralizes TLR2 from different mammals. The amino acid sequences of LRRs 11-14 from human (Uniprot code O60603), murine (Q9QUN7), cynomolgus monkey (Q95M53) and porcine (D3JEM3) TLR2 were aligned. Conserved residues identified as part of the TLR2/Fab interaction interface are highlighted in green. Residues involved in the TLR2 dimerization with TLR1 and TLR6 are highlighted in red. Alignment was performed with ClustalW version 2 (Larkin et al., 2007; Thompson et al., 1994).

The epitope analysis confirms the interpretation that the conserved and exposed amino acids highlighted in Figure IIIA-23 are likely to be involved in the TLR2/OPN-305 interaction. For verification, different residues were chosen to perform single and multiple point mutations to analyze their influence on the antibody affinity using fluorescence-activated cell sorting (FACS) and immunoprecipitation experiments. These trials are currently in progress with our cooperation partner Opsona.

## IIIA.4 Crystallization of the complex

The TLR2/Fab complex used for crystallization was shown to be pure and stable in solution in the experiments described above. In addition, no aggregates could be seen on EM images, indicating the solution to be monodisperse. More than 1000 crystallization conditions were tested at different protein concentrations (5-20 mg/mL) and temperatures (4 °C, 16 °C and 20 °C). First protein crystals of TLR2/Fab (Figure IIIA-24, A) were obtained after 3 weeks for a protein concentration of 20 mg/mL at 16 °C by cross-seeding with InlC crystals from *Listeria monocytogenes* (provided by Lilia Polle, UWC, Cape Town, South Africa) under one distinct condition, comprising 0.1 M MES buffer pH 6, 0.1 M $MgCl_2$, and 8 % PEG6000. These needle clusters were then used for crystal optimization using microseeding so as to obtain single and bigger crystals suitable for diffraction experiments. Crystals could be reproduced, however all resulted in needle clusters (Figure IIIA-24, B+C) or single, but very fragile and thin needles (Figure IIIA-24, C+D).

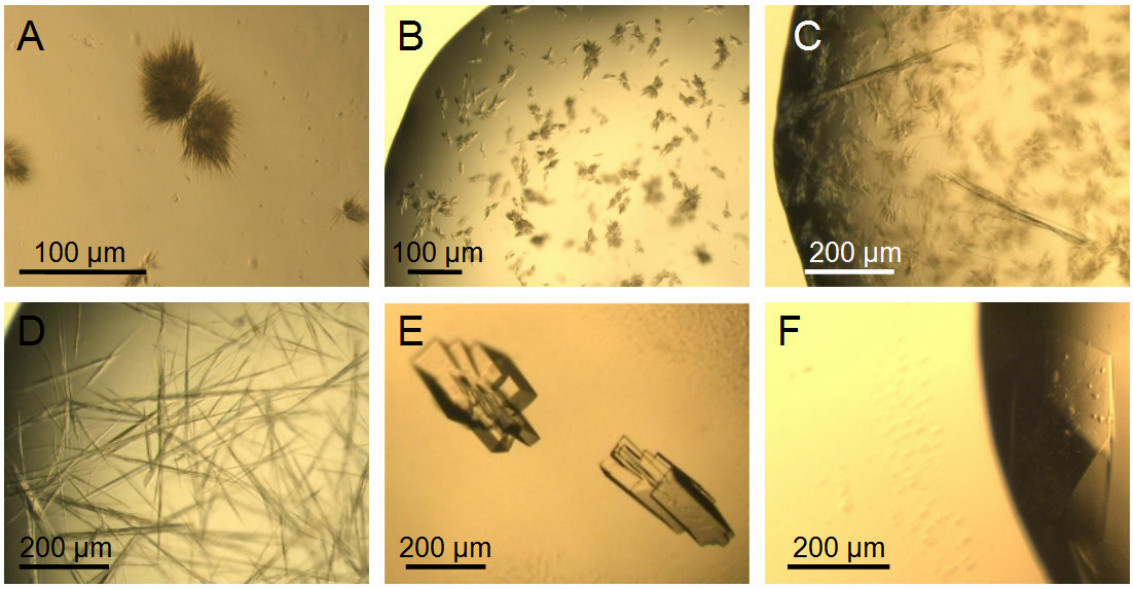


**Figure IIIA-24 Crystals of TLR2/Fab**
Different shapes of crystals from different stages of optimization are shown. **(A)** Initial needle clusters from cross-seeding. **(B)** Reproduction of needle clusters. **(C)** Sporadic single needle crystals within clusters. **(D)** Thin and long needles. **(E)** Crystals grown together. **(F)** Single crystal.

One parameter that may lead to larger and better crystals involves increasing the protein solubility to reduce the rate of crystal growth speed. This may be achieved by adding higher salt concentrations and/or glycerol. In this case higher $MgCl_2$ concentrations

proved successful in increasing the crystal size to up to 300 µm x 200 µm (250 mM $MgCl_2$, Figure IIIA-24, E).

The best crystal of TLR2/Fab was obtained after 2 month by decreasing the protein concentration to 11 mg/mL and in presence of glycerol (0.1 M MES buffer pH 6, 0.12 M $MgCl_2$, 10% PEG6000, 3% glycerol, 16 °C) (Figure IIIA-24, F). This single, large crystal (~500 µm x 200 µm x 200 µm) resulted in weak and smeared diffraction spots to ~8 Å on a rotating anode generator (Rigaku MicroMax-007HF) and CCD detector (Rigaku Saturn944HG) (Figure IIIA-25). 30 % glycerol was used as cryoprotectant. Indexing of the diffraction images using the HKL3000 package identified the most likely the Bravais lattice as C-centered orthorhombic. Unit cell dimensions are a = 176 Å, b = 310 Å, and c = 97 Å.

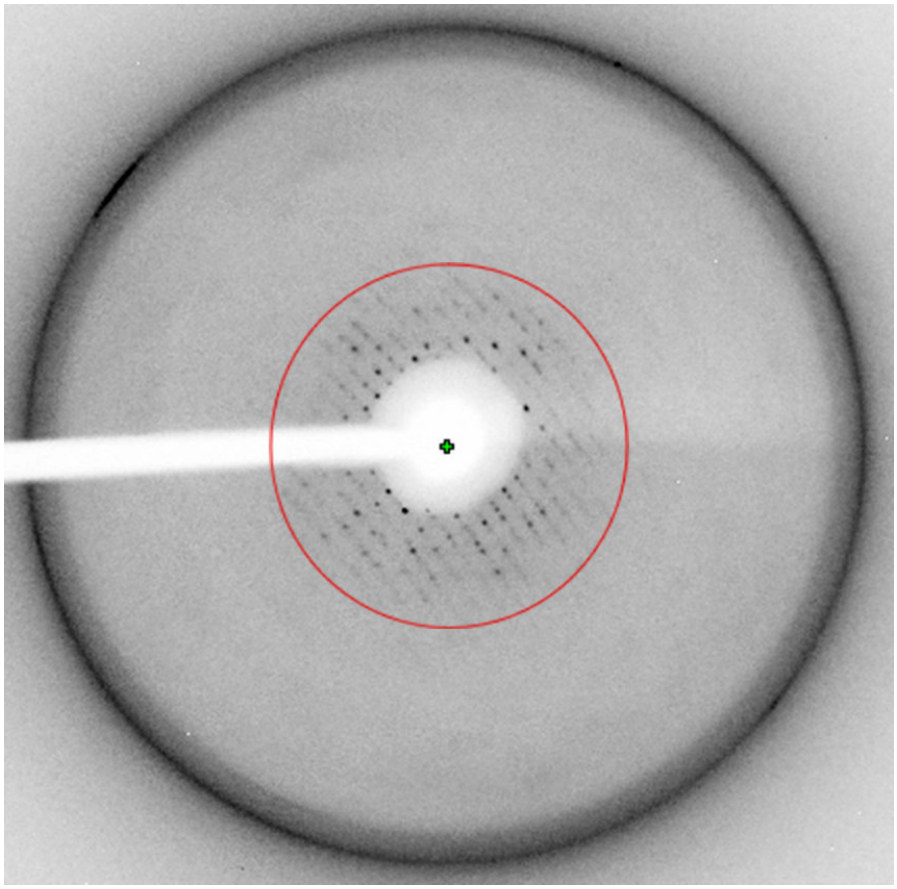

**Figure IIIA-25 Diffraction pattern of TLR2/Fab crystal**
Diffraction of TLR2/Fab (crystal see Figure IIIA-24, F). The position of the direct beam is indicated by a green cross, the red circle marks the resolution shell of 8.0 Å.

A complete dataset was collected, integrated and scaled using HKL3000 programmes Denzo and Scalepack. The weak and anisotropic diffraction pattern as well as the excessively high crystal mosaicity (>3°) resulted in poor scaling parameters and a mere

3413 unique reflections for structure solution and refinement. The completeness of this dataset to 7.9 Å resolution is 98.9 %, the redundancy amounts to 2.6. The $R_{sym}$ in the shell of highest resolution is 64 % (overall $R_{sym}$ = 16 %). Matthews coefficient calculation resulted in $V_m$ = 2.9 $Å^3$/Da assuming two molecules per asymmetric unit with a solvent content of 57 %.

Structure determination by molecular replacement was attempted using programs PHASER and MOLREP from the ccp4 software package. Search models included mTLR2 ECD with and without hagfish domain (crystal structure from Jin et al. 2007) and OPN-305 Fab domain with and without CDRs (structure modeling described in IIB.10). No significant correlation for the models and the dataset were obtained. All MOLREP runs resulted in low "contrast values" (<1.5), a score for the probability of correct solutions calculated as a ratio of the top score to the mean score. Correspondingly MOLREP did not output a coordinate file. In PHASER, likewise no unique solution with meaningful parameters could be found. The highest Z-score for a solution after the fast rotation function was 4.2. A value of >5 is considered as a probable correct solution. The best Z-score after the fast translation function was 5.3 (values >6 are considered as correct solutions). Moreover, packing check revealed numerous clashes. The fewest clashes found for a solution were 13. Solutions for which PDB files were output did not confirm the arrangement of TLR2 and Fab observed by EM. Electron density was only observable as a "random distribution".

Heterogeneous glycosylation of TLR2 can negatively affect the homogeneity of a protein solution adversely affecting protein crystal packing quality and hence diffraction quality. Therefore, in addition to the experiments with glycosylated TLR2 described above, TLR2 was also deglycosylated with PNGase F prior to complex formation and crystallization (see IIIA.1.2). Alternatively, PNGase F was added directly to the crystallization experiment using 1 unit PNGase F per crystallization drop. This treatment did, however, not improve crystal quality, though further experiments are still ongoing.

Other crystallization parameters that were explored but did not positively impact the crystal quality included incubation of crystallization plates at 4 °C, screening for new lead conditions using self-seeding, use of additives (Additive Screen, Hampton Research, California, USA) or purifying TLR2/Fab by anion-exchange rather than size exclusion chromatography.

Although attempts at solving the crystal structure of TLR2/Fab were not successful, the crystals that were obtained constitute a promising starting point for further experiments in this direction.

# IIIB Producing mouse/human Toll-like receptors 2 and 6 in insect cells using the baculovirus expression system

The work described in this chapter was undertaken during the first 1½ years of this thesis at the HZI (Braunschweig, Germany). It was discontinued due to the publishing of the crystal structure of the TLR2/TLR6 complex (Kang et al., 2009). This event further coincided with the relocation of our research group to the University of the Western Cape, Cape Town, South Africa, where a lack of insect cell culture facilities and of corresponding experience prevented the continuation of this type of investigation.

## IIIB.1 Cloning

A first step of the cloning procedure of TLR2 and TLR6 involved replacing the native secretion signal peptides by that of glycoprotein 67 (gp67) of *Autographa californica* nuclear polyhedrosis virus. The latter is known to lead to high levels of secretion and is therefore frequently used to boost the rate of secretion in the baculovirus system. The peptide is cleaved by the cell's native signal peptidase as part of the secretion process.

The central idea was to produce the TLR ECDs recombinantly as a fusion protein with a C-terminal $His_8$-tag followed by an antibody "Fragment crystallizable" (Fc)-tag for rapid purification using Ni-NTA and protein A-sepharose affinity chromatography. The inclusion of a TEV protease cleavage site between the $His_6$- and Fc-tags would allow the facile removal of the Fc-tag as part of the purification procedure (Figure IIIB-1).

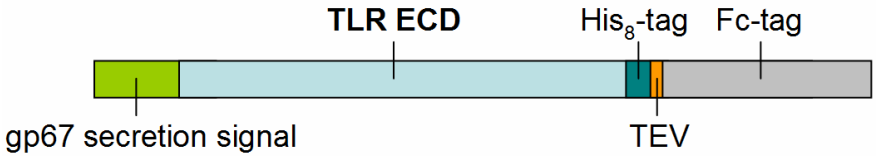


**Figure IIIB-1 Scheme of the recombinant constructs of TLR2 and TLR6 expressed in Sf21 cells**
The native signal peptide was replaced by gp67. The TLR ECD is C-terminally linked to a $His_8$- and an Fc-tag. A TEV protease cleavage site between the two tags allows for the removal of the Fc-tag during purification.

The Fc-tag, a dimer of the C-terminal half of human antibody heavy chains, is recognized by Protein A of *Staphylococcus aureus* with a nanomolar dissociation constant, theoretically allowing for a highly efficient enrichment and purification of the

protein in a single step. This strategy of combining a gp67 signal with an Fc-tag in the TLR constructs was based on a similar approach by Jin *et al.* (2007).

The produced recombinant proteins and their theoretical properties are listed in Table IIIB-1.

**Table IIIB-1 Properties of proteins**

| Construct | Length [aa] | Molecular weight [kDa] | Isoelectric point | Glycosylation sites |
|---|---|---|---|---|
| human $TLR2_{19-588}$-His8-TEV-Fc | 822 | 92,9 | 6,05 | 4 + 1 |
| human $TLR6_{32-586}$-His8-TEV-Fc | 807 | 92,1 | 6,44 | 9 + 1 |
| mouse $TLR2_{25-587}$-His8-TEV-Fc | 815 | 91,9 | 6,10 | 3 + 1 |
| mouse $TLR6_{28-584}$-His8-TEV-Fc | 809 | 91,8 | 6,53 | 10 + 1 |
| Fc | 231 | 26 | 7,72 | 1 |
| human $TLR2_{19-588}$-His8 | 588 | 66,7 | 5,77 | 4 |
| human $TLR6_{32-586}$-His8 | 573 | 65,9 | 6,23 | 9 |
| mouse $TLR2_{25-587}$-His8 | 583 | 65,7 | 5,82 | 3 |
| mouse $TLR6_{28-584}$-His8 | 575 | 65,6 | 6,33 | 10 |

The recombinant proteins have different numbers of N-linked glycosylation sites depending on the TLR type and the mammalian species plus an additional site in the Fc region (Table IIIB-1). The molecular weight (MW) shown in this table is calculated from the amino acids ignoring the glycosylation. Insect cells glycosylate proteins posttranslationally. However the variability of the glycosylation and later processing (~1-3 kDa per glycosylation site) prevent the accurate prediction of the true MW.

For simplicity, the four recombinant proteins human $TLR2_{19-588}$-$His_8$-TEV-Fc, human $TLR6_{32-586}$-$His_8$-TEV-Fc, mouse $TLR2_{25-587}$-$His_8$-TEV-Fc and mouse $TLR6_{28-584}$-$His_8$-TEV-Fc will henceforth be denoted hTLR2-His-Fc, hTLR6-His-Fc, mTLR2-His-Fc and mTLR6-His-Fc.

The cloning strategy to form the recombinant pFastBac1 (pFB) plasmids necessary for Bacmid-DNA generation involved four individual steps: i) PCR amplification of the Fc fragment from a donor plasmid using primers yielding a TEV-Fc DNA fragment flanked by appropriate restriction sites (Figure IIIB-2, A), ii) cloning of TEV-Fc into the vector pFB (Figure IIIB-2, B), iii) cloning of synthesized gp67-$hTLR6_{32-586}$-$His_8$

fragment into pFB-TEV-Fc (Figure IIIB-2, C and D), and iv) replacement of hTLR6 ECD by mTLR2 ECD, mTLR6 ECD and hTLR2 ECD genomic DNA (Figure IIIB-3). All products were verified by sequencing. Using the Tn7 sites of pFB the target DNA was then integrated into the Bacmid-DNA by site-specific transposition.

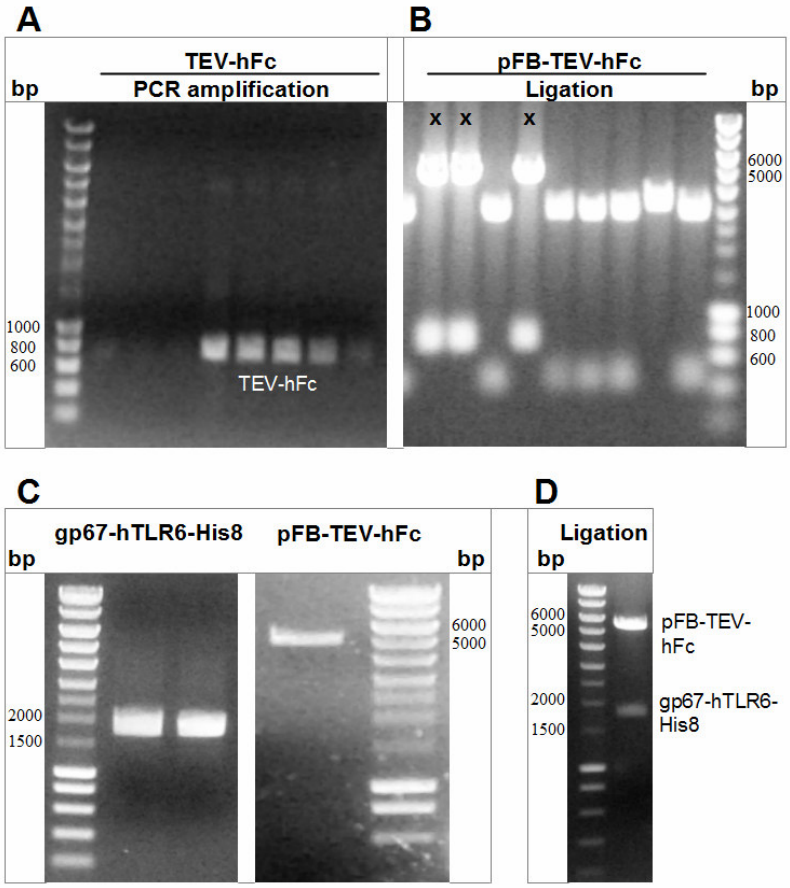


**Figure IIIB-2 Cloning of pFB-gp67-hTL6-His-TEV-Fc**
Agarose gel electrophoresis was performed to analyze the individual cloning products. **(A)** PCR products after amplification of hFc from the plasmid pCMV-hFc-XP using primers yielding a TEV-hFc DNA fragment. **(B)** TEV-hFc fragment and pFB were cut with restriction enzymes and ligated to form pFB-TEV-hFc. After cloning, a test restriction was performed to cut the insert. Samples bearing inserts with correct size are marked with an "x". **(C)** The synthesized DNA fragment gp67-hTLR6-$His_8$ (left gel) and pFB-TEV-hFc (right gel) were digested with the same restriction enzymes and analyzed on the agarose gel. **(D)** gp67-hTLR6-$His_8$ was cloned into pFB-TEV-hFc. The success of the ligation was verified by cutting of the cloned insert and analysis of the DNA fragments on the agarose gel. Molecular weight marker: Smart Ladder (Eurogentec).

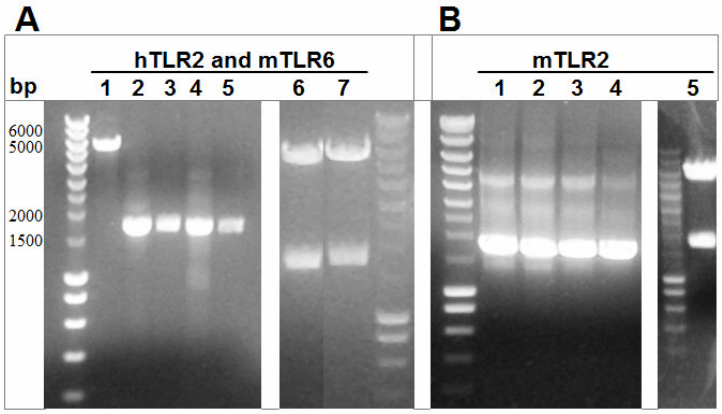


**Figure IIIB-3 Cloning of hTLR2, mTLR6 and mTLR2**
pFB plasmids bearing hTLR2, mTLR6 and mTLR2 were cloned by replacing hTLR6 in pFB-gp67-hTL6-His-TEV-Fc. **(A)** Enzymatic restriction of the plasmid yielding pFB-gp67-/-$His_8$-TEV-hFc (1), PCR products of hTLR2 (2) and mTLR6 (3), purified and restricted PCR products of hTLR2 (4) and mTLR6 (5), and test restriction of the final plasmids by cutting of hTLR2 (6) and mTLR6 (7). **(B)** PCR products of mTLR2 (1-4), and test restriction of the final plasmid by cutting of mTLR2 (5). Molecular weight marker: Smart Ladder (Eurogentec).

For a detailed description of the cloning strategy, see Materials and Methods (IIC.1).

## IIIB.2 Virus amplification

After generating and isolating bacmid-DNAs encoding the four TLR gene constructs (denotation of the clones: mouseTLR2-K9-MP1, mouseTLR6-K14-MP1, humanTLR2-K3-MP2, humanTLR6-K7-MP3), the DNA was transfected into Sf21 insect cells. The transfected cells were incubated in ExCell medium for the initial virus production. A plaque assay was performed after 48 h of incubation to determine the virus concentration in the medium (plaque forming units per milliliter, pfu/mL). Knowing the titer in solution the virus was amplified using a MOI (multiplicity of infection) of 0.1 – 0.5, which is the ratio of viruses to cells during infection. In the case of mTLR2-His-Fc and mTLR6-His-Fc three circles of amplification and plaque assay were performed to obtain a final volume of 700 mL with a virus titer of 1.0 x $10^8$ (mTLR2-His-Fc) and 0.7 x $10^8$ (mTLR6-His-Fc) pfu/mL respectively. For hTLR2-His-Fc and hTLR6-His-Fc the virus was amplified in a single step to a volume of 100 mL with a virus titer of 0.4 x $10^7$ (hTLR2-His-Fc) and 1.1 x $10^7$ (hTLR6-His-Fc) pfu/mL respectively (Table IIIB-2). An example of a plaque assay is shown in Figure IIIB-4. During amplification, the shape, cell density and vitality of the virus infected cells, were monitored daily to control the infection efficiency. Cell rounding was observed due to the virus production within the

cells, leading to a swelling of the mean cell diameter to above 20 µm (Table IIIB-2) and finally to the cell death. The viruses were harvested 4-5 days after infection, if the vitality of the cells was reduced to at least 60%.

**Table IIIB-2 Virus amplification of the four TLR clones**

| | Mean diameter | Peak diameter | Virus titer [pfu/mL] | Final volume virus solution |
|---|---|---|---|---|
| | | | | |
| | after transfection | | | |
| **mTLR2-His-Fc** | | | $3.9 \times 10^5$ | 4 mL |
| **mTLR6-His-Fc** | | | $1.6 \times 10^6$ | 4 mL |
| **hTLR2-His-Fc** | | | $1.5 \times 10^7$ | 4 mL |
| **hTLR6-His-Fc** | | | $1.1 \times 10^7$ | 4 mL |
| | after 1st virus amplification | | | |
| **mTLR2-His-Fc** | 20.9 µm | 21.9 µm | $0.5 \times 10^7$ | 15 mL |
| **mTLR6-His-Fc** | 20.4 µm | 22.1 µm | $1.5 \times 10^7$ | 15 mL |
| **hTLR2-His-Fc** | 21.1 µm | 21.2 µm | $0.4 \times 10^7$ | 100 mL |
| **hTLR6-His-Fc** | 21.1 µm | 21.3 µm | $1.1 \times 10^7$ | 100 mL |
| | after 2nd virus amplification | | | |
| **mTLR2-His-Fc** | 20.7 µm | 20.6 µm | $1.3 \times 10^7$ | 30 mL |
| **mTLR6-His-Fc** | 20.3 µm | 20.6 µm | $2.5 \times 10^6$ | 30 mL |
| | after 3rd virus amplification | | | |
| **mTLR2-His-Fc** | 22.1 µm | 22.2 µm | $1.0 \times 10^8$ | 700 mL |
| **mTLR6-His-Fc** | 22.1 µm | 22.1 µm | $0.7 \times 10^8$ | 700 mL |

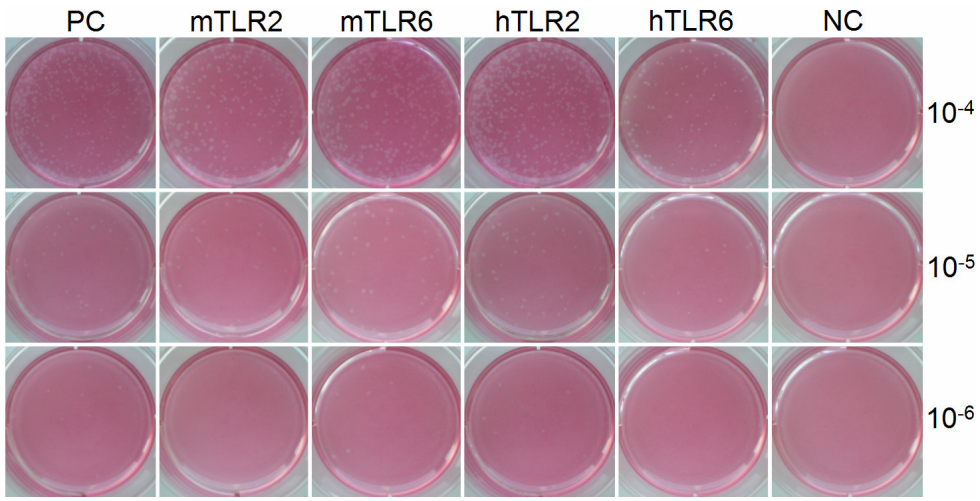


**Figure IIIB-4 Plaque assay from amplified virus**
Assay of hTLR2-His-Fc and hTLR6-His-Fc after the 1st round of virus amplification and of mTLR2-His-Fc and mTLR6-His-Fc after the 2nd round. Three virus dilutions ($10^{-4}$, $10^{-5}$, $10^{-6}$) were analyzed. White plaques were counted to calculate the virus concentration. One plaque derives from a single virus infecting a single cell. Positive controls (PC, Toshi virus with known titer) and negative controls (NC, medium) were performed.

## IIIB.3 Expression test

The amplified virus was used in an expression test to establish its ability to induce expression and secretion of soluble protein in insect cells. 20 mL of cells using a MOI of 2 were used. Samples of the cell supernatant were taken 24 h, 48 h and 72 h after infection. Produced and secreted protein in the samples was identified by Western blotting using an anti-$His_6$-tag antibody (Figure IIIB-5).

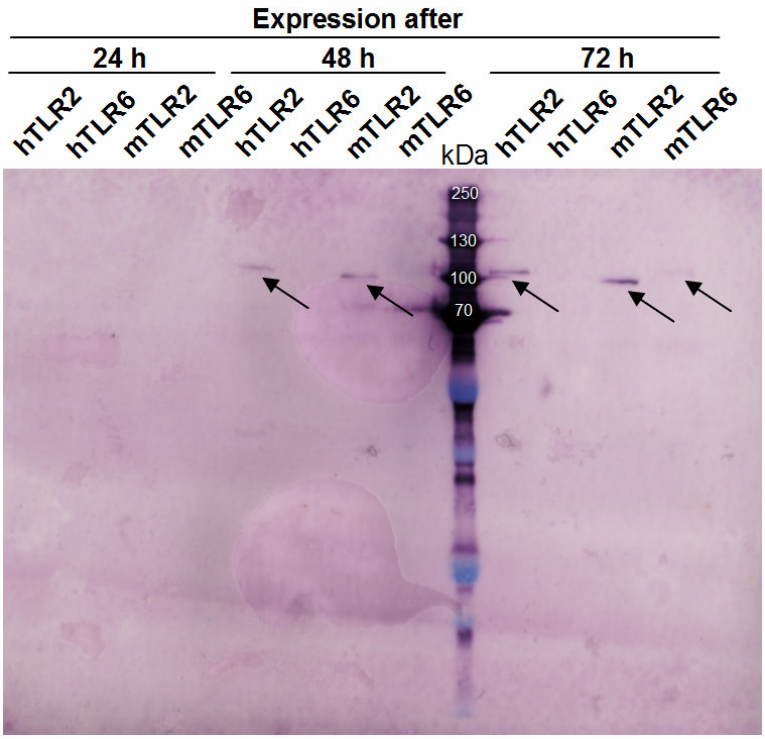


**Figure IIIB-5 Expression of TLR constructs in insect cells**
Western blot of mTLR2-His-Fc, mTLR6-His-Fc, hTLR2-His-Fc and hTLR6-His-Fc expressed in Sf21 insect cells for 24 h, 48 h and 72 h. Produced protein was detected after 48 h and 72 h in the case of mTLR2-His-Fc, mTLR6-His-Fc and hTLR2-His-Fc, but not in the case of hTLR6-His-Fc. Molecular weight marker: “Precision Plus Protein All Blue Standard” (BioRad).

The Western blot indicates that mTLR2-His-Fc and hTLR2-His-Fc had successful been produced after 48 h and 72 h incubation. Trace amounts of mTLR6-His-Fc were produced after 72 h, while hTLR6-His-Fc does not appear to be produced. Depending on the number of glycosylation sites and degree of glycosylation, the actual molecular weight of the produced proteins is about 10 kDa (mTLR2-His-Fc) to 20 kDa (mTLR6-His-Fc and hTLR2-His-Fc) higher than the theoretical weight (~92 kDa, see Table IIIB-1) calculated from the amino acid composition.

The secretion rate of mTLR2-His-Fc was compared to that of soluble and insoluble intracellular protein (Figure IIIB-6).

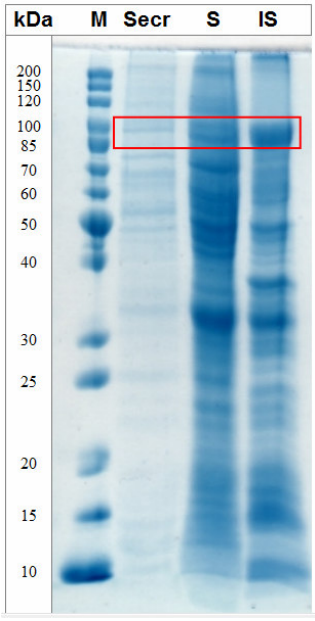


**Figure IIIB-6 Secretion rate of expressed mTLR2-His-Fc**
Protein samples were extracted with Cytobuster reagent (Novagen) from 4 x $10^6$ cells separated into (Secr), intracellular soluble (S) and intracellular insoluble (IS) fractions. Molecular weight marker (M): "PageRuler Unstained Ladder" (Fermentas).

A strong band in the insoluble fraction indicates that the largest fraction of mTLR2-His-Fc ends up in intracellular inclusion bodies. A smaller fraction is successfully secreted as seen in a band at about 100 kDa in the secretion fraction matching the band of mTLR2-His-Fc observed in the Western blot.

## IIIB.4 Protein purification

Protein purification was performed to analyze if the properties of the designed recombinant proteins with Fc-tag and TEV protease cleavage site (Figure IIIB-1) can be optimally used.

A sample of each produced protein was purified to establish whether the $His_6$- and Fc-tags as well as the TEV protease cleavage site (Figure IIIB-1) are functional. The first step involved Protein A affinity chromatography (AC): Each protein fraction was mixed with Protein A sepharose matrix to allow protein coupling. The matrix was then washed with buffer to remove any impurities. The protein composition of matrix beads and wash fractions was analyzed by SDS-PAGE (Figure IIIB-7).

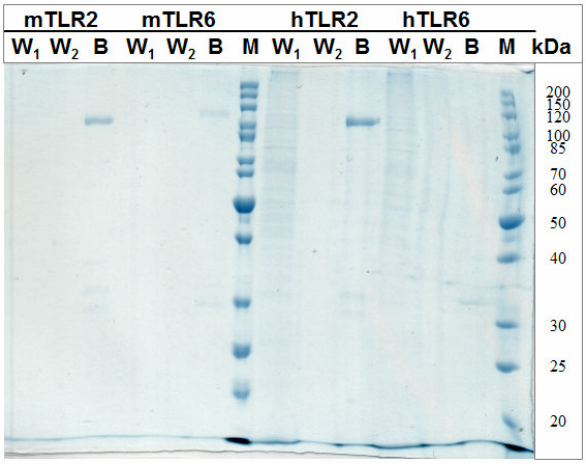


**Figure IIIB-7 Purification of TLR-His-Fc by Protein A affinity chromatography**
For each TLR species two wash fractions ($W_1$ + $W_2$) and a matrix beads fraction (B) were collected and applied on the gel. Molecular weight marker (M): "PageRuler Unstained Ladder" (Fermentas).

As previously observed in the Western blot, mTLR2-His-Fc and hTLR2-His-Fc were most strongly produced, mTLR6-His-Fc was produced to a significantly lower level, whereas hTLR6-His-Fc was not expressed at all. The band corresponding to mTLR6-His-Fc (115 kDa) ran slightly above that of mTLR2-His-Fc and hTLR2-His-Fc (105 kDa) due to the higher degree of glycosylation.

Overall the fusion proteins were enriched and separated from any other proteins very efficiently by Protein A AC. Only weak bands corresponding to impurities can be observed at ~30 kDa in the lanes containing the bead samples (Figure IIIB-7, lanes B).

In a next step, the attempt was made to elute the target proteins from the column by TEV protease cleavage, after which the Fc-tag would remain bound to the column and TLR-His could be collected in the flow through.

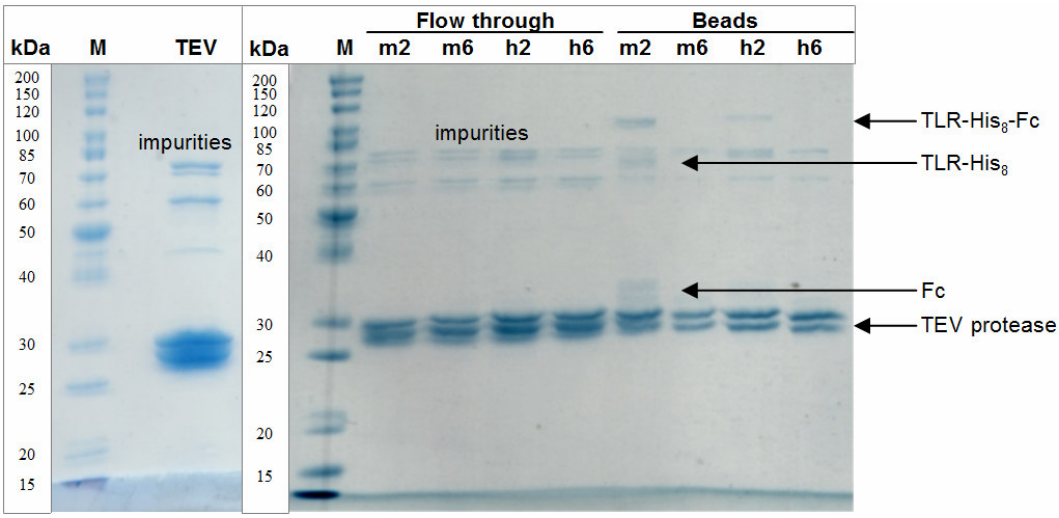


**Figure IIIB-8 TEV protease cleavage of TLR-His-Fc**
Flow through and matrix beads samples of mTLR2-His-Fc (m2), mTLR6-His-Fc (m6), hTLR2-His-Fc (h2) and hTLR6-His-Fc (h6) after TEV protease cleavage were analyzed by SDS-PAGE. TEV protease (TEV) was run as control. Molecular weight marker (M): "PageRuler Unstained Ladder" (Fermentas).

The beads were incubated with TEV protease over night at 4 °C. The soluble fraction was then eluted and the beads washed with buffer. The SDS gel (Figure IIIB-8) reveals bands at 60 kDa and between 70 kDa and 85 kDa for all protein samples. By comparison with a TEV protease control these were identified as impurities in this preparation. The common bands therefore need to be ignored in analyzing the protein samples.

The TEV protease should have cleaved each TLR-$His_8$-Fcs into two protein fragments: TLR-$His_8$ of about 70 kDa (65 kDa + glycosylation) in the flow through and Fc of about 30 kDa (26 kDa + glycosylation) bound to the matrix (see properties in Table IIIB-1). However, no bands other than the TEV protease and its impurities are visible in the eluted fractions. Instead, a weak band at 70 kDa is apparent for the bead sample m2 matching the expected size of cleaved mTLR2-His. The same lane reveals several additional bands above the TEV protease at about 32-35 kDa, which may represent the Fc-tag.

This result suggests that partial cleavage of mTLR2-His-Fc appears to have taken place but that the larger fraction of the protein was uncleaved and remained bound to the matrix. Liberated mTLR2-His possibly aggregated or bound unspecifically to the beads, preventing it from elute from the column. The same may be true for hTLR2-His-Fc, but the protein concentration was too low to visualize the protein on the gel. Longer

incubation of the protein-coupled matrix with TEV protease at room temperature did not lead to an increase in elution of the protein.

To confirm the identity of the bands between 30-35 kDa in Figure IIIB-8 as the Fc-tag, a Western blot was run on TEV protease cleaved samples using an anti-Fc antibody to identify the Fc fragment.

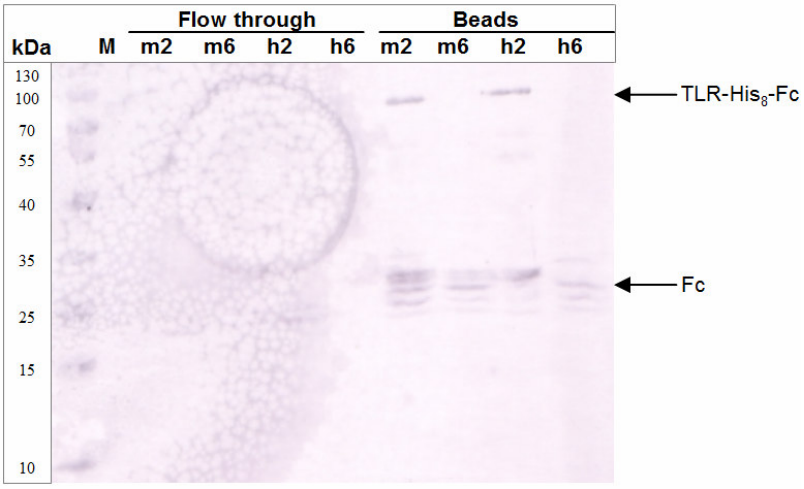


**Figure IIIB-9 Western blot of TLR-His-Fc after TEV protease cleavage**
mTLR2-His-Fc (m2), mTLR6-His-Fc (m6), hTLR2-His-Fc (h2) and hTLR6-His-Fc (h6) were incubated with TEV protease. After cleavage, flow through and matrix beads samples were analyzed on a Western blot by immunostaining with an anti-Fc antibody. Molecular weight marker (M): "PageRuler Prestained Ladder" (Fermentas).

As expected, no bands were identified in the flow through fractions by immunostaining with an anti-Fc antibody (Figure IIIB-9). The proteins mTLR2-His-Fc and hTLR2-His-Fc were stained in the beads fractions. Furthermore, several bands can be observed between 25 kDa and 35 kDa - similar to the SDS-PAGE in Figure IIIB-8 - even in the lanes for mTLR6 and hTLR6 where no uncleaved proteins could be detected. The identification of the Fc fragment confirms that all recombinant proteins were partially cleaved. The varying sizes of Fc can be explained by heterogeneous glycosylation of the protein.

Because of the high affinity of Protein A for Fc-tagged proteins, the only method of eluting the uncleaved fusion-protein would be to change the pH to below pH 4. This would risk precipitating the protein. Correspondingly, elution of fusion proteins with acidic buffer led to their irreversible denaturation.

## IIIB.5 DNA constructs: New strategies

As the last experimental part in this project, two modifications of the previous DNA constructs were designed to improve secretion and purification of the TLR variants.

The first approach involved inserting a stop codon directly downstream of the $His_8$-tag by quick change mutagenesis to remove the uncleavable Fc-tag. The aim was to test whether the Fc-tag itself negatively affected the secretion of the protein. Were this so, the four proteins could then have been produced and purified without the additional purification tag.

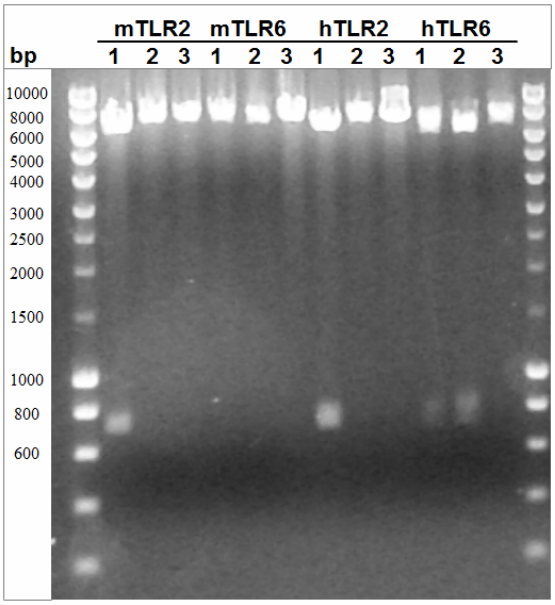


**Figure IIIB-10 Agarose gel of TLR plasmids after stop codon insertion**
NheI/NotI restriction of TLR-His-Fc plasmid-DNA after mutagenesis. From each TLR species, the DNA from three colonies (1-3) was analyzed. Successful mutagenesis would have removed a NheI site and resulting in a single, linearized band. Unchanged clones would show an additional band at 700 bp resulting from NheI/NotI. At least one positive clone could be isolated from each TLR construct. Molecular weight marker: Smart Ladder (Eurogentec).

A stop codon was inserted within a NheI restriction site, downstream of the $His_8$-tag. Successful mutagenesis would therefore remove the NheI site. For verification, the isolated DNA was digested with NheI and NotI (Figure IIIB-10). Positive clones were identified as single bands of linearized DNA on the agarose gel, whereas negative clones resulted in an additional band between 600 and 800 bp. One positive clone was chosen from each TLR variant and was sent for sequencing.

In a second approach, a 15 base pair spacer was to be inserted between the TEV protease cleavage site and the Fc-tag by quick change mutagenesis to improve steric access of TEV protease to the encoded cleavage site increasing the efficiency of the protease (Figure IIIB-11).

**TLR Spacer Forward Primer**

| 15 bases N-Term | Loop | 15 bases C-Term |
|---|---|---|
| CTTTATTTTCAGGGC | GGTGCGGGCGGTGAG | CCCAAATCTTGTGAC |
| TEV protease site | | Fc-tag |

**TLR Spacer Reverse Primer (reverse complement to forward primer)**

| 15 bases N-Term | Loop | 15 bases C-Term |
|---|---|---|
| GTCACAAGATTTGGG | CTCACCGCCCGCACC | GCCCTGAAAATAAAG |
| Fc-tag | | TEV protease site |

**Figure IIIB-11 Loop insertion between TEV site and Fc tag**
The base sequence GGTGCGGGCGGTGAG coding for the amino acids GlyAlaGlyGlyGlu was inserted as a linker between the TEV protease cleavage site and the Fc-tag to improve steric access to the cleavage site by TEV protease.

All TLR constructs were successfully modified according to both mutagenic strategies, verified by sequencing, and hence provide a potential starting point for new bacmid-DNA generation, insect cell protein expression and purification trials. These experiments were not performed as part of this thesis due to the reasons outlined above.

# IV Discussion

## IVA Negative stain EM of TLR2/OPN-305

Negative stain EM is a common technique to image macromolecules. The biomolecules are embedded in a dried film of heavy-metal salt such as uranyl acetate to fix the specimen on the grid and to surround the specimen with a strong electron scatterer. It leads to high contrast images as mainly the surrounded stain but only little the specimen is deflecting the incoming electrons. Inherently, the final resolution is limited by the grain size to ~20 Å (Wang and Sigworth, 2006). Cryo-EM is an alternative technique, in which the protein specimen is rapidly cooled to below -160 °C without any stain. It allows for molecular resolution in the range of 10 Å and higher. However, the signal-to-noise ratio and the contrast of cryo-images are lower than for negative stain EM (Wang and Sigworth, 2006). This technique is therefore more suitable for large macromolecules above 500 kDa which inherently result in a stronger signal. Examples in this size range include membrane channels (Ludtke et al., 2005), ribosome subunits (Stark, 2002) or chaperonins (Falke et al., 2005). Obtaining structural information for the 117 kDa complex of mTLR2/OPN-305 by cryo-EM was attempted as part of this project. However, these were not been successful as no molecules were observable under the microscope. The resolution for the complex of mTLR2/OPN-305 is close to the theoretical limit for negative stain experiments and is thus comparable (Kim et al., 2004) or even better (Pruitt et al., 2010) than other structures solved by negative EM.

### IVA.1 The EM docking: models and orientations

OPN-305 is a humanized version of the parent OPN-301 murine IgG1 antibody. This was done to reduce its immunogenicity in humans as compared to murine antibodies. The humanized antibody retains the efficiency of the original murine version in *in vitro* cell based bioassays (OPN-305 patent, International Patent Number WO/2011/003925, Opsona Therapeutics). However, no OPN-305 crystal structure is currently available for EM density docking. As the antibody was created by grafting CDR loops onto a human IgG4 framework, we similarly used the crystal structure of the Fab fragment of IgG4 antibody b12 (PDB code 2NY7), which shares a high sequence identity with OPN-305 of 84 % (heavy chain) and 87 % (light chain), respectively, when excluding the CDRs.

Sequence differences exclusively occur in the variable domains of light and heavy chain. To optimize the antibody model, the CDR loops of b12 were replaced with those of OPN-305, modeled using the structure modeling server Swiss-Model. Overall, Qmean4 scores of 0.818 and 0.685 for heavy chain and light chain, respectively, suggest a high reliability of the model (see Results, Figure IIIA-16). Z-scores of 0.14 for the heavy chain and -1.19 for the light chain are close to zero and indicate a high likelihood that the model is of comparable quality to experimental structures. Based on the Anolea and Qmean scores for the individual amino acid residues, the weakest reliability was calculated for the CDR regions. For more details about Swiss-Model model evaluation, see Material and Methods IIB.10.

Although an increasing number of crystal structures of antibody Fab domains are being solved, predicting the conformation of CDRs still remains a difficult task, as the variable loops demonstrate a significant range of lengths, sequences and conformations (Shirai et al., 1999). Analysis of more than 300 crystal structures of antibody variable domains, 80 conformational clusters were identified and CDRs were grouped by their length combinations (North et al., 2010). CDRs for all crystal structures except H3 fall within a favoured length distribution. Thus 45 % of light chain CDR 1 (L1) comprises 11 residues – summarized as “L1: 45%/11”. Figures for the remaining CDRs are L2: 98%/8; L3: 85%/9; H1: 93%/13; H2: 67%/10. Four of six CDRs in OPN-305 Fab (L2, L3, H1 and H2) fall within these dominant groups of CDR lengths. L1 with a length of 15 residues belongs to a minor cluster comprising 4% of structures, whereas H3 with 11 residues shares this with 8% of structures. Prediction of L2, L3, H1 and H2 conformations would therefore presumably be more accurate due to the availability of more reference structures for homology modeling. In accordance, Swiss-Model Anolea and Qmean scores indicate a lower model quality especially for H3 (see Results, Figure IIIA-16). The Swiss-Model scores for L1, L2, L3, H1, and H2 show comparable values. While the length and sequence of the CDRs for OPN-305 Fab are known and are correctly reflected in our generated structural model, the determination of the true CDR conformations would need to be determined by high resolution techniques such as X-ray crystallography.

As Fab fragments have an approximate 2-fold rotational symmetry around the longest axis of the domain, the OPN-305 Fab structural model has been initially modeled in two possible orientations (denoted Fab#1 and Fab#2) into the EM derived molecular

surface. By comparison of the two orientations, it was possible to constitute Fab#2 beeing the more probable orientation. Fab#2 reveals a better agreement of structural model and EM molecular surface by showing fewer clashes between model and EM surface (see Results, Figure IIIA-18).

Crystal structures of mTLR2 are available for lipopeptide-bound monomers (Jin et al., 2007) and for the complex with lipopeptides and mTLR6 (Kang et al., 2009). To optimally explain the EM-derived molecular surface, we chose the crystal structure of monomeric mTLR2 (PDB code 2Z81) as this provides the most accurate structural information at a resolution of 1.8 Å. All currently available TLR2 structures constitute hybrid molecules in which LRR modules of the hagfish Variable Lymphocyte Receptor (VLRs) replace the C-terminal amino acids 507-587 of the TLR2 ECD including capping domain (Jin and Lee, 2008a). We have chosen to make use of these hybrid TLR2 ECD-VLR structures in lieu of TLR2 ECD in interpreting the EM results and to analyze the interaction between OPN-305 and TLR2. This was done because i) VLRs adopt standard LRR conformations (Jin and Lee, 2008a), ii) the mTLR2-VLR chimera is similar in length to native mTLR2 and iii) the VLR domain is not itself in contact with the antibody.

Similar to the Fab fragment, the almost planar shape of TLR-ECD results in an approximate 2-fold rotational symmetry allowing mTLR2 to be placed into the EM molecular surface in two orientations (denoted as TLR#1 and TLR#2). In TLR#1, the surface area involved in dimerization with TLR1 and TLR6 faces the OPN-305 Fab fragment, whereas the dimerization site would face away from the Fab in TLR#2. Major clashes with the EM molecular surface could be observed for TLR#2 (see Results, Figure IIIA-19). Coincidentally, as outlined above, the TLR2/TLR1 or 6 dimerization surface of TLR2 faces the variable domain of OPN-305 in TLR#1, providing and immediate structural explanation for the neutralizing effect of this antibody in that this site would be completely blocked by the antibody, preventing dimerization of TLR2 with either TLR1 or TLR6 and hence downstream signaling. Based on these observations TLR#1 was identified as the correct orientation.

## IVA.2 The antibody epitope on TLR2

Following the determination of the correct orientations for both Fab and TLR2 within the EM-derived molecular surface, the inhibition of TLR2 by OPN-305 can be clearly described in structural terms as the physical blocking of the dimerization site on the TLR2 surface by OPN-305. Correspondingly, OPN-305 binding to TLR2 sterically prevents TLR1 or TLR6 from accessing the dimerization interface and hence from forming heterodimers with TLR2. OPN-305 therefore specifically inhibits the TLR2-dependent pro-inflammatory response. This interpretation directly confirms the observation that OPN-305 inhibits $Pam_3CSK_4$-induced production of IFN-γ, IL-1β, IL-6, TNF-α and IL-8 in mononuclear cells in peripheral blood and synovial fluid and also inhibits spontaneous cytokine production in rheumatoid arthritis synovial tissue explant cultures *ex vivo* (Ultaigh et al., 2011). The inhibition is dose dependant, and in a sepsis model in mice cytokine production induced by $Pam_3CSK_4$ could be completely ablated by systemic pretreatment with 2 mg/kg OPN-301 (Farrar et al., 2011). The same authors used a concentration of 10 mg/mL for *in vivo*, post-renal transplantation in mice to analyze the effect of OPN-301 on postischemic renal failure and observed a significantly improved renal function. The half-life of the antibody is 8-9 days and remains functional over a period of 14 days (Farrar et al., 2011). This observation is consistent with our laboratory experience of the antibody remaining structurally intact over weeks. For the prevention of I/R injury after organ transplants or myocardial infarction the pretreatment with antibodies with a long half-life is beneficial to stabilize the treated organ over a long time span by requirement fewer drug administrations (Arslan et al., 2010b). In animal and *in vitro* experiments no adverse effects have been noted for antibody blocked TLR2. OPN-305 is currently used in a healthy volunteer study to calculate the dosing for the phase II efficacy study (oral conservation with William McCormack, Opsona Therapeutics).

Successful purification of the TLR2/OPN-305 Fab complex by size exclusion chromatography and the stability of the complex during native PAGE suggest a high binding affinity with a dissociation constant ($K_D$) of 100 nM or below. The existence of a strong interaction is further supported by the observation that OPN-305 recognizes a discontinuous epitope involving surface-exposed residues from several LRRs. Experimental determination of the binding affinity by SPR spectroscopy yielded a $K_D$ =

11.9 nM for OPN-305 with mTLR2 and $K_D$ = 28.9 nM with hTLR2 (OPN-305 patent, International Patent Number WO/2011/003925, Opsona Therapeutics).

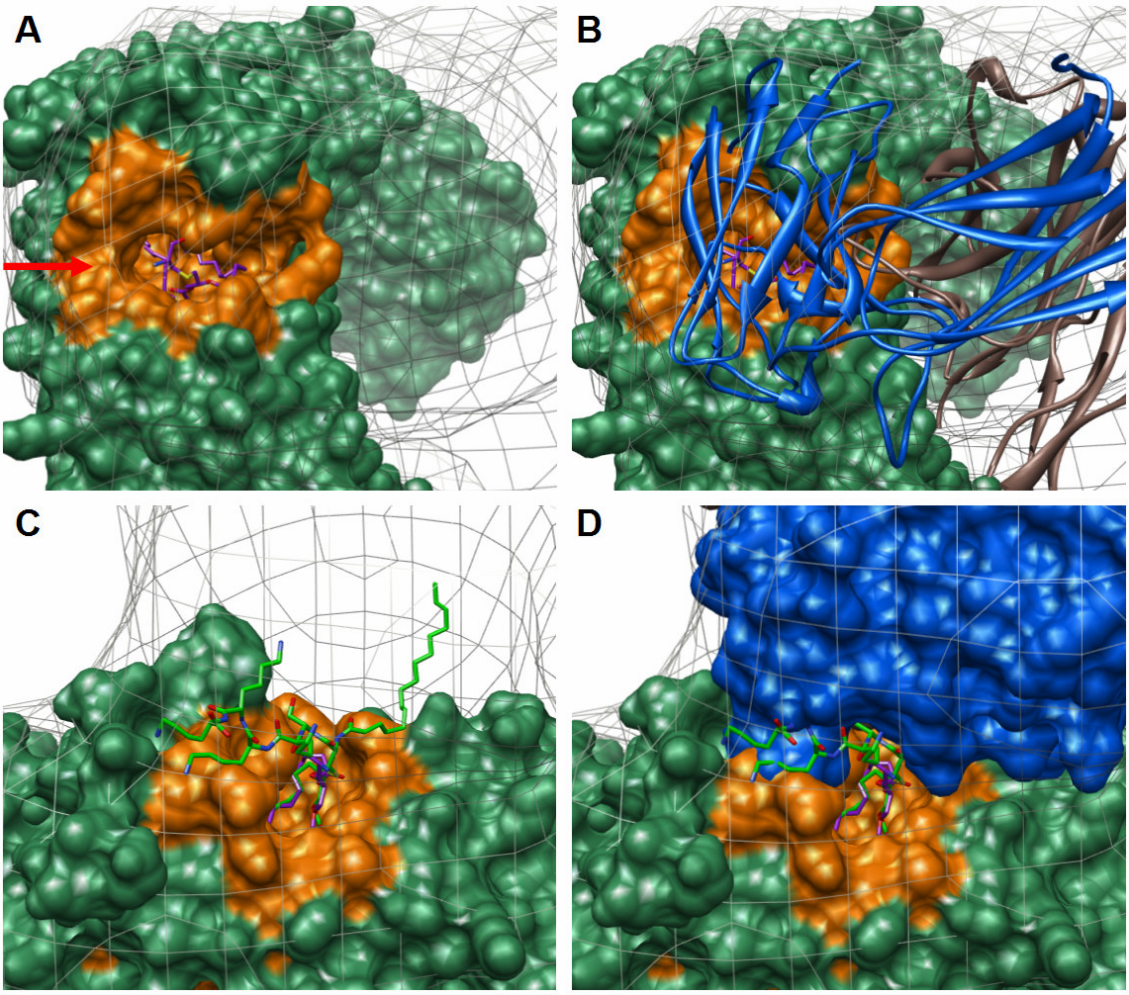


**Figure IVA-1 Blocking of the ligand binding site by OPN-305**
Molecular surface of the ligand binding site (orange) of TLR2 (mint green) with and without OPN-305. **(A)** Top view of the ligand binding site with bound diacylated lipopeptide $Pam_2C$ (pink). **(B)** As (A) but including the antibody Fab. The latter blocks the entire ligand binding site of TLR2. **(C)** The two TLR2 ligands diacylated lipopeptide $Pam_2C$ (pink) and triacylated $Pam_3CSK_4$ (green) are overlaid (direction of view indicated by a red arrow in A). **(D)** Equivalent view as C) but showing OPN-305 in molecular surface representation. The nitrogen-bound lipid chain of $Pam_3CSK_4$ as well as residues of the peptide clash with the antibody.

### IVA.2.1 Does OPN-305 blocks ligand binding?

As demonstrated above, the presence of lipopeptide is not a prerequisite for TLR2/Fab complex formation. Correspondingly, TLR2 preincubated with OPN-301 does not bind to $Pam_3CSK_4$ immobilized on a chip surface during SPR analyses (Meng *et al.* 2004). Proposedly, masking of the ligand-binding pocket of TLR2 led to its inactivation. The entrance to the lipopeptide binding pocket in TLR2 is located between LRRs 11 and 12

(Jin et al., 2007) central to both the TLR/TLR dimerization surface and the antibody epitope (Figure IVA-1, A). The inhibition observed by SPR spectroscopy was thus presumably due both to steric blocking of the $Pam_3CSK_4$ binding site as well as the physical size of the antibody preventing access to the TLR2 surface or the chip-bound ligand. Thus, while the inhibition of TLR dimerization clearly dominates the mechanism of antibody-induced TLR2 inactivation this does not resolve the question of overlapping binding sites for antibody and lipopeptide on TLR2. Hence, does binding of the ligand prevent, suppress or increase antibody binding? Alternatively, is the antibody able to displace the ligand or bind to TLR2 both in the presence and absence of the ligand? If so, are lipopeptides still able to diffuse in and out while the antibody is bound? In the case of competitive inhibition of antibody binding by the ligand, the concentration of antibody required for complete TLR2 neutralization would be significantly higher than in the case of antibody binding being independent of lipopeptide binding.

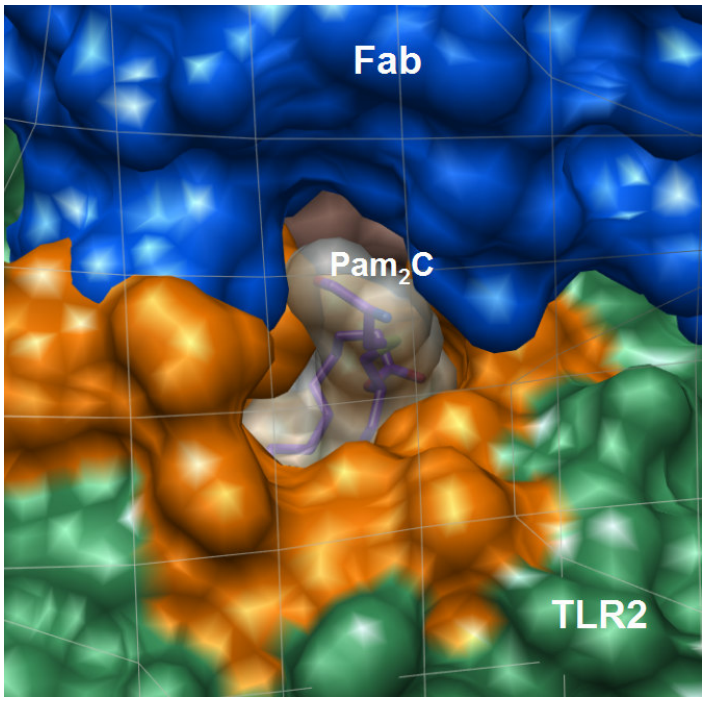


**Figure IVA-2 Ligand access to the ligand binding pocket after antibody/TLR2 complex formation**
Lateral view of the ligand binding pocket. While the antibody covers most of the binding pocket, it nevertheless provides lateral access to the binding pocket potentially allowing ligand to diffuse in or out of the binding site. The conserved elements of lipopeptides including the acyl chains and the cysteine residue are not influenced by antibody binding.

The two ester-bound acyl chains of lipopeptides fill a large pocket in TLR2 lined with hydrophobic residues from LRR modules 9-12. The third amide-bound acyl chain of

triacylated lipopeptides as well as the peptide moiety are not accommodated in this pocket but are involved in mediating TLR dimerization (Jin et al., 2007) (Figure IVA-1, A). In the TLR2/Fab complex the antibody variable domain binds the surface of LRR11-14 and covers major parts of the ligand binding pocket (Figure IVA-1, B). This would result in conflicts between the amide-bound acyl chain of triacylated lipopeptides such as $Pam_3CSK_4$ and the antibody surface (compare Figure IVA-1, C+D). Therefore, binding of the antibody and triacylated lipopeptides are mutually exclusive and partly compete for the same binding site. In addition, the peptide group of $Pam_3CSK_4$ spatially overlaps with the antibody (Figure IVA-1, D). Diacylated lipopeptides lacking the amide-bound lipid chain could potentially bind to TLR2 independently of the antibody binding, provided the peptide moiety is fairly short. In fact, the ligand binding pocket still appears accessible even after antibody binding potentially allowing small diacylated lipopeptides to diffuse in and out (Figure IVA-2). A more highly resolved crystal structure could provide more detailed information on the size of narrowed binding pocket entrance. The lipopeptides $Pam_2CSK_4$ and $Pam_3CSK_4$ are, however, small synthetic molecules, significantly shorter than physiological lipopeptides that normally have longer peptides (see Figure IB-1). In this case the antibody would directly compete with most natural lipopeptides.

OPN-305 thus prevents TLR/TLR dimerization and obstructs the ligand binding site preventing lipopeptide-dependent cytokine release. In addition, the antibody also inhibits PGN-, LTA-, and DAMPs-dependent immune responses (Farrar et al., 2011; Meng et al., 2004). To date, their active sites have not been identified and a possible competitive inhibition of antibody binding by these ligands remains to be determined.

### IVA.2.2 The protein-protein interaction surface

Our EM-based docking experiments clearly identify the surface loops of TLR2 LRR11-14 as the discontinuous epitope recognized by the OPN-305 Fab fragment. An extended, flexible loop of LRR10 in mTLR2 (Figure IVA-3) may additionally be involved but this is not certain from the current structural model. Its potential interaction partner is CDR-L1 of OPN-305, the conformation of which is also difficult to predict due to it having the rare length of 15 residues (see IVA.1). In the TLR2 dimer structures LRR10 adopts a more compact fold than in the TLR2 monomer implying that

TLR1 or TLR6 binding induces the structural change (Figure IVA-3, green and red structures, Jin *et al.* 2007). A compact structure as in the TLR dimers would move it away from CDR-L1. However, favorable interactions with CDR-L1 could, of course, result in a different interaction altogether. The degree of interaction therefore remains to be determined.

Like LRR10, LRR11 also undergoes a conformational change after TLR dimerization moving it towards the ligand and allowing it to form multiple hydrogen bonds with it (Kang et al., 2009). As the EM analysis was undertaken without ligand, LRR11 would presumably adopt a conformation as seen in the monomeric mTLR2 (PDB code 2Z81), used as the model structure (Figure IVA-3, green). The exact conformation is not critical for the current evaluation as it would remain in the centre of the epitope making its residues accessible by OPN-305.

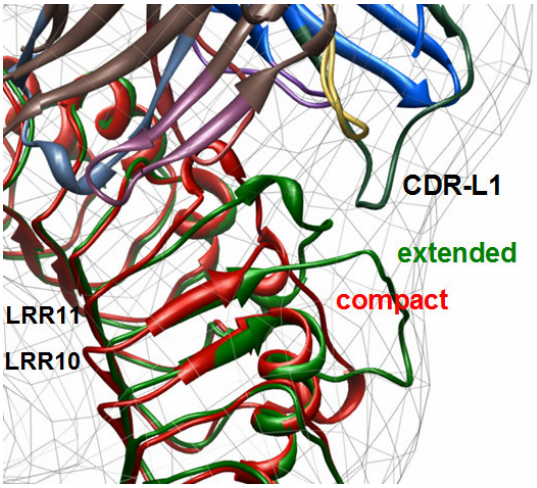


**Figure IVA-3 Structural changes in LRR10 and LRR11 induced by TLR dimerization**
Overlay of mTLR2 monomer (green, PDB code 2Z81) with mTLR2 from mTLR2/mTLR6 dimer (red, PDB code 3A79). In the crystal structure of TLR2/TLR6 the LRR10 of TLR2 adopts a compact conformation in contrast to the extended loop conformation in the crystal structure of the TLR2 monomer. Only in the extended conformation LRR10 would be in contact with CDR-L1. Also note the dimerization-induced conformational changes in LRR11.

Examining the location of the CDRs of OPN-305 relative to the surface of the LRRs, all six can be inferred to be involved in the protein-protein interaction (Figure IVA-4, A). Several CDRs are positioned to interact with more than one LRR (Figure IVA-4, B).

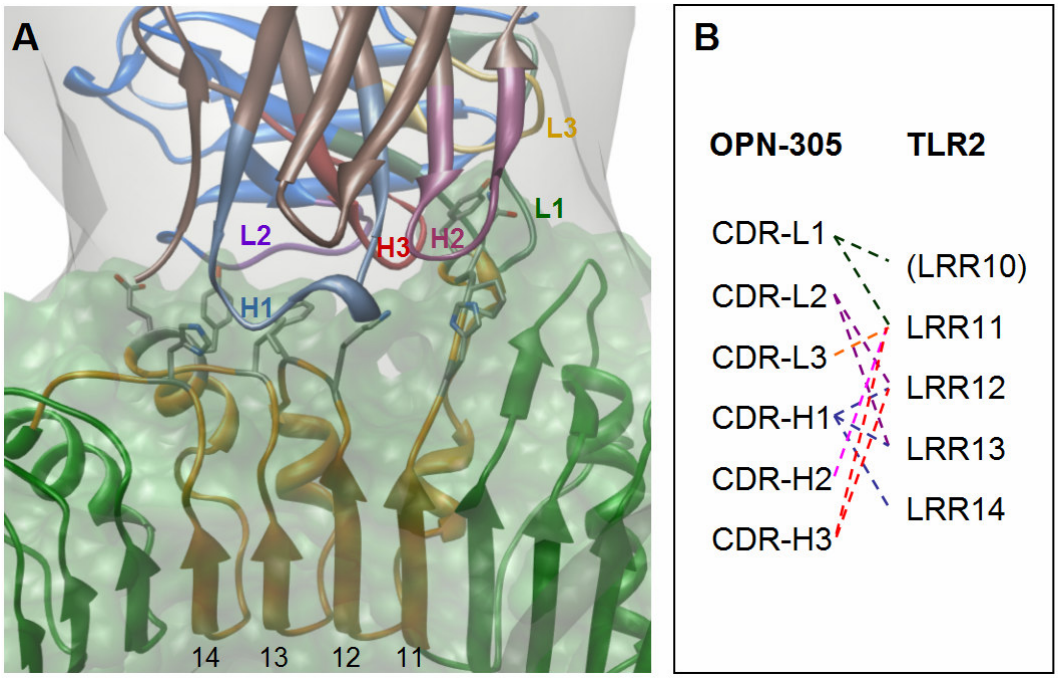


**Figure IVA-4 TLR2/OPN-305 interactions**
All six CDRs of OPN-305 appear to be involved in recognizing TLR2. **(A)** Modeled conformation of CDRs (heavy chain CDRs: H1, H2, H3; light chain CDRs: L1, L2, L3) relative to the surface of the TLR2 LRRs (LRR11-14, orange). Residues on the surface of TLR2 and potentially in contact with the antibody are highlighted in grey. **(B)** Schematic depiction of CDR/LRR interactions. The line colours correspond to the colour scheme of the CDRs in A. For a detailed description see the text below.

By flanking the concave side of LRRs 12, 13 and 14, CDR-H1 would presumably interact with all three, whereas CDR-L2 aligns with the convex side of LRR12 and LRR13. CDR-H3 is situated almost in the centre of the ligand binding site between LRR11 and LRR12. CDR-L1, CDR-L3 and CDR-H3 face towards LRR11. In total, the extended LRR11 is surrounded by four CDRs (CDR-L1, CDR-L3, CDR-H2 and CDR-H3), making this loop the major contributor within the described interaction. This underlines the preferred orientation of TLR2 within the EM surface of also being highly physiological reasonable for antibody interaction. The second, but unlikely orientation of TLR2 would strongly decrease the protein-protein interaction surface area and the number of CDR/LRR interactions (Figure IVA-5).

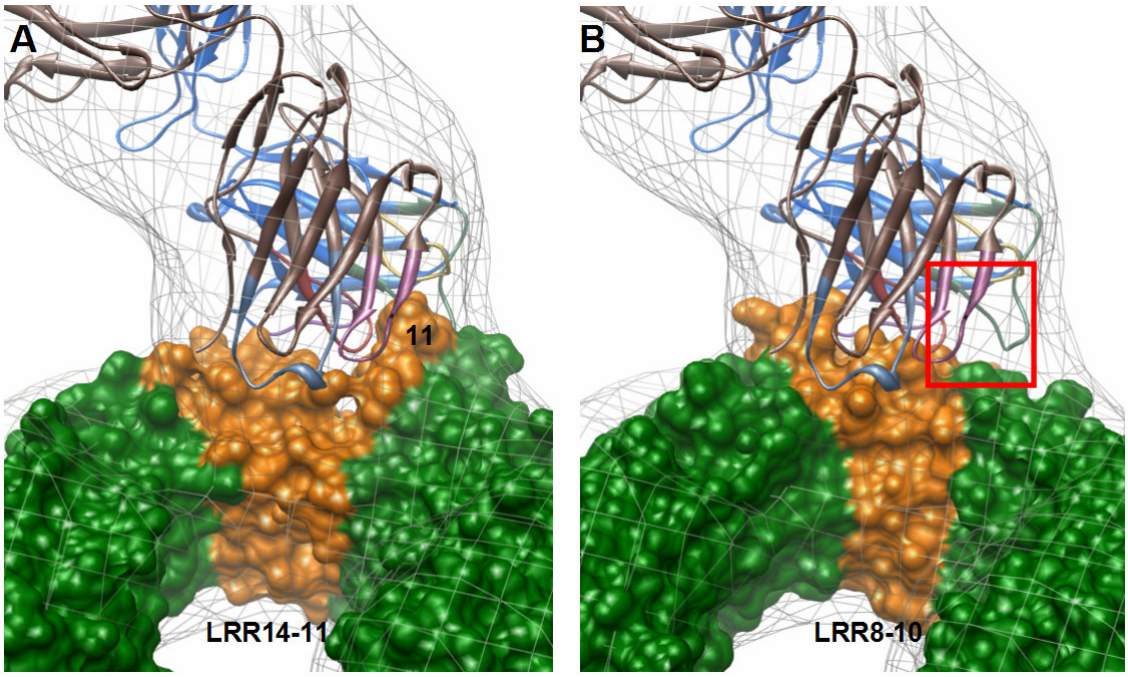


**Figure IVA-5 LRR11 is a major contributor for CDR/LRR interactions**
**(A)** LRR11 is important for a strong protein-protein interaction as it is surrounded by several CDRs of OPN-305. **(B)** Modeling the unlikely orientation of TLR2 into the EM surface results in no comparable extended LRR at the position of LRR11 as seen in (A), which would strongly decrease the binding affinity and would leave several CDRs unbound. The more likely TLR2 orientation #1 as identified in Figure IIIA-19 is thus highly physiological reasonable.

Details of the interactions between OPN-305 CDRs and TLR surface residues can at present not be identified due to both the ambiguity of the modeled CDR region and the resolution inherent to the method. Nevertheless, potentially interacting residues in LRR11-14 have been identified based on the premise that the side chains should be directed outward and they should be conserved in the mammalian TLRs which OPN-305 is known to antagonize. Of ten amino acids on the surface of LRR11-14 fulfilling the criteria outlined above for involvement in the interaction, eight are conserved in murine, human, apish (aTLR2) and porcine TLR2 (pTLR2) (see Figure IIIA-22, Figure IIIA-23). Compared to mTLR2, differences include an arginine at position 321 in hTLR2 instead of glutamine, and a phenylalanine at position 323 in porcine TLR2 instead of tyrosine. SPR experiments previously indicated that OPN-305 has a slightly higher affinity to mTLR2 than to hTLR2 (mTLR2 $K_D$ = 11.9 nM, and hTLR2 $K_D$ = 28.9 nM) (OPN-305 patent, International Patent Number WO/2011/003925, Opsona Therapeutics). This may be explained by the fact that the humanized antibody OPN-305 is based on the murine anti-TLR2 antibody T2.5 (OPN-301), which was initially selected from mTLR2 immunized mice. The CDRs of OPN-305 are therefore optimized

for the recognition of mTLR2 surface residues. The exchange of glutamine 321 in mTLR2 to arginine 321 in hTLR2 could lead to the observed decrease in the binding affinity.

### IVA.2.3 Cross-reactivity of OPN-305

The cross-reactivity of OPN-305 in a range of mammals is due to the conserved nature of the TLR dimerization interface indicating the specific interaction of TLR2 with TLR1 and TLR6 to predate the divergence of the mammalian lineages. The sequence identity of LRR11-14 between mTLR2 and hTL2 is 83 % compared to 63 % for the remainder of the ECD. Similar degrees of conservation can be observed between mTLR2/aTLR2 and mTLR2/pTLR2 (Table IVA-1). As this region is critical for ligand binding and heterodimerization of TLR2 and hence for the protein functionality, amino acids within this area intolerant to spontaneous mutations. Mutations would immediately impact the TLR-mediated immune response and increase the risk of disease, making TLR2 an excellent antagonistic drug target (Hennessy et al., 2010).

**Table IVA-1 Sequence identities**

| | **mTLR2/ hTLR2** | **mTLR2/ aTLR2** | **mTLR2/ pTLR2** |
|---|---|---|---|
| **LRR11-LRR14** | 83 % | 81 % | 75 % |
| **ECD (w/o LRR11-LRR14)** | 63 % | 63 % | 61 % |
| **ECD** | 67 % | 66 % | 64 % |

Although cross-reactivity of OPN-305 with TLR2 from mammals other than human, mouse, cynomolgus monkey and pig have not been shown experimentally, it is likely that this antibody would also neutralize TLR2 from other species – the proviso being that the residues in the TLR2 epitope that are involved in the recognition are conserved. The amino acid sequences for TLR2 LRR11-14 from a range of animals have therefore been aligned to identify other potential targets for OPN-305 (Figure IVA-6). In addition to the four mammals named above, TLR2 sequences came from chimpanzee, dog, cattle, goat, sheep, horse and Chinese hamster.

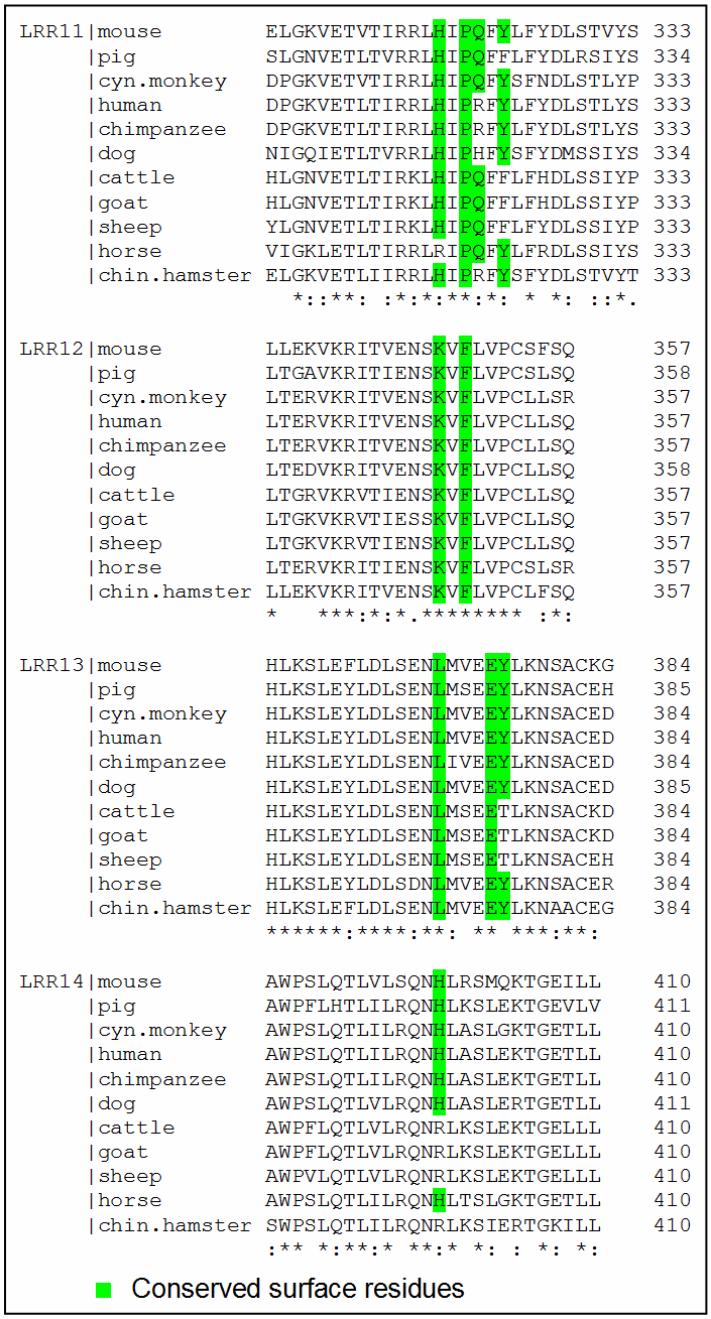


**Figure IVA-6 Multi-sequence alignment of the TLR2 epitope**
Murine, human, cynomolgus monkey and porcine TLR2 are known to be silenced by OPN-305. Their amino acid sequences were aligned with representatives of four additional mammalian families. Conserved residues in the proposed epitope of OPN-305 on TLR2 are highlighted in green. Alignment was performed with ClustalW version 2 (Larkin et al., 2007; Thompson et al., 1994).

The amino acid sequence alignment reveals that despite individual mutations in the recognition site residues, all species share at least 7 of 10 residues of the mTLR2 epitope. Proline 320 (mTLR2 numbering), lysine 347, phenylalanine 349, leucine 371 and glutamate 375 are all perfectly conserved in all species. Histidine 318 is only replaced by arginine in equine TLR2. Even-toed ungulates (cattle, goat and sheep) have the lowest consensus, sharing only 7 of 10 critical residues with mTLR2. The sequence

of the hominid chimpanzee is identical to that of hTLR2, which coincidentally is also identical to that of canine TLR2.

The sequence alignment implies that OPN-305 will presumably antagonize all studied TLR2s. The affinity may, however, be lower in some compared to mTLR2 due to fewer conserved interactions. The lowest affinity may be expected for cattle, goat and sheep.

## IVA.3 Crystallization of TLR2/OPN-305

Although the TLR2/OPN-305 crystal structure could not be solved in this work, some major obstacles such as the purification of the corresponding molecules and the production of diffracting crystals up to a resolution of 8 Å were achieved. This chapter discusses the results in this work and how the strategies could be modified in future efforts to solve the crystal structure of TLR2/OPN-305.

### IVA.3.1 Optimization of protein purification

A pure and monodisperse protein solution is crucial for the generation of high quality crystals. EM images reveal no aggregation of TLR2 and TLR2/OPN-305 (see Figure IIIA-12) indicating that the purified proteins is essentially monodisperse and the interaction is stable. Correspondingly, the complex gives rise to a homogenous peak during AEC (see Figure IIIA-11). By contrast, two Fab variants with a mass difference of 436 Da were identified by MS. These could not be separated completely (see Figure IIIA-7). The size difference between the variants implies the loss of the amino acids Ser-Lys-Tyr-Gly at the C-terminus of the Fab heavy chain and is presumably the result of unspecific papain cleavage (see Figure IIIA-8). Due to the similar size, shape and charge distribution, the complete separation of the two molecular species by liquid chromatography such as SEC (see Figure IIIA-6) and cation exchange chromatography (data not shown) was not successful. Inhomogeneous papain cleavage has previously been observed (Bennett et al., 1997) and is due to the enzyme being a nonspecific sulfhydryl protease that cleaves most peptide bonds, though the rates of hydrolysis may differ by several orders of magnitude (Bennett et al., 1997). Antibodies are preferentially cleaved in the accessible hinge region (see Figure IIIA-5) and papain has thus traditionally been used to generate Fab fragments. The broad substrate specificity

of papain can, however, lead to heterogeneous cleavage of the hinge region requiring some experimentation to identify the optimal digestion conditions for a particular substrate (Adamczyk et al., 2000). For monoclonal antibodies digestion parameters may vary considerably for different types and subclasses (Milenic et al., 1989). As a thiol protease, papain needs to be activated by a reducing agent (usually cysteine) prior to digestion. Much effort went into identifying conditions under which adequate amounts of high quality Fab fragments could be generated. For this purpose both enzyme and antibody concentrations were varied, as were the buffer constituents, the cysteine concentration and the incubation time. However, the secondary cleavage implies that the parameter will need to be further optimized. Possibly a longer incubation time or increase of enzyme concentration could potentially allow the secondary digestion to continue to completion producing a homogeneous sample of the shorter variant.

A fundamentally different approach would be the recombinant production of a so called single-chain variable fragment (scFv) of OPN-305. A scFv is a fusion protein of the variable regions of heavy and light chain, connected by a short linker (Holliger and Hudson, 2005). The protein retains the specificity and affinity for its antigen and can be produced in bacteria (*E. coli*) as a homogenous protein, without the need of papain cleavage.

mTLR2 is a glycoprotein containing three N-linked glycosylation sites in the ECD (Jin et al., 2007). Although some TLR crystal structures have been solved with attached glycan chains (Bell et al., 2005; Jin et al., 2007), this may not be possible in all cases as the crystal packing and associated crystal contacts may require their removal. The heterogeneity and flexibility introduced by glycosylation is known to cause problems during crystallization (Baker et al., 1994). Therefore, several strategies to optimize the glycosylation state of the protein were derived. In addition to insect cell production, which reduces glycosylation compared to most eukaryotic cell lines, mTLR2 was produced in CHO lec3.2.8.1 glycosylation mutant cells, a cell line developed to produce glycoproteins with dramatically simplified surface carbohydrates (Stanley, 1989; Wilke et al., 2010). Sf21 insect cells by contrast give rise to significantly more complex glycoproteins (Kulakosky et al., 1998). Expression in CHO lec3.2.8.1 cells is expected to result in a homogenous $Man_5$ oligomannosyl form linked to the two proximal N-acetylglucosamines (GlcNAc) (Stanley, 1989).

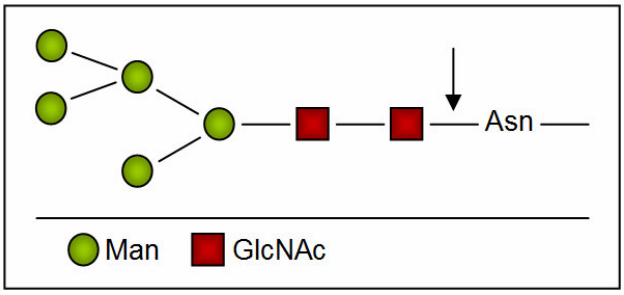


**Figure IVA-7 N-glycosylation of CHO lec3.2.8.1**
The two proximal N-Acetylglucosamine (GlcNAc) units are linked to 5 mannose (Man) moieties. The arrow indicates the PNGase F cleavage site between the innermost GlcNAc and the asparagine residue.

Apart from the cell line, the degree of glycosylation also depends on the protein-specific accessibility during processing. This can thus result in micro-heterogeneity in the target protein.

We exposed mTLR2 to PNGase F prior to crystallization. PNGase F is an amidase that cleaves the link between the glycosylated asparagine and the first GlcNAc in N-linked glycoproteins (Tarentino et al., 1985) (Figure IVA-7). The outcome of this treatment could be verified by SDS-PAGE only for glycosylated TLR2 produced in Sf21 insect cells due to the large size of the glycosylation structures (see Figure IIIA-4). For CHO lec3.2.8.1 cells, the size of the sugar moiety amounts to a mere 1.34 kDa (5x Man + 2x GlcNAc) and is below the resolution limit for SDS-PAGE. However, the cleavage conditions established for mTLR2 from Sf21 were similarly used for CHO cell produced protein. Overall deglycosylation of mTLR2 reduces the heterogeneity and entropy associated with oligosaccharide chain flexibility.

In the course of this thesis, mTLR2 was purified using a non-cleavable, C-terminal $His_6$-tag. As $His_6$-tags are assumed to be largely unstructured and flexible they may potentially interfere with contacts required for the growth of protein crystals. A recommendation is therefore to remove the tag by cleavage after purification (Carson et al., 2007). In fact, to date more than 11500 proteins have been successfully crystallized and their structures solved (statistic from www.pdb.org) despite the presence of a C- or N-terminal $His_6$ (or longer) tag. In the context of TLR2/OPN-305 Fab crystallization removing of the tag may be a reasonable step in overcoming the crystallization problems described and to improve crystal quality. For this, the gene construct would need to be recloned to add a protease cleavage site between TLR2 and the $His_6$-tag.

TEV protease is a commonly used enzyme for protein cleavage and shows a high specificity and activity.

### IVA.3.2 Alternative crystallization strategies

Although a variety of approaches and strategies were employed to produce well diffracting TLR2/Fab crystals, a maximal diffraction of only 8 Å could be achieved. The diffraction data nevertheless permitted unit cell parameters and the space group to be determined: space group C222 with unit cell dimensions of a = 176 Å, b = 310 Å, and c = 97 Å. The diffraction pattern revealed moderate anisotropy resulting in a higher diffraction limit in the vertical as compared to the horizontal direction (see Figure IIIA-25). One very long unit cell axis (b = 310 Å) may contribute to the anisotropy, as the unit cells need to retain the proper packing over three times the distance in this direction compared to c in order to reach the same resolution. Alternatively, diffraction anisotropy may indicate crystal packing interactions to be more uniform in one direction than another. Crystal contacts might be more easily formed on one side of the complex molecule than on another. The improvements of purification pointed out above could help to increase crystal contacts and packing.

Further efforts to improve crystal quality would be an even more extensive sampling of crystallization conditions including more temperatures, starting conditions, protein concentrations or additives. There is evidence that microseed matrix screening is a promising approach to crystallize antibody-antigen complexes, in which seeds are systematically transferred into new conditions to promote crystal growth (Obmolova et al., 2010). It is based on the concept that the conditions that are best for crystal growth may be different from those that favor nucleation. Therefore it is reasonable to increase efforts in finding new crystallization conditions.

# IVB Establishing TLR2 / TLR6 production in eukaryotic cells

As an increasing number ligands are being identified for TLR2 and its partners TLR1 and TLR6, their complexes will remain a focus of structural analysis. Although crystal structures for TLR2/TLR1 and TLR/TLR6 in complex with lipopeptides have been solved, the epitopes of other TLR2 ligands such as LTA, PGN or Zymosan still remain to be identified. Several adaptor proteins are known to be involved in dimerization and/or ligand binding. For example, CD36 is believed to be required for full signaling efficacy through TLR2/TLR6 in complex with LTA or the lipopeptide MALP-2 (Beutler et al., 2006). In addition, potential agonists and antagonists can be structurally analyzed in complex with TLRs. For this purpose the production of mouse/human TLR2 and TLR6 in insect cells using the baculovirus expression system may be of continued interest. Suggestions with respect to their improved production and purification ability are discussed below.

## IVB.1 Insect cell production of mouse/human TLR2 and TLR6

As outlined above, we successfully generated DNA constructs, baculoviral DNA and produced sufficient baculovirus for murine and human TLR2 and TLR6 extracellular domains. However, protein production was only partly successful. In particular the expression of mouse/human TLR6 was significantly weaker or completely absent (hTLR6) compared to that of mouse/human TLR2 (see Figure IIIB-5). One reason may involve the number of glycosylation sites as hTLR6 (9 N-glycans) and mTLR6 (10 N-glycans) have twice to three times the number of hTLR2 (4 N-glycans) and mTLR2 (3 N-glycans). Complex glycosylation can reduce protein production in insect cells leading to less soluble and less stable protein. Interestingly the crystal structure of the TLR2/TLR6 complex was solved using the murine proteins (Kang et al., 2009), despite the complex of human TLR2/TLR1 having been solved before (Jin et al., 2007). Possibly, the authors of that study encountered similar difficulties in producing hTLR6 as described above.

The protein secretion rate in this study was lower than expected resulting in a large fraction of the protein being diverted to intracellular inclusion bodies (see Figure IIIB-6). Additional attempts at using other signal peptides or other cell lines could be undertaken to identify conditions yielding higher protein solubility and more efficient

secretion rates. Alternatively, instead of utilizing secreted protein, the soluble intracellular fraction could also be isolated and tested for folded protein. Our own efforts to refold protein solubilized from inclusion bodies were not successful (data not shown).

## IVB.2 Purification of produced TLR2 and TLR6

The yield of protein in eukaryotic cells in general and of TLR2 in particular is rather low (Results, IIIA.1.1) providing a mere 500 µg per L after affinity chromatography. The number of purification steps is known to be proportional to the rate of protein loss. However, screening for crystallization conditions and optimization of crystals usually requires significantly higher amounts of protein. Protein expression therefore developed into one of the bottlenecks for this project and had major cost and infrastructure implications. We originally designed novel recombinant proteins that would have allowed their purification in a single affinity chromatography step by making use of the high affinity between the C-terminal Fc-tag and Protein A matrix. As the Fc-tagged proteins cannot be eluted easily from Protein A columns, a TEV protease cleavage site was inserted between tag and protein to allow for its facile release.

mTLR2 and hTLR2 were produced in the derived system, while evidence for weak expression of mTLR6 was obtained by SDS-PAGE. The single bands in SDS-PAGE analysis confirmed the excellent purification efficiency (see Figure IIIB-7). However, the TEV protease cleavage site between the protein and the Fc-tag proved inaccessible to the protease possibly due to steric hindrance preventing the release of the TLR-ECD proteins (see Figure IIIB-8, Figure IIIB-9). Elution of the immobilized protein by pH shift for digestion in solution denatured the protein and hence did not provide an alternative route. A new construct was therefore designed that incorporates a five amino acid spacer between the TEV protease cleavage site and the Fc-tag to facilitate the protease interaction (see Figure IIIB-11). The insertion into the original construct by quick change mutagenesis was successful. Alternatively, the Fc-tag was removed by inserting a stop codon by quick change mutagenesis to test whether the Fc-tag itself negatively affects protein secretion (see Figure IIIB-10). Due to time constraints the new construct were not used during this thesis. They, nevertheless, provide a good starting point for continuing the project by other researchers.

# V Outlook

## VA.1 Inhibition of TLR2 with a monoclonal antibody

The described structural results for TLR2 in complex with an antagonistic antibody represent the first insights into a mechanism of TLR2 inhibition with a potential therapeutic drug. The identification of the OPN-305 epitope on TLR2 together with its surface residues in this thesis is the basis for a new patent application from Opsona to isolate epitope fragments or to construct template molecules onto which chemical groups which mimic the epitope are grafted having the specified residues and structure coordinates and to facilitate the generation or identification of new binding members having the same or similar functional properties as OPN-305. It may be possible to use the hybrid LRR technique for the development of a scaffold for epitope grafting or to stabilize and/or modify shorter epitope-containing fragments of TLR2 without compromising their structural integrity (Jin and Lee, 2008a). It would be further interesting to substitute an array of epitope surface residues identified in this work to verify their contribution on antibody interaction. Different combinations of single mutations should be performed and the influence of the TLR2 mutants on OPN-305 binding could be well characterized with techniques such as flow cytometry by using a fluorescent-labeled antibody. By solving the crystal structure of TLR2/OPN-305 the exact structure coordinates of the epitope residues could be determined and possible deviations from the available TLR2 crystal structures could be declared. LRR10 and LRR11 appear in two conformations dependent if TLR2 is a monomer or not. Crystallization analysis could reveal the orientation of these loops in the antibody-bound state. Further analysis of the cross-reactivity property of OPN-305 was performed in this work by multi-sequence alignment of the identified epitope with TLR2 from other mammals. Based on the sequence consensus it revealed that OPN-305 is likely to inhibit TLR2 of most of mammalian classes. This analysis leads to a possible additional application of the antibody for the treatment of domestic and farm animals like dogs, horses, cattle and sheep, for example in septic shock pathology. Dogs are known to suffer from canine rheumatoid arthritis (CRA) and SLE-related diseases correlating with increased cytokine expression (Carter et al., 1999; Hegemann et al., 2003; Wilbe et al., 2009). Thus, the cross-reactivity of OPN-305 is not only a beneficial

feature to study the effectiveness of the antibody in animal models prior to human treatment, but also a promising attribute to treat diverse disease patterns in animals. Therefore, more binding studies with TLR2 from other origins should be carried out to eventually extend the application range of OPN-305.

## VA.2 Producing mouse/human Toll-like receptors 2 and 6 in insect cells using the baculovirus expression system

Efficient production of TLRs in a eukaryotic expression system is a prerequisite for structural analysis. Replacing the secretion signal and the utilization of very specific purification tags are strategies that could improve overall protein yield. In this work we could show that using an Fc-tag for purification results in a very high purity as expected. However, the fusion tag could not be cleaved following purification, but efforts have been started to modify the current protein constructs by insertion of a spacer between cleavage site and fusion tag. Future experiments should concentrate on the establishing of the production of the new modified proteins in the baculovirus expression system. To determine the efficiency of the chosen signal peptide gp67, it might be reasonable to additionally test the native signal peptides of the respective proteins. CHO cells - a mammalian cell line and thus evolutionary more close to humans and mice - could be tested for protein expression instead of insect cells to improve overall protein quality. TLR2 and TLR6 remain in the focus of interest for crystallography for structural analysis on the interaction of TLR2/TLR6 with LTA or MALP-2 and in complex with adaptor proteins such as CD36.

# VI References

Adamczyk M, Gebler JC, Wu J (2000) Papain digestion of different mouse IgG subclasses as studied by electrospray mass spectrometry. J Immunol Methods 237:95-104.

Aikawa N, Okubo Y, Lynn M, Rossignol DP, Wong YN, Schuck E, Kitahara Y, Nakano T, Sivak O, Wasan KM, Nagy C, Yen M (2012) Safety, pharmacokinetics and pharmacodynamics of four-hour intravenous infusions of eritoran in healthy Japanese and Caucasian men. Innate Immun (Epub).

Akira S (2009) Innate immunity to pathogens: diversity in receptors for microbial recognition. Immunol Rev 227:5-8.

Akira S, Takeda K (2004) Toll-like receptor signalling. Nat Rev Immunol 4:499-511.

Akira S, Uematsu S, Takeuchi O (2006) Pathogen recognition and innate immunity. Cell 124:783-801.

Alexopoulou L, Holt AC, Medzhitov R, Flavell RA (2001) Recognition of double-stranded RNA and activation of NF-kappaB by Toll-like receptor 3. Nature 413:732-738.

Aliprantis AO, Yang RB, Mark MR, Suggett S, Devaux B, Radolf JD, Klimpel GR, Godowski P, Zychlinsky A (1999) Cell activation and apoptosis by bacterial lipoproteins through toll-like receptor-2. Science 285:736-739.

Altschul SF, Madden TL, Schaffer AA, Zhang J, Zhang Z, Miller W, Lipman DJ (1997) Gapped BLAST and PSI-BLAST: a new generation of protein database search programs. Nucleic Acids Res 25:3389-3402.

Anderson KV (2000) Toll signaling pathways in the innate immune response. Curr Opin Immunol 12:13-19.

Apostolopoulos V, McKenzie IF (2001) Role of the mannose receptor in the immune response. Curr Mol Med 1:469-474.

Arakawa T, Philo JS, Ejima D, Ejima D, Tsumoto K, Arisaka F (2006) Aggregation analysis of therapeutic proteins, part 1: General aspects and techniques for assessment. Bioprocess International 4:42-49.

Arnold K, Bordoli L, Kopp J, Schwede T (2006) The SWISS-MODEL workspace: a web-based environment for protein structure homology modelling. Bioinformatics 22:195-201.

Arslan F, Keogh B, McGuirk P, Parker AE (2010a) TLR2 and TLR4 in ischemia reperfusion injury. Mediators Inflamm 2010:704202.

Arslan F, Smeets MB, O'Neill LA, Keogh B, McGuirk P, Timmers L, Tersteeg C, Hoefer IE, Doevendans PA, Pasterkamp G, de Kleijn DP (2010b) Myocardial ischemia/reperfusion injury is mediated by leukocytic toll-like receptor-2 and reduced

by systemic administration of a novel anti-toll-like receptor-2 antibody. Circulation 121:80-90.

Asea A, Rehli M, Kabingu E, Boch JA, Bare O, Auron PE, Stevenson MA, Calderwood SK (2002) Novel signal transduction pathway utilized by extracellular HSP70: role of toll-like receptor (TLR) 2 and TLR4. J Biol Chem 277:15028-15034.

Baker HM, Day CL, Norris GE, Baker EN (1994) Enzymatic deglycosylation as a tool for crystallization of mammalian binding proteins. Acta Crystallogr D Biol Crystallogr 50:380-384.

Bell JK, Botos I, Hall PR, Askins J, Shiloach J, Segal DM, Davies DR (2005) The molecular structure of the Toll-like receptor 3 ligand-binding domain. Proc Natl Acad Sci USA 102:10976-10980.

Benkert P, Biasini M, Schwede T (2011) Toward the estimation of the absolute quality of individual protein structure models. Bioinformatics 27:343-350.

Benkert P, Tosatto SC, Schomburg D (2008) QMEAN: A comprehensive scoring function for model quality assessment. Proteins 71:261-277.

Bennett KL, Smith SV, Truscott RJ, Sheil MM (1997) Monitoring papain digestion of a monoclonal antibody by electrospray ionization mass spectrometry. Anal Biochem 245:17-27.

Berg M, Offermanns S, Seifert R, Schultz G (1994) Synthetic lipopeptide Pam3CysSer(Lys)4 is an effective activator of human platelets. Am J Physiol 266:C1684-C1691.

Bessler WG, Cox M, Lex A, Suhr B, Wiesmuller KH, Jung G (1985) Synthetic lipopeptide analogs of bacterial lipoprotein are potent polyclonal activators for murine B lymphocytes. J Immunol 135:1900-1905.

Beutler B (2009) Microbe sensing, positive feedback loops, and the pathogenesis of inflammatory diseases. Immunol Rev 227:248-263.

Beutler B, Jiang Z, Georgel P, Crozat K, Croker B, Rutschmann S, Du X, Hoebe K (2006) Genetic analysis of host resistance: Toll-like receptor signaling and immunity at large. Annu Rev Immunol 24:353-389.

Bieback K, Lien E, Klagge IM, Avota E, Schneider-Schaulies J, Duprex WP, Wagner H, Kirschning CJ, Ter M, V, Schneider-Schaulies S (2002) Hemagglutinin protein of wild-type measles virus activates toll-like receptor 2 signaling. J Virol 76:8729-8736.

Botos I, Segal DM, Davies DR (2011) The structural biology of Toll-like receptors. Structure 19:447-459.

Bowdish DM, Sakamoto K, Kim MJ, Kroos M, Mukhopadhyay S, Leifer CA, Tryggvason K, Gordon S, Russell DG (2009) MARCO, TLR2, and CD14 are required for macrophage cytokine responses to mycobacterial trehalose dimycolate and Mycobacterium tuberculosis. PLoS Pathog 5:e1000474.

Boyd JH, Mathur S, Wang Y, Bateman RM, Walley KR (2006) Toll-like receptor stimulation in cardiomyoctes decreases contractility and initiates an NF-kappaB dependent inflammatory response. Cardiovasc Res 72:384-393.

Carson M, Johnson DH, McDonald H, Brouillette C, Delucas LJ (2007) His-tag impact on structure. Acta Crystallogr D Biol Crystallogr 63:295-301.

Carter SD, Barnes A, Gilmore WH (1999) Canine rheumatoid arthritis and inflammatory cytokines. Vet Immunol Immunopathol 69:201-214.

Carty M, Goodbody R, Schroder M, Stack J, Moynagh PN, Bowie AG (2006) The human adaptor SARM negatively regulates adaptor protein TRIF-dependent Toll-like receptor signaling. Nat Immunol 7:1074-1081.

Chang L, Karin M (2001) Mammalian MAP kinase signalling cascades. Nature 410:37-40.

Chang ZL (2010) Important aspects of Toll-like receptors, ligands and their signaling pathways. Inflamm Res 59:791-808.

Choe J, Kelker MS, Wilson IA (2005) Crystal structure of human toll-like receptor 3 (TLR3) ectodomain. Science 309:581-585.

Cohen J (2002) The immunopathogenesis of sepsis. Nature 420:885-891.

Collaborative Computational Project Number 4 (1994) The CCP4 suite: programs for protein crystallography. Acta Cryst D50:760-763.

Diaz M, Flajnik MF (1998) Evolution of somatic hypermutation and gene conversion in adaptive immunity. Immunol Rev 162:13-24.

Dommett RM, Klein N, Turner MW (2006) Mannose-binding lectin in innate immunity: past, present and future. Tissue Antigens 68:193-209.

Falke S, Tama F, Brooks CL, III, Gogol EP, Fisher MT (2005) The 13 angstroms structure of a chaperonin GroEL-protein substrate complex by cryo-electron microscopy. J Mol Biol 348:219-230.

Farrar CA, Keogh B, McCormack W, O'Shaughnessy A, Parker A, Reilly M, Sacks SH (2011) Inhibition of TLR2 promotes graft function in a murine model of renal transplant ischemia-reperfusion injury. FASEB J 26:799-807.

Favre J, Musette P, Douin-Echinard V, Laude K, Henry JP, Arnal JF, Thuillez C, Richard V (2007) Toll-like receptors 2-deficient mice are protected against postischemic coronary endothelial dysfunction. Arterioscler Thromb Vasc Biol 27:1064-1071.

Fitzgerald KA, McWhirter SM, Faia KL, Rowe DC, Latz E, Golenbock DT, Coyle AJ, Liao SM, Maniatis T (2003) IKKepsilon and TBK1 are essential components of the IRF3 signaling pathway. Nat Immunol 4:491-496.

Frank J, Radermacher M, Penczek P, Zhu J, Li Y, Ladjadj M, Leith A (1996) SPIDER and WEB: processing and visualization of images in 3D electron microscopy and related fields. J Struct Biol 116:190-199.

Frank J, Shimkin B, Dowse H (1981) Spider - A modular software system for electron image processing. Ultramicroscopy 6:343-357.

Fukata M, Vamadevan AS, Abreu MT (2009) Toll-like receptors (TLRs) and Nod-like receptors (NLRs) in inflammatory disorders. Semin Immunol 21:242-253.

Gantner BN, Simmons RM, Canavera SJ, Akira S, Underhill DM (2003) Collaborative induction of inflammatory responses by dectin-1 and Toll-like receptor 2. J Exp Med 197:1107-1117.

Gay NJ, Gangloff M (2007) Structure and function of Toll receptors and their ligands. Annu Rev Biochem 76:141-165.

Goddard TD, Huang CC, Ferrin TE (2007) Visualizing density maps with UCSF Chimera. J Struct Biol 157:281-287.

Goh FG, Midwood KS (2011) Intrinsic danger: activation of Toll-like receptors in rheumatoid arthritis. Rheumatology (Oxford) 51:7-23.

Goodridge HS, Reyes CN, Becker CA, Katsumoto TR, Ma J, Wolf AJ, Bose N, Chan AS, Magee AS, Danielson ME, Weiss A, Vasilakos JP, Underhill DM (2011) Activation of the innate immune receptor Dectin-1 upon formation of a 'phagocytic synapse'. Nature 472:471-475.

Hashimoto C, Hudson KL, Anderson KV (1988) The Toll gene of Drosophila, required for dorsal-ventral embryonic polarity, appears to encode a transmembrane protein. Cell 52:269-279.

Hayashi F, Smith KD, Ozinsky A, Hawn TR, Yi EC, Goodlett DR, Eng JK, Akira S, Underhill DM, Aderem A (2001) The innate immune response to bacterial flagellin is mediated by Toll-like receptor 5. Nature 410:1099-1103.

Hayden MS, Ghosh S (2008) Shared principles in NF-kappaB signaling. Cell 132:344-362.

Hegemann N, Wondimu A, Ullrich K, Schmidt MF (2003) Synovial MMP-3 and TIMP-1 levels and their correlation with cytokine expression in canine rheumatoid arthritis. Vet Immunol Immunopathol 91:199-204.

Heil F, Hemmi H, Hochrein H, Ampenberger F, Kirschning C, Akira S, Lipford G, Wagner H, Bauer S (2004) Species-specific recognition of single-stranded RNA via toll-like receptor 7 and 8. Science 303:1526-1529.

Hemmi H, Kaisho T, Takeuchi O, Sato S, Sanjo H, Hoshino K, Horiuchi T, Tomizawa H, Takeda K, Akira S (2002) Small anti-viral compounds activate immune cells via the TLR7 MyD88-dependent signaling pathway. Nat Immunol 3:196-200.

Hennessy EJ, Parker AE, O'Neill LA (2010) Targeting Toll-like receptors: emerging therapeutics? Nat Rev Drug Discov 9:293-307.

Hochrein H, Schlatter B, O'Keeffe M, Wagner C, Schmitz F, Schiemann M, Bauer S, Suter M, Wagner H (2004) Herpes simplex virus type-1 induces IFN-alpha production via Toll-like receptor 9-dependent and -independent pathways. Proc Natl Acad Sci USA 101:11416-11421.

Hoebe K, Georgel P, Rutschmann S, Du X, Mudd S, Crozat K, Sovath S, Shamel L, Hartung T, Zahringer U, Beutler B (2005) CD36 is a sensor of diacylglycerides. Nature 433:523-527.

Hohn M, Tang G, Goodyear G, Baldwin PR, Huang Z, Penczek PA, Yang C, Glaeser RM, Adams PD, Ludtke SJ (2007) SPARX, a new environment for Cryo-EM image processing. J Struct Biol 157:47-55.

Holliger P, Hudson PJ (2005) Engineered antibody fragments and the rise of single domains. Nat Biotechnol 23:1126-1136.

Hotchkiss RS, Karl IE (2003) The pathophysiology and treatment of sepsis. N Engl J Med 348:138-150.

Huang Q, Pope RM (2010) Toll-like receptor signaling: a potential link among rheumatoid arthritis, systemic lupus, and atherosclerosis. J Leukoc Biol 88:253-262.

Huang Q, Sobkoviak R, Jockheck-Clark AR, Shi B, Mandelin AM, Tak PP, Haines GK, III, Nicchitta CV, Pope RM (2009) Heat shock protein 96 is elevated in rheumatoid arthritis and activates macrophages primarily via TLR2 signaling. J Immunol 182:4965-4973.

Ishii KJ, Kawagoe T, Koyama S, Matsui K, Kumar H, Kawai T, Uematsu S, Takeuchi O, Takeshita F, Coban C, Akira S (2008) TANK-binding kinase-1 delineates innate and adaptive immune responses to DNA vaccines. Nature 451:725-729.

Janeway CA, Jr. (1989) Approaching the asymptote? Evolution and revolution in immunology. Cold Spring Harb Symp Quant Biol 54 Pt 1:1-13.

Janeway CA, Jr. (1992) The immune system evolved to discriminate infectious nonself from noninfectious self. Immunol Today 13:11-16.

Jin MS, Kim SE, Heo JY, Lee ME, Kim HM, Paik SG, Lee H, Lee JO (2007) Crystal structure of the TLR1-TLR2 heterodimer induced by binding of a tri-acylated lipopeptide. Cell 130:1071-1082.

Jin MS, Lee JO (2008a) Application of hybrid LRR technique to protein crystallization. BMB Rep 41:353-357.

Jin MS, Lee JO (2008b) Structures of TLR-ligand complexes. Curr Opin Immunol 20:414-419.

Jung D, Alt FW (2004) Unraveling V(D)J recombination; insights into gene regulation. Cell 116:299-311.

Kagan JC, Su T, Horng T, Chow A, Akira S, Medzhitov R (2008) TRAM couples endocytosis of Toll-like receptor 4 to the induction of interferon-beta. Nat Immunol 9:361-368.

Kaiser WJ, Offermann MK (2005) Apoptosis induced by the toll-like receptor adaptor TRIF is dependent on its receptor interacting protein homotypic interaction motif. J Immunol 174:4942-4952.

Kajava AV (1998) Structural diversity of leucine-rich repeat proteins. J Mol Biol 277:519-527.

Kang JY, Nan X, Jin MS, Youn SJ, Ryu YH, Mah S, Han SH, Lee H, Paik SG, Lee JO (2009) Recognition of lipopeptide patterns by Toll-like receptor 2-Toll-like receptor 6 heterodimer. Immunity 31:873-884.

Kiefer F, Arnold K, Kunzli M, Bordoli L, Schwede T (2009) The SWISS-MODEL Repository and associated resources. Nucleic Acids Res 37:D387-D392.

Kim HM, Park BS, Kim JI, Kim SE, Lee J, Oh SC, Enkhbayar P, Matsushima N, Lee H, Yoo OJ, Lee JO (2007) Crystal structure of the TLR4-MD-2 complex with bound endotoxin antagonist Eritoran. Cell 130:906-917.

Kim LA, Furst J, Gutierrez D, Butler MH, Xu S, Goldstein SA, Grigorieff N (2004) Three-dimensional structure of I(to); Kv4.2-KChIP2 ion channels by electron microscopy at 21 Angstrom resolution. Neuron 41:513-519.

Kobe B, Kajava AV (2001) The leucine-rich repeat as a protein recognition motif. Curr Opin Struct Biol 11:725-732.

Kovach MA, Standiford TJ (2011) Toll like receptors in diseases of the lung. Int Immunopharmacol 11:1399-1406.

Kulakosky PC, Hughes PR, Wood HA (1998) N-Linked glycosylation of a baculovirus-expressed recombinant glycoprotein in insect larvae and tissue culture cells. Glycobiology 8:741-745.

Kumar H, Kawai T, Akira S (2009) Toll-like receptors and innate immunity. Biochem Biophys Res Commun 388:621-625.

Laemmli UK (1970) Cleavage of structural proteins during the assembly of the head of bacteriophage T4. Nature 227:680-685.

Larkin MA, Blackshields G, Brown NP, Chenna R, McGettigan PA, McWilliam H, Valentin F, Wallace IM, Wilm A, Lopez R, Thompson JD, Gibson TJ, Higgins DG (2007) Clustal W and Clustal X version 2.0. Bioinformatics 23:2947-2948.

Leemans JC, Stokman G, Claessen N, Rouschop KM, Teske GJ, Kirschning CJ, Akira S, van der PT, Weening JJ, Florquin S (2005) Renal-associated TLR2 mediates ischemia/reperfusion injury in the kidney. J Clin Invest 115:2894-2903.

Lemaitre B, Nicolas E, Michaut L, Reichhart JM, Hoffmann JA (1996) The dorsoventral regulatory gene cassette spatzle/Toll/cactus controls the potent antifungal response in Drosophila adults. Cell 86:973-983.

Leulier F, Lemaitre B (2008) Toll-like receptors--taking an evolutionary approach. Nat Rev Genet 9:165-178.

Liu L, Botos I, Wang Y, Leonard JN, Shiloach J, Segal DM, Davies DR (2008a) Structural basis of toll-like receptor 3 signaling with double-stranded RNA. Science 320:379-381.

Liu S, Liu Y, Hao W, Wolf L, Kiliaan AJ, Penke B, Rube CE, Walter J, Heneka MT, Hartmann T, Menger MD, Fassbender K (2011) TLR2 Is a Primary Receptor for Alzheimer's Amyloid beta Peptide To Trigger Neuroinflammatory Activation. J Immunol 188:1098-1107.

Liu X, Ukai T, Yumoto H, Davey M, Goswami S, Gibson FC, III, Genco CA (2008b) Toll-like receptor 2 plays a critical role in the progression of atherosclerosis that is independent of dietary lipids. Atherosclerosis 196:146-154.

Ludtke SJ, Serysheva II, Hamilton SL, Chiu W (2005) The pore structure of the closed RyR1 channel. Structure 13:1203-1211.

Maley F, Trimble RB, Tarentino AL, Plummer TH, Jr. (1989) Characterization of glycoproteins and their associated oligosaccharides through the use of endoglycosidases. Anal Biochem 180:195-204.

Mansell A, Smith R, Doyle SL, Gray P, Fenner JE, Crack PJ, Nicholson SE, Hilton DJ, O'Neill LA, Hertzog PJ (2006) Suppressor of cytokine signaling 1 negatively regulates Toll-like receptor signaling by mediating Mal degradation. Nat Immunol 7:148-155.

Mathur S, Walley KR, Wang Y, Indrambarya T, Boyd JH (2011) Extracellular heat shock protein 70 induces cardiomyocyte inflammation and contractile dysfunction via TLR2. Circ J 75:2445-2452.

Matsushima N, Tanaka T, Enkhbayar P, Mikami T, Taga M, Yamada K, Kuroki Y (2007) Comparative sequence analysis of leucine-rich repeats (LRRs) within vertebrate toll-like receptors. BMC Genomics 8:124.

McCartney SA, Colonna M (2009) Viral sensors: diversity in pathogen recognition. Immunol Rev 227:87-94.

McCoy AJ, Grosse-Kunstleve RW, Adams PD, Winn MD, Storoni LC, Read RJ (2007) Phaser crystallographic software. J Appl Crystallogr 40:658-674.

Medzhitov R (2001) Toll-like receptors and innate immunity. Nat Rev Immunol 1:135-145.

Medzhitov R, Preston-Hurlburt P, Janeway CA, Jr. (1997) A human homologue of the Drosophila Toll protein signals activation of adaptive immunity. Nature 388:394-397.

Melo F, Feytmans E (1998) Assessing protein structures with a non-local atomic interaction energy. J Mol Biol 277:1141-1152.

Meng G, Rutz M, Schiemann M, Metzger J, Grabiec A, Schwandner R, Luppa PB, Ebel F, Busch DH, Bauer S, Wagner H, Kirschning CJ (2004) Antagonistic antibody prevents toll-like receptor 2-driven lethal shock-like syndromes. J Clin Invest 113:1473-1481.

Milenic DE, Esteban JM, Colcher D (1989) Comparison of methods for the generation of immunoreactive fragments of a monoclonal antibody (B72.3) reactive with human carcinomas. J Immunol Methods 120:71-83.

Minor W, Cymborowski M, Otwinowski Z, Chruszcz M (2006) HKL-3000: the integration of data reduction and structure solution--from diffraction images to an initial model in minutes. Acta Crystallogr D Biol Crystallogr 62:859-866.

Mitsuzawa H, Wada I, Sano H, Iwaki D, Murakami S, Himi T, Matsushima N, Kuroki Y (2001) Extracellular Toll-like receptor 2 region containing Ser40-Ile64 but not Cys30-Ser39 is critical for the recognition of Staphylococcus aureus peptidoglycan. J Biol Chem 276:41350-41356.

Mogensen TH (2009) Pathogen recognition and inflammatory signaling in innate immune defenses. Clin Microbiol Rev 22:240-273.

Mühlradt PF, Kiess M, Meyer H, Sussmuth R, Jung G (1997) Isolation, structure elucidation, and synthesis of a macrophage stimulatory lipopeptide from Mycoplasma fermentans acting at picomolar concentration. J Exp Med 185:1951-1958.

Murata M (2008) Activation of Toll-like receptor 2 by a novel preparation of cell wall skeleton from Mycobacterium bovis BCG Tokyo (SMP-105) sufficiently enhances immune responses against tumors. Cancer Sci 99:1435-1440.

Nakata T, Yasuda M, Fujita M, Kataoka H, Kiura K, Sano H, Shibata K (2006) CD14 directly binds to triacylated lipopeptides and facilitates recognition of the lipopeptides by the receptor complex of Toll-like receptors 2 and 1 without binding to the complex. Cell Microbiol 8:1899-1909.

North SJ, Huang HH, Sundaram S, Jang-Lee J, Etienne AT, Trollope A, Chalabi S, Dell A, Stanley P, Haslam SM (2010) Glycomics profiling of Chinese hamster ovary cell glycosylation mutants reveals N-glycans of a novel size and complexity. J Biol Chem 285:5759-5775.

Nyman T, Stenmark P, Flodin S, Johansson I, Hammarstrom M, Nordlund P (2008) The crystal structure of the human toll-like receptor 10 cytoplasmic domain reveals a putative signaling dimer. J Biol Chem 283:11861-11865.

O'Neill LA (2008) The interleukin-1 receptor/Toll-like receptor superfamily: 10 years of progress. Immunol Rev 226:10-18.

O'Neill LA, Bowie AG (2007) The family of five: TIR-domain-containing adaptors in Toll-like receptor signalling. Nat Rev Immunol 7:353-364.

Obmolova G, Malia TJ, Teplyakov A, Sweet R, Gilliland GL (2010) Promoting crystallization of antibody-antigen complexes via microseed matrix screening. Acta Crystallogr D Biol Crystallogr 66:927-933.

Otwinowski Z, Minor W (1997) Processing of X-ray diffraction data collected in oscillation mode. In: Methods in Enzymology - Macromolecular Crystallography Part A (Charles WC, ed), pp 307-326. Academic Press.

Palm NW, Medzhitov R (2009) Pattern recognition receptors and control of adaptive immunity. Immunol Rev 227:221-233.

Park BS, Song DH, Kim HM, Choi BS, Lee H, Lee JO (2009) The structural basis of lipopolysaccharide recognition by the TLR4-MD-2 complex. Nature 458:1191-1195.

Peitsch MC, Wells TN, Stampf DR, Sussman JL (1995) The Swiss-3DImage collection and PDB-Browser on the World-Wide Web. Trends Biochem Sci 20:82-84.

Penczek P, Radermacher M, Frank J (1992) Three-dimensional reconstruction of single particles embedded in ice. Ultramicroscopy 40:33-53.

Pettersen EF, Goddard TD, Huang CC, Couch GS, Greenblatt DM, Meng EC, Ferrin TE (2004) UCSF Chimera--a visualization system for exploratory research and analysis. J Comput Chem 25:1605-1612.

Piccinini AM, Midwood KS (2010) DAMPening inflammation by modulating TLR signalling. Mediators Inflamm 2010.

Pierik M, Joossens S, Van SK, Van SN, Vlietinck R, Rutgeerts P, Vermeire S (2006) Toll-like receptor-1, -2, and -6 polymorphisms influence disease extension in inflammatory bowel diseases. Inflamm Bowel Dis 12:1-8.

Poltorak A, He X, Smirnova I, Liu MY, Van HC, Du X, Birdwell D, Alejos E, Silva M, Galanos C, Freudenberg M, Ricciardi-Castagnoli P, Layton B, Beutler B (1998) Defective LPS signaling in C3H/HeJ and C57BL/10ScCr mice: mutations in Tlr4 gene. Science 282:2085-2088.

Prakken AB, van Hoeij MJ, Kuis W, Kavelaars A, Heynen CJ, Scholtens E, de K, I, Rijkers GT, van EW (1997) T-cell reactivity to human HSP60 in oligo-articular juvenile chronic arthritis is associated with a favorable prognosis and the generation of regulatory cytokines in the inflamed joint. Immunol Lett 57:139-142.

Pruitt RN, Chambers MG, Ng KK, Ohi MD, Lacy DB (2010) Structural organization of the functional domains of Clostridium difficile toxins A and B. Proc Natl Acad Sci U S A 107:13467-13472.

Ramos HJ, Gale M, Jr. (2011) RIG-I Like Receptors and Their Signaling Crosstalk in the Regulation of Antiviral Immunity. Curr Opin Virol 1:167-176.

Roach JC, Glusman G, Rowen L, Kaur A, Purcell MK, Smith KD, Hood LE, Aderem A (2005) The evolution of vertebrate Toll-like receptors. Proc Natl Acad Sci U S A 102:9577-9582.

Sakata Y, Dong JW, Vallejo JG, Huang CH, Baker JS, Tracey KJ, Tacheuchi O, Akira S, Mann DL (2007) Toll-like receptor 2 modulates left ventricular function following ischemia-reperfusion injury. Am J Physiol Heart Circ Physiol 292:H503-H509.

Santegoets KC, van BL, van den Berg WB, Wenink MH, Radstake TR (2011) Toll-like receptors in rheumatic diseases: Are we paying a high price for our defense against bugs? FEBS Lett 585:3660-3666.

Sato S, Sugiyama M, Yamamoto M, Watanabe Y, Kawai T, Takeda K, Akira S (2003) Toll/IL-1 receptor domain-containing adaptor inducing IFN-beta (TRIF) associates with TNF receptor-associated factor 6 and TANK-binding kinase 1, and activates two distinct transcription factors, NF-kappa B and IFN-regulatory factor-3, in the Toll-like receptor signaling. J Immunol 171:4304-4310.

Segonzac C, Zipfel C (2011) Activation of plant pattern-recognition receptors by bacteria. Curr Opin Microbiol 14:54-61.

Seifert R, Schultz G, Richter-Freund M, Metzger J, Wiesmuller KH, Jung G, Bessler WG, Hauschildt S (1990) Activation of superoxide formation and lysozyme release in human neutrophils by the synthetic lipopeptide Pam3Cys-Ser-(Lys)4. Involvement of guanine-nucleotide-binding proteins and synergism with chemotactic peptides. Biochem J 267:795-802.

Shaikh TR, Gao H, Baxter WT, Asturias FJ, Boisset N, Leith A, Frank J (2008a) SPIDER image processing for single-particle reconstruction of biological macromolecules from electron micrographs. Nat Protoc 3:1941-1974.

Shaikh TR, Trujillo R, LeBarron JS, Baxter WT, Frank J (2008b) Particle-verification for single-particle, reference-based reconstruction using multivariate data analysis and classification. J Struct Biol 164:41-48.

Sharma S, tenOever BR, Grandvaux N, Zhou GP, Lin R, Hiscott J (2003) Triggering the interferon antiviral response through an IKK-related pathway. Science 300:1148-1151.

Shinohara M, Hirata K, Yamashita T, Takaya T, Sasaki N, Shiraki R, Ueyama T, Emoto N, Inoue N, Yokoyama M, Kawashima S (2007) Local overexpression of toll-like receptors at the vessel wall induces atherosclerotic lesion formation: synergism of TLR2 and TLR4. Arterioscler Thromb Vasc Biol 27:2384-2391.

Shirai H, Kidera A, Nakamura H (1999) H3-rules: identification of CDR-H3 structures in antibodies. FEBS Lett 455:188-197.

Slack JL, Schooley K, Bonnert TP, Mitcham JL, Qwarnstrom EE, Sims JE, Dower SK (2000) Identification of two major sites in the type I interleukin-1 receptor cytoplasmic region responsible for coupling to pro-inflammatory signaling pathways. J Biol Chem 275:4670-4678.

Stanley P (1989) Chinese hamster ovary cell mutants with multiple glycosylation defects for production of glycoproteins with minimal carbohydrate heterogeneity. Mol Cell Biol 9:377-383.

Stark H (2002) Three-dimensional electron cryomicroscopy of ribosomes. Curr Protein Pept Sci 3:79-91.

Takahashi K (2011) Mannose-binding lectin and the balance between immune protection and complication. Expert Rev Anti Infect Ther 9:1179-1190.

Takeda K, Takeuchi O, Akira S (2002) Recognition of lipopeptides by Toll-like receptors. J Endotoxin Res 8:459-463.

Takeuchi O, Kawai T, Muhlradt PF, Morr M, Radolf JD, Zychlinsky A, Takeda K, Akira S (2001) Discrimination of bacterial lipoproteins by Toll-like receptor 6. Int Immunol 13:933-940.

Tang SC, Arumugam TV, Xu X, Cheng A, Mughal MR, Jo DG, Lathia JD, Siler DA, Chigurupati S, Ouyang X, Magnus T, Camandola S, Mattson MP (2007) Pivotal role for neuronal Toll-like receptors in ischemic brain injury and functional deficits. Proc Natl Acad Sci U S A 104:13798-13803.

Tarentino AL, Gomez CM, Plummer TH, Jr. (1985) Deglycosylation of asparagine-linked glycans by peptide:N-glycosidase F. Biochemistry 24:4665-4671.

Thompson JD, Higgins DG, Gibson TJ (1994) CLUSTAL W: improving the sensitivity of progressive multiple sequence alignment through sequence weighting, position-specific gap penalties and weight matrix choice. Nucleic Acids Res 22:4673-4680.

Ultaigh SN, Saber TP, McCormick J, Connolly M, Dellacasagrande J, Keogh B, McCormack W, Reilly M, O'Neill LA, McGuirk P, Fearon U, Veale DJ (2011) Blockade of Toll-like receptor 2 prevents spontaneous cytokine release from rheumatoid arthritis ex vivo synovial explant cultures. Arthritis Res Ther 13:R33.

Underhill DM, Ozinsky A, Smith KD, Aderem A (1999) Toll-like receptor-2 mediates mycobacteria-induced proinflammatory signaling in macrophages. Proc Natl Acad Sci U S A 96:14459-14463.

Urbonaviciute V, Furnrohr BG, Meister S, Munoz L, Heyder P, De MF, Bianchi ME, Kirschning C, Wagner H, Manfredi AA, Kalden JR, Schett G, Rovere-Querini P, Herrmann M, Voll RE (2008) Induction of inflammatory and immune responses by HMGB1-nucleosome complexes: implications for the pathogenesis of SLE. J Exp Med 205:3007-3018.

Vagin A, Teplyakov A (2010) Molecular replacement with MOLREP. Acta Crystallogr D Biol Crystallogr 66:22-25.

Walk A, Callahan J, Srisawangvong P, Leuschner J, Samaroo D, Cassilly D, Snyder ML (2011) Lipopolysaccharide enhances bactericidal activity in Dictyostelium discoideum cells. Dev Comp Immunol 35:850-856.

Wang J, Hu Y, Deng WW, Sun B (2009) Negative regulation of Toll-like receptor signaling pathway. Microbes Infect 11:321-327.

Wang L, Sigworth FJ (2006) Cryo-EM and single particles. Physiology (Bethesda ) 21:13-18.

Werts C, Tapping RI, Mathison JC, Chuang TH, Kravchenko V, Saint G, I, Haake DA, Godowski PJ, Hayashi F, Ozinsky A, Underhill DM, Kirschning CJ, Wagner H, Aderem A, Tobias PS, Ulevitch RJ (2001) Leptospiral lipopolysaccharide activates cells through a TLR2-dependent mechanism. Nat Immunol 2:346-352.

Wilbe M, Jokinen P, Hermanrud C, Kennedy LJ, Strandberg E, Hansson-Hamlin H, Lohi H, Andersson G (2009) MHC class II polymorphism is associated with a canine SLE-related disease complex. Immunogenetics 61:557-564.

Wilke S, Krausze J, Gossen M, Groebe L, Jager V, Gherardi E, van den HJ, Bussow K (2010) Glycoprotein production for structure analysis with stable, glycosylation mutant CHO cell lines established by fluorescence-activated cell sorting. Protein Sci 19:1264-1271.

Wolfs TG, Buurman WA, van SA, de VB, Daemen MA, Hiemstra PS, van ', V (2002) In vivo expression of Toll-like receptor 2 and 4 by renal epithelial cells: IFN-gamma and TNF-alpha mediated up-regulation during inflammation. J Immunol 168:1286-1293.

Yoon SI, Kurnasov O, Natarajan V, Hong M, Gudkov AV, Osterman AL, Wilson IA (2012) Structural basis of TLR5-flagellin recognition and signaling. Science 335:859-864.

Zhou T, Xu L, Dey B, Hessell AJ, Van RD, Xiang SH, Yang X, Zhang MY, Zwick MB, Arthos J, Burton DR, Dimitrov DS, Sodroski J, Wyatt R, Nabel GJ, Kwong PD (2007) Structural definition of a conserved neutralization epitope on HIV-1 gp120. Nature 445:732-737.

# Danksagung

Meinen besonderen Dank aussprechen möchte ich Prof. Wolf-Dieter Schubert für die Aufnahme in seine Arbeitsgruppe, das sehr interessante Projekt sowie seine uneingeschränkte Unterstützung. Seine fachliche Kompetenz und sein Engagement waren wesentlich zum Gelingen dieser Arbeit, nicht zuletzt durch sein immer offenes Ohr für Fragen und Diskussionen. Mit unermüdlichem Einsatz hat er alles dafür getan, den aufwändigen Umzug nach Südafrika schnell und organisiert zu vollenden und gute Bedingungen in Südafrika für erfolgreiche Forschung auf hohem Niveau zu gewährleisten. Zudem stand er uns bei sämtlichen Problemen abseits des Labors, die ein Umzug in ein neues Land so mit sich bringen, stets mit helfender Hand zur Seite, und hat uns damit das Einleben in seiner „alten Heimat“ möglichst leicht gemacht. Auch dafür möchte ich an dieser Stelle „Danke“ sagen.

Bedanken möchte ich mich bei Prof. Dirk Heinz für die Möglichkeit der Anfertigung dieser Doktorarbeit in seiner Abteilung und der zur Verfügungstellung einer modernen Laborausstattung und Infrastruktur während der Zeit am HZI. Auch nach dem Umzug nach Südafrika wurden wir durch seine Abteilung weiterhin tatkräftig unterstützt. Ich bedanke mich ebenfalls für die Teilnahme an meinen „Thesis Komitees“ und den sehr hilfreichen Anregungen und Diskussionen.

Sehr herzlich bedanke ich mich bei Prof. Dieter Jahn für die Übernahme des Erstgutachtens.

Ebenso bedanke ich mich bei Prof. Ralf-Rainer Mendel für die Übernahme des Prüfungsvorsitzes.

An Dr. Joop van den Heuvel und seine Arbeitsgruppe geht ein großes Dankeschön für die regelmäßige Produktion und Versendung frischen TLR2-Proteins von Kontinent zu Kontinent, was mit einem nicht geringen Organisations- und Arbeitsaufwand verbunden war und stets erfolgreich verlief. Als Teilnehmer der „Thesis Komitees“ hat Dr. Joop van den Heuvel zusätzlich einen wichtigen Beitrag zum Projekt geleistet.

Prof. Trevor Sewell und seiner Arbeitsgruppe danke ich sehr für die freundliche Aufnahme und Unterstützung während meiner Arbeit in der Elektronenmikroskopie. Insbesondere den Mitarbeitern Mohamed Jaffer und Jean Watermeyer gilt mein Dank für die geduldige und ausführliche Einarbeitung in die Welt der Elektronen, Partikel und Rekonstruktionen.

Ebenfalls bedanke ich mich bei Peter McGuirk, William McCormack, Anne-Marie Carr und allen Beteiligten von Opsona Therapeutics für die effektive und erfolgreiche Kooperation.

Dr. Manfred Nimtz und Team, Rita Getzlaff sowie Salome Smit danke ich für die unzähligen massenspektrometrischen Untersuchungen und N-terminalen Sequenzierungen.

„*The germans*“ sind erst mit Lilia und Edu so richtig komplett. Auch wenn Edu ohne Zweifel nicht dieser Nationalität zuzuordnen ist, so haben wir doch gemeinsam anscheinend alles dafür getan, recht schnell diesen augenzwinkernden Titel im südafrikanischen Labor zu verdienen. Die Arbeit mit euch war immer angenehm, witzig, stets produktiv und gespikt mit fachlichen Diskussionen. Danke für eure vorzüglichen Kochkünste und das Verständnis für meine weniger vorzüglichen Kochkünste. Danke Lilia für die Zustimmung der Einquartierung meiner Geschwister im Wohnzimmer unserer kleinen Bude und das nicht-anmerken-lassen möglichen Schlafentzugs aufgrund etwaiger Schnarchgeräusche. Durch deine lebhafte und fröhliche Art war das Kapitel Südafrika immer kurzweilig und einfacher zu meistern. Edu ist natürlich erst so richtig komplett mit seiner Frau Devi. Danke euch allen für die schöne Zeit unter einem Dach während unseres Kapstadt-Abenteuers.

Ein großes „Dankeschön“ geht an Ute Widow, die beste TA ever. Wenn wir eine Person in Kapstadt auf der Arbeit vermisst haben, dann dich. An dieser Stelle auch danke dafür, dass du bei meiner Musikwahl im Labor immer zwei Augen – bzw. Ohren – zugedrückt hast.

Sämtlichen aktuellen und ehemaligen Kolleginnen und Kollegen in der Strukturbiologie am HZI sowie der Biotechnologie an der UWC in Südafrika möchte ich uneingeschränkt danken für das tolle Arbeitsklima, lustigen Mittagspausen und diversen „After Work“-Veranstaltungen. Besonderer Dank gilt Daniela Gebauer, Nadine Konisch und Stephanie Schulz für die geduldige Einweisung in die Insektenzellkultur, Sabine Schmidt (nicht nur) für ihre Hilfe bei der Umzugsvorbereitung und natürlich meinen ehemaligen Büronachbarn Christian Strube und Ulrich Wiesand, mit denen es nie langweilig, dagegen immer witzig (und produktiv) zuging. Außerdem danke ich sehr „meiner“ Master-Studentin Donné für die gute Zusammenarbeit (und den äußerst leckeren Namibia-Kuchen deiner Mutter).

Diese Arbeit wäre ohne die großartige Unterstützung meiner Familie nicht möglich gewesen. Vom Studium bis Südafrika – euer Rückhalt war zu allen Zeiten und in allen Lebenslagen stets deutlich zu spüren. Ihr habt immer an mich geglaubt und mir die 10.000 km Entfernung durch eure Besuche kleiner fühlen lassen. Danke euch allen dafür.

Sarah, ich kann hier gar nicht schreiben, für was ich dir am Liebsten alles danken möchte. Die zwei Jahre auf unterschiedlichen Kontinenten waren für uns mit vielen Entbehrungen verbunden und ohne deine Hilfe hätte ich es nicht geschafft. Dass wir diese Zeit so gut überstanden haben, ist das größte Geschenk, das du mir geben konntest. Danke, Danke, DANKE!!!